Effects of Monoglycerides on Rhodamine 123 Accumulation, Estradiol 17 β-D-Glucuronide Bidirectional Transport and MRP2 Protein Expression within Caco-2 cells

by

Xi Jessica Jia

Honours B.Sc., University of British Columbia, 2006

A THESIS SUBMITTED IN PARTIAL FULFILLMENT OF
THE REQUIREMENTS FOR THE DEGREE OF

MASTER OF SCIENCE

in

The Faculty of Graduate Studies

(Pharmaceutical Sciences)

THE UNIVERSITY OF BRITISH COLUMBIA
(Vancouver)

October 2008

ABSTRACT

Purpose: Oral drug development had been hindered by the bioavailability issue despite vast market popularity. Lipid excipients have shown to enhance bioavailability of several reformulated hydrophobic oral drugs, yet the underlying mechanisms of action by lipids are still unclear. One proposed mechanism is that lipid could facilitate drug uptake by altering the activities of apical membrane intestinal efflux transporters. Thus, this study aimed to investigate the effects of specific monoglycerides on the efflux activity and protein expression of multidrug resistance-associated protein 2 (MRP2) *in vitro*.

Methods: A preliminary study was first conducted to determine the effect of Peceol®, a mono- and di-glyceride mixture, on MPR2 efflux activity. Then, the 24-hour non-cytotoxic ranges of specific monoglycerides (1-monopalmitin, 1-monostearin and 1-monoolein) were determined using MTS and LDH assays in Caco-2 cells. Then, the effects of chosen monoglycerides on the functional activity of MRP2 were assessed via rhodamine 123 (Rh123) accumulation and estradiol 17 β-D-glucuronide ($E_2$17βG) bidirectional transport studies. The dose-responses of Rh123 accumulation with each monoglyceride treatment were also determined. Lastly, Western blotting was used to probe the monoglycerides effect on MRP2 protein expression.

Results: In the preliminary study, significant increase in Rh123 accumulation and decrease in $E_2$17βG efflux ratio were observed in Peceol® treated cells. The non-cytotoxic concentration ranges for 1-monopalmitin, 1-monostearin and 1-monoolein were within 1 mM, 1 mM and 500 μM, respectively. Cells treated with 1 mM 1-monoplamitin, 1 mM 1-monostearin, 500 μM 1-monoolein and 50 μM MK571 (a MRP2 inhibitor) resulted in significant increases in Rh123 accumulation and decreases in $E_2$17βG efflux ratio compared to the control (medium treated only). The three monoglycerides did not show Rh123 accumulation in a dose-responsive manner. MRP2 protein expressions in 1-monopalmitin and 1-monoolein treated cells were decreased by 19% and 35%, respectively; however, there was no change of MRP2 protein expression in 1-monostearin treated cells.

Conclusions: These findings suggested that 1-monoolein, 1-monostearin and 1-monopalmitin could attenuate the activity of MRP2 and possibly other efflux transporters in Caco-2 cells. The reduction of efflux activity of MRP2 by 1-monoolein treatment could be partially explained by the non-specific down-regulation of MRP2 protein expression.

TABLE OF CONTENTS

LIST OF TABLES

LIST OF FIGURES

LIST OF ABBREVIATIONS

ABC	ATP-binding cassette
AmpB	Amphotericin B
ANOVA	Analysis of variance
BCRP	Breast cancer resistant protein
BCS	Biopharmaceutics classification system
BSA	Bovine serum albumin
cMOAT	Canalicular multispecific organic anion transporter
cMRP	Canalicular multidrug resistance-associated protein
CYP	Cytochrome P450
CMC	Critical micelle concentration
CAR	Constitutive androstane receptor
Dpm	Disintegrations per minute
$E_2$17βG	Estradiol 17 β-D-glucuronide
EDTA	Ethylenediaminetetraacetic acid
FAT	Fatty-acid transporters
FDA	Food and drug administration
FXR	Farnesoid receptor
GI	Gastro-intestinal
GSH	Glutathione
GST	Glutathione *S*-transferase
HBSS	Hanks' balanced salt solution
HEPES	(4-(2-hydroxyethyl)-1-piperazineethanesulfonic acid

INT	*p*-iodonitrotetrazolium
K_m	Michaelis-Menton constant
LBDDS	Lipid-based drug delivery systems
LBP	Lipid-binding proteins
LDH	Lactate dehydrogenase
MDCK	Madin-Darby canine kidney
MDR1	Multidrug resistance gene product 1
MRP	Multidrug resistance-associated protein
MSD	Membrane spanning domains
MTS	5-(3-carboxy-methoxyphenyl)-2-(4.5-dimethylthiazolyl)-3-(4-sulphonyl)
MTT	Methylthiazol tetrazolium
NBD	Nucleotide binding domains
OATP	Organic Anion Transporting Polypeptide
P_{app}	Apparent permeability coefficients
$P_{app,ab}$	Apparent permeability coefficient from apical to basolateral side
$P_{app,ba}$	Apparent permeability coefficient from basolateral to apical side
Pgp	P-glycoprotein
PMSF	Phenylmethanesulphonylfluoride
Rh123	Rhodamine 123
RIPA	Radioimmunoprecipitation assay
RAR	Retinoic acid receptor
SD	Standard deviation

SDS-PAGE	Sodium Dodecyl Sulfate -polyacrylamide electrophoresis
SLC	Solute carrier
SXR	Steroid-activated receptor
TBS	Tris buffered saline
TEER	Transepithelial electrical resistance
TEMED	N, N, N', N'-Tetra-methyl-ethelenediamine
TM	Transmembrane
UGT	Uridine diphosphate–glucuronosyltransferase

ACKNOWLEDGEMENTS

I would like to thank my supervisor, Dr. Wasan, for his support and continuous mentoring throughout my Master's program. You have provided an excellent environment for me to grow both personally and academically. Your passion, dedication and generosity had influenced me greatly for years to come. Thanks again for giving me this opportunity to be part of your laboratory.

To members of my M.Sc committee members, Dr. Riggs, Dr. Bandiera, Dr. Chang, Dr. Kumar and Dr. Hill, your constructive feedbacks and suggestions had been extremely helpful in guiding me through my Master's project.

I would also like to thank all my colleagues both in the lab and in the faculty, whom I have interacted with in the past two years. To Dr. Carlos, thank you so much for your support as a colleague and a friend. To Olena, you have welcomed and embraced me since my first day here in the lab. To Cheri and Rita, thank you for your companionship during this unique period of my life. I am grateful to establish a good friendship with you and truly wishing all the best in your future endeavors. To all the labmates, Steve, Sheila, Kristina, Pavel, Jackie and Jennifer, I am so thankful to work along side of you during the course of my training. To all the undergraduate students worked in the lab, I had so many fun moments talking with you all. To my fellow graduate students whom I often share tissue culture and dark room with, Tony, Eugene and Prasanth, our conversations and discussions had been one of the most intriguing and memorable moments during my graduate training.

Furthermore, I would like to thank my dear friends, Martin Ding, Carol Chen, Gijo Huang, Magnolia Pak, Michelle Zhou, Wendy Zhou, Xingxing Cheng, Vivian Chow and Tiffany Cheung. Thanks so much for being good listeners when I was frustrated by an unsuccessful experiment. Your encouragement and comforts had enlightened my spirit.

Last not the least, special thanks are owed to my parents for their genuine supports throughout these years of my education. Your words of encouragement, patience and kindness had enabled me to retain faith in myself. Words could not express my deepest gratification and appreciation for your love.

To my beloved parents and grandparents

CHAPTER 1

INTRODUCTION

1.1 Lipid-Based Drug Delivery Systems (LBDDS)

1.1.1 LBDDS in Orally Administered Drugs

A large number of drugs on the market are formulated for oral intake. The main advantage of oral administration over other routes is that it is usually the most convenient and economical route (1). However, the major constraint in oral drug development is the low bioavailability issue, especially for hydrophobic drugs. Bioavailability is defined as the extent of a therapeutically active drug reaching the site of action (1). For most oral drugs, they are delivered to their sites of action through systemic circulation. Some barriers effecting oral drug bioavailability include drug degradation prior to absorption at the gastro-intestinal (GI) tract, poor drug absorption along the GI tract and drug elimination via hepatic first-pass metabolism (2). Approximately 40% of all new drug candidates suffer from low aqueous solubility, partially due to lipophilic groups in these chemical compounds (3, 4).

Excipients used to be considered as the non-active ingredient in the drug dosage form, and their traditional role was limited to bind and provide bulk to the dosage form. However, lipid excipients or lipid based drug delivery system (LBDDS), which essentially encompassing different forms of natural and synthetic lipids, offer advantages beyond the boundary of the primary role of excipients. LBDDS are versatile tools for drug administration because they can be formulated into many types of preparations, such as solutions, suspensions,

emulsions, self-emulsifying systems, and micro-emulsions (3). In addition, LBDDS are usually more stable, cost-effective and less toxic than some other drug delivery systems (5). For decades, LBDDS were implemented in parenteral dosage forms as triglyceride emulsions, micellar systems and liposomes (6). Only in recent years, LBDDS have generated considerable interest by the pharmaceutical industry to be applied in the oral drug formulation after the commercial successes of lipid formulated hydrophobic oral drugs, such as Neoral® (Cyclosporine A), Fortovase® (Saquinavir) and Norvir® (Ritonavir) (7).

For oral drug administration, lipids can be roughly divided into the digestible and the non-digestible groups in the GI tract (8). The non-digestible lipids such as mineral oil, when administered, remain in the lumen and can decrease drug absorption by retaining a fraction of the co-administered drugs (8). As for the digestible lipids, they are mainly composed of dietary lipids such as glyceride, fatty acids, phospholipids, cholesterol, and cholesterol esters, as well as various synthetic derivatives that can be hydrolyzed by lingual, gastric and pancreatic lipases in the stomach (9, 10). It's widely documented that ingested lipids in food enhance the absorption and bioavailability of many hydrophobic oral drugs (11, 12). This project will focus on the role of digestible lipids, in particularly monoglycerides, in facilitating oral drug absorption across the intestine.

1.1.2 Mechanisms of Lipid Enhanced Oral Drug Bioavailability

Although lipid excipients have generated tremendous interest due to their significant beneficial effects on the absorption of lipophilic oral drugs, the mechanisms of improved drug bioavailability by lipid excipients are still under intensive investigation. Thus far, there are several proposed mechanisms aiming to explain the possible clinical benefits of LBDDS in oral drug applications (3). The three primary theories that have attracted the most attention for lipid-enhanced bioavailability are the following: alteration of the composition and character of the intestinal environment of oral drugs (11); bypass of the first pass hepatic metabolism via the lymphatic system (13, 14); interaction of lipids with enterocyte-based transporters (15) (Figure 1).

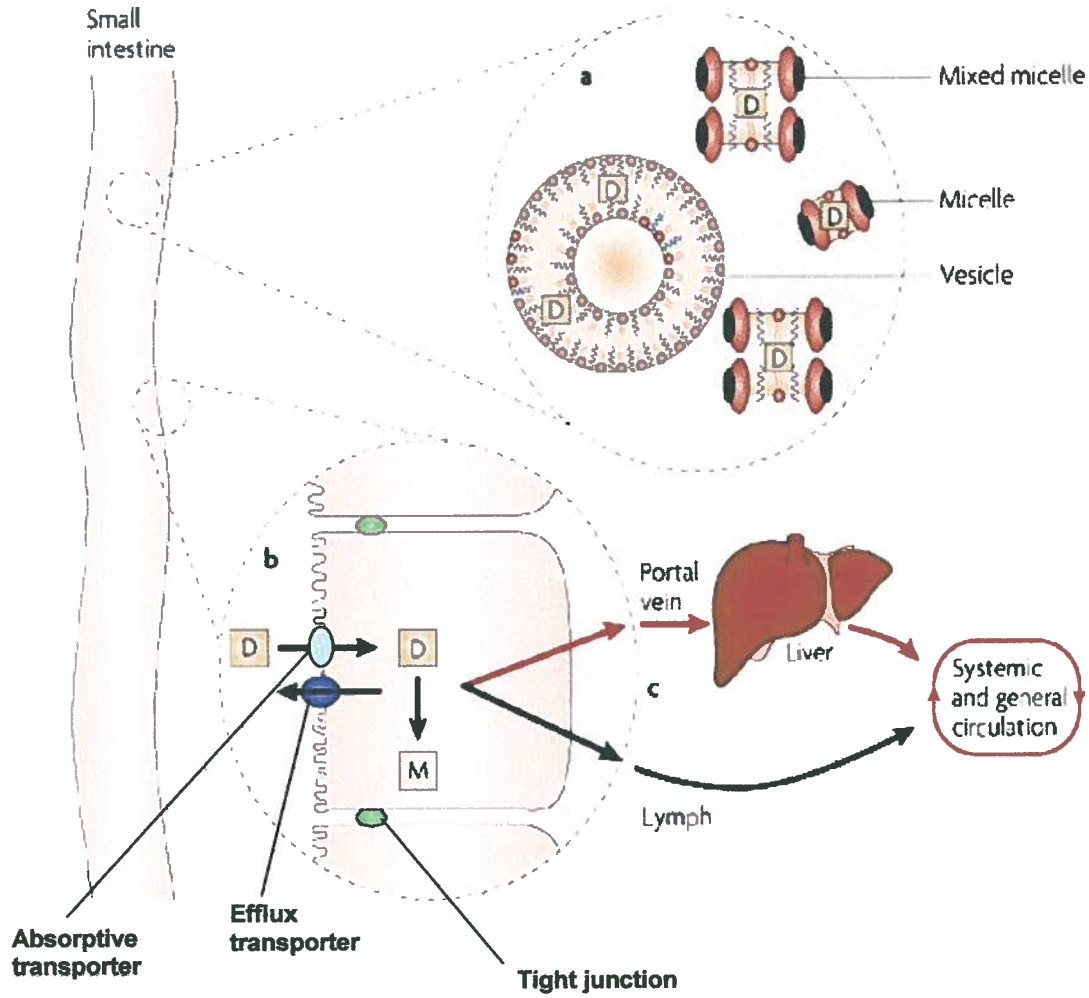

Figure 1. Potential Mechanisms that Lipids and Lipid Excipients Used in Improving Oral Drug Bioavailability. Lipids could alter the composition and character of micro-environment surrounding the drug in the intestine (a); interact with enterocyte-based transport systems (b); bypass the first pass hepatic metabolism via the lymphatic system (c). This figure was modified from Porter, C. *et al.*'s review paper (2).

The absorption of lipophilic drugs from lipid-based formulations is determined by their patterns of dispersion and solubilization in the GI tract in Figure 1a. After the drug is orally administered, the presence of lipids in the oral formulation can stimulate the secretion of gastric and pancreatic lipases (16-18). The presence of lipids and lipid-digestion products in the GI tract also stimulates bile secretion which facilitating lipophilic drugs to become more dispersed and incorporated into colloidal structures (19). The absorption of poorly water-soluble drugs is also often limited by their diffusion rates across the unstirred water layer. The unstirred water layer is essentially a static aqueous diffusion layer adjacent to the intestinal membrane. Solubilization of fatty acids and lipophilic drugs in micellar and mixed-micellar structures greatly enhanced the mass transport across the unstirred water layer which indirectly improved lipophilic drug absorption along the GI tract (20, 21).

Subsequent to the dissolution and diffusion along the GI tract, oral hydrophobic drugs need to partition across the enterocytes before entering the systemic circulation via either paracellular or transcellular route. Only small, hydrophilic and polar molecules are capable of crossing the epithelial monolayer through the paracellular space (22, 23). The more common transcellular route allows drugs to enter the enterocytes before passing through the monolayer by passive diffusion, facilitated diffusion or active transport. There are two main families of transporters on enterocytes, and they are the solute carrier (SLC) transporter family and the ATP-binding cassette (ABC) transporter family. SLC

transporters mostly function as absorptive pumps, which take up substances from surrounding environment into the cells; on the other hand, ABC transporters usually act as efflux pumps that exclude substances out of the cells (24-27). They work concertedly to regulate the absorption of orally administered drugs on the apical side of the enterocytes. Several studies have pointed out that lipids could interact and attenuate the activities of transporters on the apical side of enterocytes, which in turn cause increased bioavailability of some hydrophobic oral drugs as shown in Figure 1b (2,15,28-32). Lipid interaction with enterocytes' transporters will be further investigated in this project.

The gastrointestinal tract is richly supplied with both lymphatic and blood vessels; hence, materials that are absorbed across the enterocytes can potentially enter either lymphatic or blood capillaries. Usually, once orally administered drugs are taken up by the enterocytes, most drugs enter the hepatic portal blood more rapidly than the mesenteric lymph. This is due to the fact that the rate of flow of portal blood is about 500-fold higher than that of the mesenteric lymph (33). A significant amount of oral drugs is extensively altered and removed from the body by hepatic first-pass metabolism before reaching the systemic circulation. Lipids enabled drugs to bypass the hepatic first-pass metabolism via the intestinal lymphatic transport system (2). Following uptake into the enterocytes, fatty acids and monoglyceride digestion products are re-synthesized to triglyceride and assembled into colloidal lipoproteins within the endoplasmic reticulum. These lipoproteins are exocytosed across the basolateral

membrane of the enterocytes and preferentially access the mesenteric lymph vessels as their size precludes easy diffusion across the vascular endothelium. Highly lipophilic drugs (log P > 5 and long chain triglyceride solubility > 50 mg/g) may therefore access the intestinal lymph via post-absorptive association with developing lipoproteins in the enterocytes (34). This mechanism is supported by studies with highly lipophilic drugs, such as halofantrine and amphotericin B (35-39). The majority of these lymphatically transported drugs are solubilized within the apolar lipid core of lymph lipoproteins (2). Hence, this is the other major mechanism to account for the enhanced bioavailability in lipid-formulated oral drugs as shown in Figure 1c.

1.2 Biopharmaceutics Classification System (BCS)

Recognizing the importance of drugs' aqueous solubility and intestinal permeability, the BCS was first drafted by Amidon *et al.* in 1995 and later was adopted and defined by the Food and Drug Administration (FDA) (40, 41). Within this scheme, drugs are categorized into four classes according to their solubility and permeability characteristics: class 1 drugs have high solubility and high permeability; class 2 drugs have low solubility and high permeability; class 3 drugs have high solubility and low permeability; class 4 drugs have low solubility and low permeability (Table 1). A substance is considered highly soluble when the highest dose is soluble in 250 mL or less of aqueous media over pH 1-7.5 at 37 °C. A substance is considered to be highly permeable when the extent of

absorption in humans is 90% or more of an administered dose based on a mass balance determination or in compassion to an intravenous dose.

Table 1. Biopharmaceutics Classification System (BCS). (40, 41)

Class	Permeability	Solubility
I	High	High
II	High	Low
III	Low	High
IV	Low	Low

A generalized scheme of interplay between transporters and these four classes of oral drugs has been proposed by Wu and Benet in 2005 (42). For class 1 oral drugs, the transporter effects were minimal; for class 2 oral drugs, the efflux transporter effects predominate; for class 3 oral drugs, the absorptive transporter effects predominate; for class 4 oral drugs, both the absorptive and efflux transporter effects are important. Since most new molecular compounds developed nowadays have high molecular weights and low water solubility, they are often classified as class 2 compounds (43, 44). The effect of lipids on efflux transporters is of particular interest in this project.

Metabolizing enzymes also play an important role in effecting the bioavailability of these four classes of drugs. The Class 1 and Class 2 compounds are eliminated primarily via metabolism, whereas Class 3 and Class 4 compounds are primarily eliminated unchanged into the urine and bile.

Transporter-enzyme interplay in the intestines will be important primarily for Class 2 compounds that are substrates for CYP3A and Phase 2 conjugation enzymes. For such compounds, intestinal uptake transporters will generally be unimportant due to the rapid permeation of the drug molecule into the enterocytes as a function of their high lipid solubility. That is, absorption of Class 2 compounds is primarily passive and a function of lipophilicity. However, due to the low solubility of these compounds, there will be little opportunity to saturate apical efflux transporters and intestinal enzymes such as CYP 3A4 and uridine diphosphate-glucuronosyltransferases (UGTs). Thus, changes in transporter expression, and inhibition or induction of efflux transporters will cause changes in intestinal metabolism of drugs that are substrates for the intestinal metabolic enzymes. A large number of Class 2 compounds which are substrates for CYP3A are also substrates of the efflux transporters like P-glycoprotein (43, 44).

1.3 Interaction between Lipids and the Enterocyte-based Transporters

1.3.1 The Small Intestine

The small intestine is part of the GI tract between the stomach and the large intestine which is responsible for nutrients digestion and absorption into the body. The small intestine is one of the most important sites for oral drug absorption that regulates the extent of orally administered drugs reaching the liver and ultimately the systemic circulation. The small intestine can be further

divided into three major sections: the duodenum, the jejunum and the ileum, where digestion occurs mostly in duodenum and absorption takes place in the jejunum and ileum. The small intestinal wall consists of the serosa, the *muscularis externa*, the submucosa and the intestinal mucosa (45). The intestinal mucosa is considered the gate that controls drug and nutrient absorption. The surface of the mucosa is the monolayer of columnar epithelial cells which are often referred to as enterocytes (45). To maximize the surface area for optimal nutrient absorption, the small intestinal lining is covered with villi and microvilli (45). Hence, oral drug absorption occurs mostly in the small intestine where the surface area is the greatest along the GI tract.

1.3.2. Drugs and the Enterocyte

Enterocytes are the mucosal cells in the small intestine, and fully differentiated polarized enterocytes have anatomically and physiologically distinctive apical and basolateral sides (45). The apical surface of the enterocytes is the side that faces the lumen of the intestine; whereas the basolateral surface of the enterocytes is the side that faces the basal lamina and the blood vessels (44). Another characteristic of enterocytes is that they form tight junctions between cells, and the intercellular space is only 0.8 nm in human jejunum (22). As a result, most oral drugs utilize the transcellular route to cross the enterocytes (46). After a drug has penetrated into the cytosol of an enterocyte, it is subject to either efflux by apical membrane ABC efflux

transporters, for instance, P-glycoprotein (Pgp), multidrug resistance-associated protein 2 (MRP2) and breast cancer resistance protein (BCRP); or degradation by intracellular metabolizing enzymes, for example, the cytochrome P450 (CYP), the uridine diphosphate–glucuronosyltransferase (UGT) families and the glutathione *S*-transferase (GST). Enterocytes regulate the absorption of drugs mainly through these two processes to effectively remove xenobiotics from the body (10, 11). Hence, modulating the activity of apical membrane ABC efflux transporters has became a popular pursuit by pharmaceutical companies to enhance the bioavailability of orally administered drugs.

1.3.3 Lipids and Transporters on the Enterocytes

Three types of transporters in the enterocytes have been identified to interact with lipids so far, and they are the apical membrane lipid transporters, cytosolic lipid-binding proteins and apical membrane efflux transporters.

The apical membrane lipid transporters are mainly facilitating the uptake and transport of lipid digestion products, such as fatty acids and monoglycerides, into the enterocytes via either active or passive processes (47, 48). Some of the identified apical membrane fatty-acid transporters include CD36 and the fatty-acid transporters (FAT) (2).

The other type of lipid-interacting transporters is the cytosolic lipid-binding proteins (LBPs). After lipids pass through the apical membrane of the enterocytes, they can be associated with LBPs which are cytosolic storage sinks for excess and potentially toxic fatty-acids and exogenous substances. Cytosolic LBPs are likely to alter the intracellular disposition of lipophilic drugs indirectly through their effects on intestinal lipid absorption and pooling within enterocytes (49).

The last major group of transporters linked to lipids is the apical membrane ABC efflux transporters. Although lipids could be physically pumped out of cells by ABC efflux transporters, their interaction with ABC transporters is not limited to them simply being substrates. Lipids have been shown to attenuate the functional activities of certain apical ABC efflux transporters in the intestine, which results in less drugs being effluxed back into the GI lumen (2).

1.4 ATP-Binding Cassette (ABC) Transporters

1.4.1 Overview of ABC Transporters

The diversity of apical absorptive transporters in the intestine is counteracted by the presence of ABC drug efflux transporters that reduce drug absorption and bioavailability. ABC transporters are the largest superfamily of transporters in human, and they can be found in all eukaryotes (50). Their presence and function were initially discovered in many malignant cancer cells

conferring multidrug resistance properties, with Pgp as the first ABC efflux transporter identified (50, 51). Their transport activities were powered by energy harnessed from ATP hydrolysis. Mammalian ABC transporters transport a vast range of exogenous and endogenous substrates across cell membrane, such as, lipids, amino acids, small ions, steroids, bile salts and drugs.

The term ABC transporter was first introduced by Higgins in 1992 (27). It was based on the highly conserved ATP-binding cassette. Currently, there are 49 ABC transporters identified, which are categorized into 7 branches, designated A through G. The majority of them are energy-dependent, with the exception of ABCC7, a cystic fibrosis transmembrane conductance regulator (52, 53). Defects in ABC genes can cause inherited disorders like Tangier disease (ABCA1) (54), Stargardt macular dystrophy (ABCA4) (55), Dubin-Johnson syndrome (ABCC2) (56), cystic fibrosis (ABCC7) (53), pseudoxanthoma elasticum (ABCC6) (57).

The general structural features of ABC transporters have been elucidated based on the study of its most well-characterized member, the Pgp. The core function unit of the ABC transporters consists of two hydrophobic membrane spanning domains (MSDs) which share a high degree of sequence similarity and two nucleotide binding domains (NBDs) as shown in Figure 2 (51). The hydrophilic NBDs are located at the cytoplasmic face of the membrane. They contain Walker A and B motifs which are essential for ATP binding and

hydrolysis. Motifs are structural elements in a protein containing a small number of amino acids that are often directly involved in a protein's function. In addition, they contain a motif known as the "C" signature that is characteristic of ABC transporters' ATPase function with a core sequence of LSGGQ (50, 51). Studies have shown that Walker A and Walker B are separated by a 90-120 amino acid long spacer region which extensively hydrogen bond with the attached ATP (58, 59). The ATPs are in a sandwiched position between adjacent Walker A and ABC signature motif C. A study has shown that the serine residue in each ABC signature motif is required for the interaction between Walker A and ABC signature sequence, where the transporter is interacting with the γ-phosphate of ATP (60, 61). Pgp, MRP2 and BCRP are three of the most important apical ABC efflux transporters that are responsible for the efflux of many xenobiotics and clinically important drugs on the enterocytes that affect oral drug bioavailability.

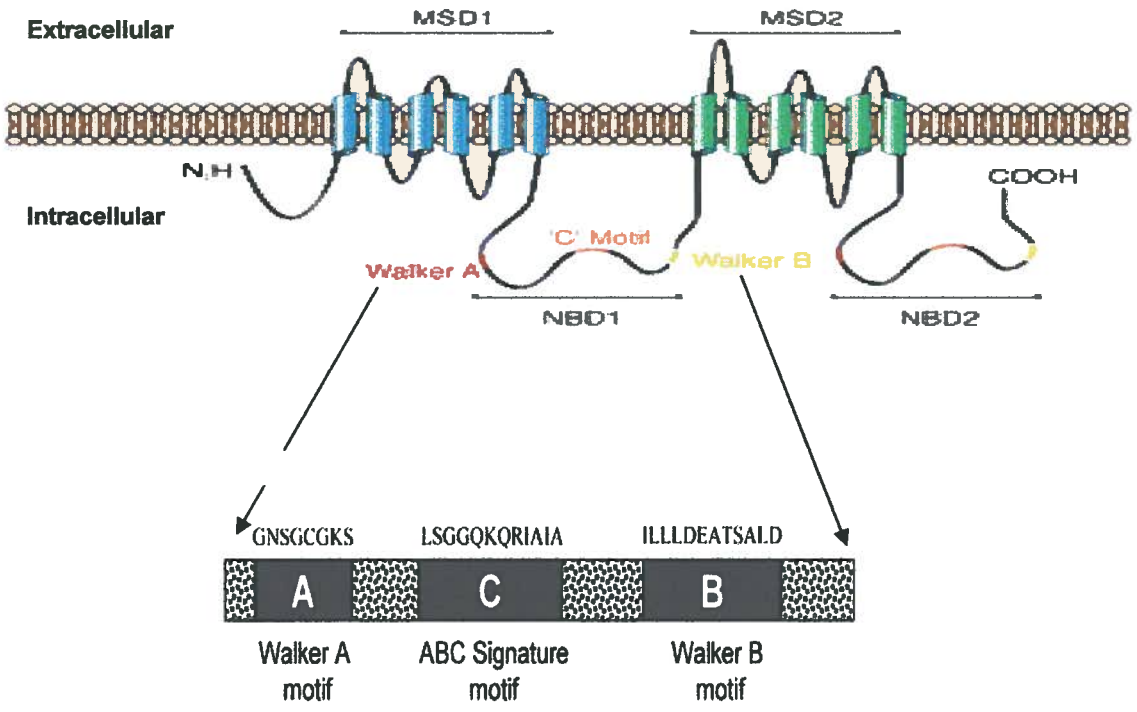

Figure 2. Schematic Structure of a Typical ABC Transporter. The ABC transporter contains two membrane spanning domains (MSD) and two nucleotide binding domains (NBD). The NBD of ABC transporters contains the Walker A and Walker B motifs which are found in all ATP-binding proteins. In addition, an ABC signature motif, motif C, is also presented. The amino acid sequence above the signature motif C is the core sequence for this motif. This figure was adapted from Choudhuri, S' review paper. (51)

Predictions of secondary structures of membrane transport proteins are based on hydropathy analysis (1). However, secondary structures provide little information on how ABC transporters translocate their substrates. The tertiary structures of ABC transporters from high resolution X-ray crystallography are needed with complementary molecular information about the residues involved in the recognition, association, and dissociation of its substrates to solve the puzzle.

Up till now, there are only a handful of membrane transporters that have been crystallized, and MsbA is one of them. In 2001, the first complete crystal structure of an MDR-ABC transporter, MsbA, was determined by x-ray crystallography at 4.5A resolution (62). MsbA was isolated from *E. coli* with homology to human multidrug-resistance efflux transporters. Like other human ABC transporters, MsbA hydrolyzes ATP to export its substrates. Based on the elucidated x-ray crystal structure of MsbA, it forms a homodimer consisting of two six-transmembrane (TM) units with the NBD on the cytoplasmic surface (62). The Walker A motifs interact with α and β phosphates of di- and tri-nucleotides; the Walker B motifs help to coordinate Mg^{2+}. Thus, it is believed that the dimers are central to the ABC transporters' transport mechanism (62).

Since Pgp was the first ABC transporter identified, much attention and studies have been done on Pgp to study the general transport mechanism of ABC transporters. The three most well perceived models are the classical model, the hydrophobic vacuum cleaner model, and the flippase model (63). In the

classical pore model, drugs in the cytosolic compartment are associated with an ATP transporter and then transported out to the extracellular space through a channel formed by the ATP transporter (64). According to the hydrophobic vacuum cleaner model, drugs in the lipid bilayer of the plasma membrane can be recognized by ABC transporters and thus expelled from cells without actually entering the cytosol (65-68). As for the flippase model, the substance diffuses laterally until encountering and binding to a site on the ABC transporter that is in the inner leaflet of the lipid bilayer. The ABC transporter then flips the substance from the inner leaflet to the outer leaflet of the plasma membrane using energy generated from ATP hydrolysis (67). Then the substance can diffuse into the aqueous phase outside the cell. Flipping of the substance triggers structural re-arrangement of the ABC transporter. The flippase model is the most widely accepted model and is also supported by X-ray crystallography data (67, 68).

1.4.2 P-glycoprotein (Pgp)

Pgp is a membrane-bound ABC efflux transporter that mediates active transport, "efflux," of a wide range of drugs and other xenobiotics out of the cells. It is sometimes referred to as the multidrug resistance gene product 1 (MDR1) because it can confer resistance to a large number of structurally diverse drugs with different mechanisms of action (65, 66). It is coded by the gene ABCB1. It is mostly expressed in the intestine, the liver, the kidney, the blood-brain barrier, and the placenta. Intestinal P-gp is located on the apical side of the epithelial

cells. Pgp drives the efflux of wide range of substrates against a concentration gradient and thus reduces their intracellular concentration (68, 69). It contains two membrane spanning domains (MSD) with 6 TM segments for each domain. Drug binding sites are located in the membrane spanning regions, especially TM 4, 5, 6 and 10, 11, 12. There are two functionally linked drug binding regions: the H site and R site. The H-site binds to H33342, whereas the R-site binds to the rhodamine 123. Drugs binding to the H or R-sites mutually stimulate each other's transport (51). Drug efflux by Pgp is blocked by MDR modulators, such as verapamil (69). Many drug substrates of Pgp are also substrates of drug metabolizing enzymes, particularly, CYP3A4. The broad and overlapping substrate specificities of CYP3A4 and MDR1, and their coordinated regulation and expression in organs such as the liver and the intestine, led to the hypothesis that these two proteins evolved to protect the host organism from exposure to environmental or dietary toxins (70, 71)

1.4.3 Multidrug Resistance-Associated Protein 2 (MRP2)

1.4.3.1 MRPs

In humans, there are 13 proteins in the ABCC family, and of these 13 proteins, there are 9 ABCC members belonging to the MRP family (61). Eight of those can confer cellular resistance to various anticancer agents by acting as efflux pumps for a diverse range of lipophilic anions (61). The MRPs can be classified into two groups based on whether they possess a third (N-terminal)

MSD. The "large" MRP members possess an additional MSD domain in addition to the functional core which is composed of two MSDs and two NBDs. The "large" MRP family members include MRP1, MRP2, MRP3, MRP6 and MRP7 (72). The "short" members of the MRP family, such as MRP4, MRP5, MRP8 and MRP9, only have the functional core of a typical ABC transporter. All large MRPs are capable of conferring resistance to at least some natural product agents; whereas, the short MRPs have been characterized by conferring resistance to nucleoside-based agents as well as transporting cyclic nucleotides (73).

MRP1, MRP2, MRP3 are predicted to have 17 TM regions. The protein sequence homology between MRP1 and 2 is 49%, while the homology between MRP1 and MRP3 is 58%, making MRP3 the closest relative to MRP1. While the amino acid sequence homology of MRP1 and 3 is greater than for MRP1 and 2, the latter two seem to share a greater number of substrates (74).

MRP1 was the first protein of this subfamily to confer drug resistance, and it was initially identified in a human lung cancer cell line (75). MRP1 ubiquitously expresses in the human body and is typically localized to the basolateral membrane of polarized human cells. MRP1 has a broad substrate-specificity, and its substrates include many conjugated and unconjugated organic anions, and a limited number of cations, such as leucotriene C_4 , oxidized glutathione, doxorubicin, saquinavir (76-79).

MRP2 is also referred as canalicular MRP (cMRP) or canalicular multispecific organic anion transporter (cMOAT) because of its ability to extrude a range of lipophilic anions into the bile (80-82). They are mainly distributed in the epithelial membrane of the intestine, the canalicular membranes of the liver, the proximal tubules of the kidney, the blood-brain barrier of the brain and the syncytiotrophoblast cells of the placenta (83). MRP2 is localized on the apical side of polarized cells. MRP2 was first cloned from normal rat liver using cDNA probes corresponding to predicted highly conserved regions of human MRP1. MRP2 substrates are typically phase II glutathione, glucouronide conjugates, sulfated conjugates, hydrophobic xenobiotics, steroid, bilirubin and bile salt conjugates (84, 85). MRP1 and MRP2 share a large number of common substrates such as vincristine, doxorubicin, leukotriene C_4 and bilirubin glucuronides (84, 86-87). Although MRP2 and MRP1 transport similar substrates, they tend to have different substrate affinities; for instance, MRP2 exhibits a greater preference for the bilirubin glucuronides (87).

MRP3 is largely found on basolateral membranes of polarized cells. MRP3 protein is highly expressed in the adrenal cortex, and its expression is much lower in liver, kidney, small intestine, pancreas, and colon (88). MRP3 does not transport GSH itself and has markedly lower affinity for LTC_4 and GSH-conjugates (89). MRP3 shows particularly high affinity for glucuronidated xenobiotics such as acetaminophen or morphine (90, 91).

MRP4 and MRP5 also belong to the subfamily C of the ABC-transporter superfamily. But unlike MRP1-3, MRP4 and MRP5 possess only 12 TM α-helices. In polarized cells, MRP4 and MRP5 both localize to the basolateral membrane. MRP4 protein has been detected in human kidney, lung, liver, prostate, brain, pancreas (92-97). MRP5 protein was detected in smooth muscle cells of the corpus cavernosum, ureter, urethra, bladder, blood vessels, the genitourinary tract, cardiomyocytes, and the brain. Both MRP4 and MRP5 transport the endogenous cyclic nucleotides cAMP and cGMP (98). The endogenous function(s) of MRP4 and 5 are not yet fully understood.

MRP6 is a poorly characterized but clinical relevant MRP family member. The exact range of substrates for MRP6 has not yet been determined, but studies suggested that MRP6 may be involved in the transport of certain anticancer agents. Mutations in the *MRP6* gene can cause pseudoxanthoma elasticum, an inheritable disorder of the connective tissue involving impaired visual acuity, skin lesions, and cardiovascular complications (99). High *MRP6* mRNA levels were reported in liver and kidney, whereas low expression was found in a range of other tissues, including lung, intestines, retina, skin, and vessel walls (100). The human *MRP6* encodes a protein of 1503 amino acid residues which shares 45% identity and 55% similarity with *MRP1*, its most closely related *MRP* homologue (100). The biochemical and physiological function of MRP6 protein remain unknown.

The recently discovered MRP7 and MRP8 proteins remain uncharacterized, with respect to either their natural substrates or normal physiological function including a possible role in drug resistance (101, 102).

1.4.3.2 MRP2

MRP2 has three MSD as shown in Figure 3. Human MRP2 is composed of 1541 amino acids and the MRP2 gene is found at chromosome position 10q24 (82). There are 32 exons in a MRP2 mRNA transcript (83). A site-directed mutagenesis study suggested that TM6, TM9, TM16 and TM17 segments in human MRP2 could be involved in substrate-binding sites (81). MRP2 contains two similar but non-identical ligand-binding sites: one binding site for the substance to be transported and the other binding site for substrate regulating the binding affinity of the transport site (103). Furthermore, MSD0 and L0 domains are crucial for the routing of MRP2 to apical membranes (104).

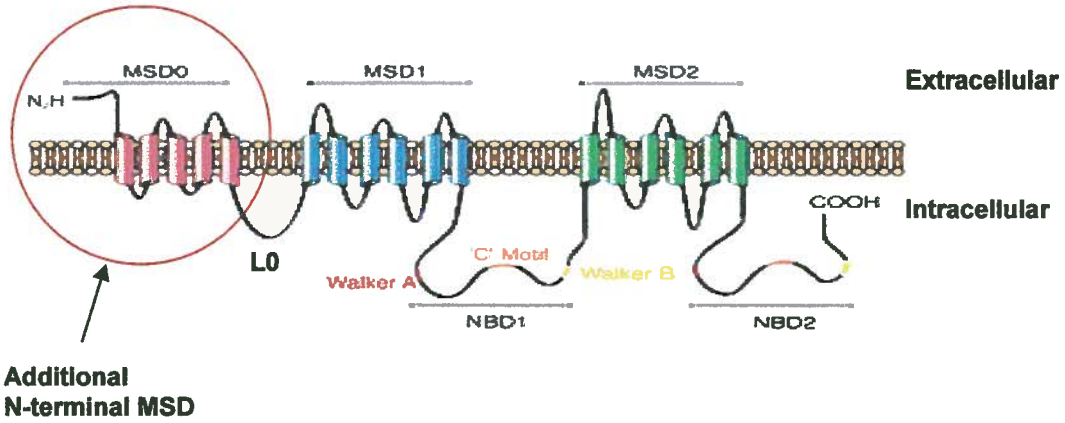

Figure 3. Schematic Structure of MRP2. MSD stands for membrane spanning domain; NBD stands for nucleotide binding domain. This figure was modified from Kruh, G.D. *et al.* (73).

Defects in MRP2 lead to a genetic disease named Dubin-Johnson Syndrome (85). Dubin-Johnson syndrome is an autosomal recessive disease characterized by conjugated hyperbilirubinemia. Human MRP2 has two unglycosylated isoforms with molecular masses of 150 kDa and 174 kDa (83). When MRP2 is N-glycosylated in its mature form, it will have an apparent molecular mass of about 190 kDa. MRP2 have a similar core structure to that of MDR, for example Pgp, which has an internally duplicated structure of two cytosolic nucleotide ATP-binding sites and two putative 6-TM segments. However, MRP2 has an extra N-terminal MSD containing 5 membrane-spanning helices compared to the traditional topology of Pgp (105) (Figure 2 & 3).

1.4.4 Breast Cancer Resistance Protein (BCRP)

Similar to MRP1, BCRP, the protein encoded by ABCG2 was first discovered in multidrug-resistant cell lines. Following the discovery and first structural evaluations, BCRP was grouped into the G-family of ABC-transporters together with other half transporters to form multimers to be functional. The BCRP monomer consists of only one ATP-binding site and 6 transmembrane regions. The polypeptide length is therefore considerably shorter than any of the MRPs. BCRP needs to form multimers in order to be functional and transport its many substrates (106). As BCRP was first identified in drug-resistant cancer cell lines, it is not surprising that many chemotherapeutic compounds are substrates of this efflux transporter, such as mitoxantrone, daunorubicin, and doxorubicin

(106). Many xeno- and endo-biotic BCRP substrates are also transported by other efflux transporters, especially P-glycoprotein, thus extrapolating BCRP related *in vitro* data to the *in vivo* situation may be difficult. In contrast to MRP1 or 2, BCRP does not require GSH for transport and does not transport GSH. BCRP is expressed in many tissues of importance to drug disposition or organ compartments, in particularly small intestine, bile canaliculi and blood vessels (106).

1.5 Interaction of Lipids with ABC Transporters

1.5.1 Peceol® and Efflux transporters

Peceol® is a commercially available product from Gattefossé (Montreal, Canada) which is often used as a lipid excipient. It is in a liquid form which has an acid value of 0.71mgKOH/g. It has an iodine value of 68.7gI_2/100g. As shown in Table 2, Peceol® is mainly composed of mono- and di-glycerides. Out of all the fatty acids attached to the glyceride backbone, oleic acid, linoleic acid, stearic acid and palmitic acid account for 78%, 12.3%, 2% and 3.5%.

Table 2. Chemical Composition of Peceol®

Composition	Percentage (%)
Free Glycerol	1.3
Total Monoglycerides	44.3
Total Diglycerides	45.4
Total triglycerides	8.7
Others	0.3

The effect of lipids on apical efflux transporters in the enterocytes was first identified and studied extensively with Pgp. Several *in vivo* and *in vitro* studies have shown that Peceol® can decrease Pgp protein expression and functional activities (14-15, 22). In contrast to Pgp, the interaction of lipids with other ABC transporters in the intestine is frequently overlooked. Therefore, the effect of lipids on another important apical ABC efflux transporter multidrug resistance-associated protein 2 (MRP2) will be investigated in this study.

1.5.2 Monoglycerides and Efflux Transporters

The simplest lipids are fatty acids, and more than 100 different fatty acids that have been identified in various species (107). Most fatty acids have a long-chain of hydrocarbons with a carboxylate group at one end. They have pK_a ranging from 4.5 to 5.0; therefore, they are ionized at physiological pH. Fatty acids differ from one another in the length of their hydrocarbon tails, the degree

of unsaturation (the number of carbon-carbon double bonds), and the positions of the double bonds in the chains (107). Fatty acids without a carbon-carbon double bond are classified as saturated, whereas those with at least one carbon-carbon double bond are classified as unsaturated.

Fatty acids are commonly attached to a glycerol backbone in our body because high concentration of free fatty acids could disrupt cell membranes. A study by Konishi *et al.* has shown that monoglycerides could down-regulate the activity of Pgp (28). The three monoglycerides used in this project are 1-monostearin, 1-monopalmitin and 1-monoolein, and their chemical structure and physical properties were shown in Table 3 (108). All these three fatty acids used are attached to the glycerol backbone at C1 position. Monostearin, monopalmitin and monoolein are the three most predominant fatty acid residues in plants and animal (107).

Table 3. Chemical Structures and Physical Properties of Monoglycerides. (108)

Compounds	Fatty Acid Chain	Physical Properties	Structure
1-monoolein $C_{21}H_{40}O_4$	C18:1	MW: 356.54 mp: 35 °C.	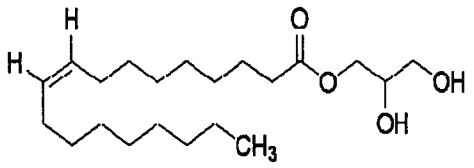
1-monostearin $C_{21}H_{42}O_4$	C18:0	MW: 358.56 mp: 78-81 °C	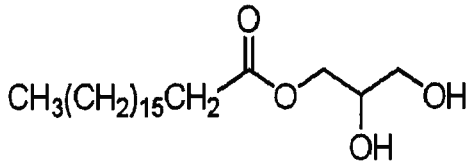
1-monopalmitin $C_{19}H_{38}O_4$	C16:0	MW: 330.50 mp: 74-76 °C	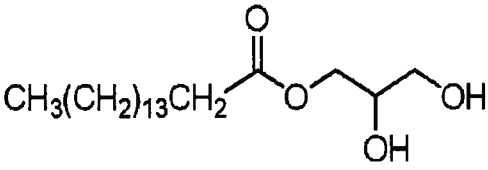

1.6 *In vitro* Cell Models

1.6.1 Madin-Darby Canine Kidney (MDCK) Cells Transfected with MRP2

MDCK cells are from a dog renal epithelia cell line. It is a common model for studying cell growth regulation, metabolism, and transport mechanisms in distal renal epithelia (109, 110). When grown under standard culture conditions, MDCK cells differentiate into columnar epithelium and form tight junctions in a

shorter period of time than Caco-2 cells, which is a well established cell line for studies of intestinal transporters (3 days MDCK vs. 21 days Caco-2 typically) (111). Therefore, MDCK cells have become an alternative to Caco-2 cells for permeability measurements. However, the non-human (canine) and non-intestinal (renal) origin of MDCK cells may be considered a disadvantage. Also, these cells have a low expression level of transporter proteins and a low metabolic activity (112). In the late 1990s, MDCK cell lines that over-expressing MRP2 were generated by transfecting human MRP2 genes into MDCK cells, and the resulting MDCK-MRP2 cell line have been used as models of the intestinal mucosa (113). A good correlation between the permeation of passively absorbed drugs in Caco-2 cells and MDCK cells has been reported (111). A study by Tang *et al* has shown that MDCK-MRP2 cells only over-expresses the unglycosylated form of MRP2, not the fully glycosylated form compared to MRP2 expression levels in Caco-2 cells (114). As a result, this cell model was not chosen for purpose of this study.

1.6.2 Caco-2 Cells: An Intestinal Cell Model

The proper reconstitution of a human differentiated epithelial cell monolayer *in vitro* allows a better prediction of oral drug absorption in humans. One of the most popular *in vitro* systems for intestinal transport studies was the Caco-2 cell line (115). This model is generally regarded as a "gold-standard" in vitro model that resembles the small intestine. Caco-2 cells are from human colon

carcinoma cells of a 72 year-old patient. They express a number of key efflux ABC transporters mimicking the expression level of these transporters in human small intestinal epithelial cells (116). In tissue culture, Caco-2 cells slowly differentiate into monolayers with differentiated phenotypes, which resemble the small intestinal villus epithelium (117).

A study by Englund *et al.* showed that the expression of transporters in Caco-2 was closest to the expression pattern in the small intestine. Similarly, an mRNA expression study compared a number of important ABC efflux transporters from healthy human jejunum biopsies and Caco-2 cells, and found that BCRP and MRP2 transcripts were more abundant than MDR1 and other ABC efflux transporters in the jejunum and Caco-2 cells (118). Transcript levels of ABC transporters correlated well between jejunum and Caco-2 cells, except BCRP, which exhibited a 100-fold lower transcript level in Caco-2 cells compared with jejunum. In addition, the expression level of MRP2 in Caco-2 cells is much higher than that of Pgp, which suggested the roles of MRP2 in intestinal drug efflux have been underestimated (116).

CHAPTER 2

SUMMARY OF RESEARCH PROJECT

2.1 Overall Objective

The overall objective of this research project is to investigate the effects of specific monoglycerides (1-monostearin, 1-monoolein and 1-monopalmitin) on MRP2 activity and protein expression *in vitro*.

2.2 Hypotheses

2.2.1 Hypothesis I

MRP2 functional activities could be reduced by 24-hour exposure to specific monoglycerides (1-monostearin, 1-monoolein and 1-monopalmitin) in Caco-2 cells, a human intestinal cell model.

2.2.2 Hypothesis II

Reduction in MRP2 activity caused by these specific monoglycerides (1-monostearin, 1-monoolein and 1-monopalmitin) could be the result of down-regulation of MRP2 protein expression.

2.3 Specific Aims

2.3.1 Aim I

To determine the 24-hour non-cytotoxic concentration ranges of Peceol®, 1-monostearin, 1-monopalmitin and 1-monoolein in Caco-2 cells.

2.3.2 Aim II

To conduct a preliminary study on the effects of mono- and di- glycerides on MRP2 activity and protein expression after Caco-2 cells are exposed to Peceol® (a mixture of mono- and di- glycerides) for 24 hours.

2.3.3 Aim III

To characterize the effects of 1-monostearin, 1-monopalmitin and 1-monoolein on MRP2 functional activities after Caco-2 cells are exposed at non-toxic concentrations for 24 hours.

2.3.4 Aim IV

To assess the effects of 1-monostearin, 1-monopalmitin and 1-monoolein on MRP2 protein expression after Caco-2 cells are exposed at non-toxic concentrations for 24 hours.

2.4 Rationale

My research project will focus on understanding of the effect of specific monoglycerides on one of the most abundant apical efflux transporters in the intestine, MRP2. Many studies have shown that lipid-based drug delivery systems could attenuate the functional activities of the intestinal ABC efflux transporters, which in turn, increase drug bioavailability when co-administered orally with the drug of interest. Most of these studies were focused on Pgp, an apical-membrane ABC efflux transporter. Several *in vivo* animal studies have

shown that when highly non-soluble drugs like ontazolast and AmpB were incorporated into Peceol®, there were significant increases in the bioavailability of these orally formulated drugs (14, 119). In addition, a number of studies using natural lipids like castor oil, Peceol® and monoglycerides have shown to inhibit Pgp-mediated drug efflux *in vitro* (15, 28, 46).

In contrast to Pgp, the interaction of lipids with other major intestinal apical-membrane ABC efflux transporters, for instance MRP2, has received less attention. MRP2 shares many similarities with Pgp in terms of tissue distribution, function and localization on polarized cells (83) as shown in Table 2. MRP2 is mainly located in the gut, liver, kidney, blood-brain barrier and placenta which overlap with the tissue distribution of Pgp (51). Furthermore, MRP2 is anchored on the apical side of polarized cells acting as an efflux pump in a similar fashion as Pgp. In addition, both MRP2 and Pgp transport a wide-spectrum of substrates (73).

Table 4. Comparison between Pgp and MRP2 (73).

Transporter	Function	Tissue Distribution	Cellular Location	Substrate Specificity
Pgp/MDR1 (ABCB1)	Efflux	Intestine, Kidney, Liver, Placenta, Blood-brain Barrier	Apical	Neutral and cationic organic compounds and drugs, such as doxorubicin, daunorubicin and paclitaxel.
MRP2 (ABCC2)	Efflux	Liver, Kidney, Intestine, Placenta, Blood-brain Barrier	Apical	Glutathione and other conjugates, organic anions, leukotriene C4. Many hydrophobic drugs; common drug such as methotrexate, doxorubicin, sulfinpyranzone

Since Peceol ® is a mixture of mono- and di-glycerides, the effect of Peceol ® on MRP2 functional activity will be looked at first in specific aim 2 as a preliminary study before testing the effects of specific monoglycerides on MRP2 activity. However, before proceeding to aims 2 to 4, the cells non-cytotoxic ranges of all these lipid treatments (Peceol®, mono-stearin, -palmitin and –olein) need to be determined using two colorimetric assays in aim 1. This step is crucial to eliminate any effect that might associate with cell death.

In the past, studies of lipid effects on transporters were mostly focused on the more complicated lipid excipients, which are often composed of a mixture of long- or medium-chain fatty acids, mono-, di- and tri-glycerides, various types of surfactants and hydrophilic solvents. However, the effects of the specific components in those lipid excipients on ABC efflux transporters have not been adequately assessed. Therefore, the effects of monoglycerides on efflux transporters' functional activity, in particularly MRP2, will be investigated using Rh123 and $E_2$17βG in aim 3. $E_2$17βG is an endogenous metabolite of estradiol belonging to the family of glucuronide conjugates of the estrogen D-ring with cholestatic properties (120).

Although lipid excipients have been shown to inhibit the functional activities of ABC efflux transporters, particularly Pgp, the mechanism of action exerted by these lipids excipients is still unclear. Some theories include disrupting the cell membrane integrity, depleting available intracellular ATP, blocking binding sites on the transporters, inhibiting the transporters' ATPase

activity, reducing the protein expression of the transporters (105, 121-122). An *in vitro* study by Sachs-Barrable *et al.* has shown that Peceol® inhibits Pgp protein expression (105); however, there have been few studies to address whether the lipid-effect on expression was due to the reduction of protein expression of other ABC efflux transporters besides Pgp. In aim 4, the effect of monoglycerides on MRP2 protein expression in Caco-2 cells will be investigated.

CHAPTER 3

MATERIALS AND METHODS

3.1 TISSUE CULTURE

3.1.1 Tissue Culture Reagents

Fetal bovine serum (FBS, USA source), 10 mM MEM non-essential amino acids solution, 100 mM (4-(2-hydroxyethyl)-1-piperazineethanesulfonic acid (HEPES) buffer solution, 100 mM sodium pyruvate solution, penicillin-streptomycin (contains 10,000 units of penicillin and 10,000 µg of streptomycin per mL), phosphate-buffered saline (PBS), Hanks' balanced salt solution (HBSS), minimum essential medium supplemented with Earle's salts and L-glutamine with phenol-red (MEM), Trypsin-EDTA (0.25% Trypsin with EDTA·4Na) 1X, were purchased from Invitrogen™ Technologies (Grand Island, NY, USA). Caco-2 cells (human colon adenocarcinoma cells) were purchased from American Type Culture Collection (ATCC) (Rockville, MD, USA). 0.4% Trypan blue solution was purchased from Sigma (St. Louis, MO, USA)

3.1.2 Tissue Culture Equipment

Sterile 50mL conical tubes, disposable 5 mL, 10 mL and 25 mL serological pipettes were purchased from Starstedt (Montreal, QB, CA). Angle-vented neck T-75 flasks, sterile 12-well plates, 48-well plates and 96-well plates were purchased from Corning Incorporated (Corning, NY, USA). The biological safety cabinet (Class II, Type A2) used was the Labgard 437 from NuAire (Plymouth, MN, USA). The Isotemp 228 water bath and Micromaster phase contrast microscope (100 x magnifications) were purchased from Fisher Scientific, Inc.

(Pittsburgh, PA, USA). The incubator, Forma® series II 3110 CO_2 water jacketed incubator, was purchased from Thermo Scientific, Inc. (Marietta, Ohio, USA). The Allegra™ 6R centrifuge was purchased from Beckman Coulter, Inc. (Fullerton, CA, USA). The Axiovert 25 microscope with 100x magnification was purchased from Carl Zeiss (Stockholm, Sweden). Hausser Nageotte Bright-line hemacytometer was purchased from Fisher Scientific, Inc (Horsham, PA, USA).

3.1.3 Preparation of Caco-2 Cell Media (Complete MEM)

The media were prepared under sterile condition in a Class II biological safety cabinet. The surfaces of all reagents taken into the cabinet were cleaned with 70% ethanol. The complete Caco-2 culture medium was prepared by supplementing commercially available MEM (Earl's salts and L-glutamine, 500 mL) with 10% fetal bovine serum (50 mL), 0.1mM MEM non-essential amino acids solution (5.8 mL), 1mM HEPES buffer solution (5.8 mL), 1mM sodium pyruvate solution (5.8 mL), 100 U/mL penicillin and 100 µg/mL streptomycin (5.8 mL). The completed MEM medium was stored at 4°C.

3.1.4. Initial Cell Culture from Frozen Caco-2 Cells

The completed MEM medium was warmed up in 37°C water bath for at least 30 minutes. Frozen Caco-2 cells from ATCC (Passage 18) were shipped in a 1.2 mL cryovial with traces of DMSO as a cryoprotectant. After receiving the order, cryovial containing Caco-2 was submersed in a liquid nitrogen tank prior to use. To establish the culture, one cryovial was took out of the nitrogen tank and

placed immediately in a 37°C water bath with constant agitation to rapidly thaw cells for 3 minutes. The vial was wiped with 70% ethanol before opening it in the cell culture hood. Then, 1mL of the thawed cells were transferred to a sterile 75 cm^2 flask filled with 10mL of supplemented warmed MEM medium. The flask was incubated at 37 °C in humidified air containing 5% CO_2. On the next day, the MEM medium in the flask was changed with fresh medium to remove the cytotoxic DMSO.

3.1.5. Subculture of Caco-2 Cells

The Caco-2 cells were maintained between passages 18 to 59. The passages used for experiments were from passages of 28 to 59. The doubling time of Caco-2 cells was 62 hours. Therefore, by monitoring the doubling time of Caco-2 cells, I determined when the cells were ready to be used for experiments. The medium was changed every other day. The flask was first washed with 10mL of pre-warmed sterile PBS. Then the flask was refilled with 15mL of fresh pre-warmed completed MEM medium. Once the Caco-2 cells reached 90% confluency in the T-75 flask, the old medium was discarded from the flask and it was washed with 10mL of pre-warmed sterile PBS. The PBS washing was discarded afterward. Cells were pre-treated with 7mL of 0.25% trypsin, and then they were incubated at 37 °C in humidified air containing 5% CO_2 for 5 minutes. After the incubation time, 13mL of the completed MEM medium was added immediately afterward to the T-75 flask to inhibit further activity by trypsin which may damage cells. Then the whole solution with suspended cells was completely

transferred to a 50mL conical tube. The cells were pelleted down at 1000 rotations per minute (rpm) for 8 minutes using Allegra™ 6R centrifuge. The supernatant was decanted and the cells were re-suspended with MEM medium. Caco-2 cells were counted using a hemocytometer.

3.1.6 Caco-2 Cell Counting

After the cell suspension had been prepared, 50µL of the cell suspension was transferred to a well in a 96-well plate. Then 50µL of Trypan blue was added to the well containing the cell suspension. Cell suspension and Trypan blue were mixed thoroughly by pipetting. The dead or dying cells are stained by Trypan blue, while viable cells repel the dye and remain non-stained. Subsequently, 50µL of this mix was pipetted into a cover-slipped chamber of a hemocytometer. The hemocytometer was placed under a Micromaster phase contrast microscope at magnification of a 10X ocular and a 10X objective to count viable cells in all four quadrants using a hand tally counter. A common convention used to count cells is that cells touch the lines to the left and top but not the right and bottom of the square are counted. To count the total number of cells were calculated as following:

Cells/mL in the counting mix = (Total # of cells counted / 4) x (10^4 cells / ml)

Cells/mL in the original cell suspension= (cells/mL in the counting mix) x 2

3.2 Cytotoxicity Study

3.2.1 Materials in Cytotoxicity Study

CytoTox96® Non-Radioactive Cytotoxicity Assay was purchased from Promega Corporation (Madison, WI, USA). The MEM medium without phenol red was purchased from Invitrogen™ Technologies (Grand Island, NY, USA). The reason for choosing growth media without phenol red is because the color of phenol red can interfere with the readings of spectrophotometric assays. The complete MEM medium was prepared as listed in 3.1.3 except replaced with the MEM medium without phenol red. All the tissue culture materials listed in 3.1.1. Peceol® were kindly provided by Gattefossé Inc. (Montreal, QC, CA). The α-monopalmitin, α-monostearin, α-monoolein (purity >99%) and Triton X-100 were purchased from Sigma-Aldrich (St. Louis, MO, USA).

3.2.2 Equipment in Cytotoxicity Study

Bransonic® 3510 table top sonicator was purchased from Branson (Cleveland, Ohio, USA). Ascent® Multiskan is a microplate photometer purchased from Thermo Scientific, Inc. (Pittsburgh, PA, USA). All the other equipment and supplies were listed in 3.1.2. Disposable 25mL reagent reservoirs were purchased from Thermo Scientific, Inc. (Pittsburgh, PA, USA). Sterile 10cc syringe with needle was purchased from BD (Franklin Lakes, NJ, USA).

3.2.3 Preparation of Lipid Treatments

Peceol®, α-monopalmitin, α-monostearin and α-monoolein were prepared with the fully supplemented MEM medium containing no phenol red. The molecular weight of α-monopalmitin, α-monostearin and α-monoolein are 330.51 g/mole, 358.57 g/mole and 356.55 g/mole, respectively. First, a 5mM stock solution of monostearin and monopalmitin were prepared. Then, both stock solutions were subjected to sonication at 37 °C using the Bransonic® 3510 table top sonicator for 30 minutes. Subsequently, the following concentrations of monostearin and monopalmitin treatments were prepared from the 5 mM stock solution: 100, 250, 500, 750, 1000, 1250, 1500, 1750 and 2000 µM. Monoolein and Peceol® were prepared in a similar fashion to monostearin and monopalmitin except that 1mM monoolein and 5% v/v Peceol® stock solution were prepared. The subsequent concentrations prepared from monoolein stock solution were at 100, 250, 500 and 750 µM; the subsequent concentrations prepared from Peceol® stock solution were at 0.1, 0.25, 0.5, 0.75, 1, 1.25, 1.5, 1.75 and 2% v/v. All the prepared lipid treatments were stored at 4 °C until use.

3.2.4 Seeding 96-well Plates

Pelleted cells were re-suspended and counted in completed MEM media (with phenol red) as described in sections 3.1.5 and 3.1.6. The reason for choosing medium with phenol red is to use it as a pH indicator to monitor the health of tissue culture. Phenol red exhibits a gradual color transition from yellow to red over the pH range from 6.6 to 8.0. Under normal condition (pH close to 7),

phenol red added to the growth medium will have a pink-red color. The waste products produced by the mammalian cells will slowly decrease the pH, gradually turning the solution orange and then yellow. Therefore, this color change is an indication that the medium needs to be replaced. The re-suspended Caco-2 cells were diluted to 200,000 cells per mL, and 100µL of the diluted stock cell solution was added to each well in a 96-well plate. Thus, 20,000 Caco-2 cells seeded per well in a 96-well plate. The medium was changed every other day. When the cells reached 90% confluency, the lipid-treatments could be added to the wells.

3.2.5 24-hour Cytotoxicity Study (LDH Assay)

The toxicity profile of Caco-2 cells in response to each lipid treatment was obtained using a commercially available enzymatic assay, The CytoTox® 96 Non-radioactive cytotoxicity assay, which is often referred to as the LDH assay. The LDH assay is a colorimetric alternative enzymatic assay to ^{51}Cr release cytotoxicity assay, with the advantages of being a much simpler and accurate colorimetric assay for dead and plasma membrane-damaged cells. LDH assay quantitatively measures lactate dehydrogenase (LDH), a stable cytosolic enzyme, which is released upon cell lysis. LDH presented in the culture medium (due to plasma membrane damage) participates in a coupled reaction which converts a yellow tetrazolium salt, *p*-iodonitrotetrazolium (INT) into a red, formazan-class dye which is measured by absorbance at 492 nm (Figure 4). The amount of formazan is directly proportional to the amount of LDH in the culture, which is in

turn directly proportional to the number of dead or damaged cells. The amount of LDH released positively correlates to the number of cell deaths.

$$NAD^+ + \text{Lactate} \xrightarrow{\text{LDH}} \text{Pyruvate} + NADH$$

$$NADH + INT \xrightarrow{\text{Diaphorase}} NAD^+ + \text{formazan (red)}$$

Figure 4. Schematic chemical reaction of LDH assay.

On the day of the experiment, the lipid treatments prepared were first sonicated and warmed up using the Bransonic® 3510 table top sonicator at 37°C for 15 minutes. A 0.1% triton X-100 solution was prepared with the MEM medium containing no phenol red. The cells were treated with Peceol® at 0, 0.1, 0.25, 0.5, 0.75, 1, 1.25, 1.5, 1.75, 2, 5% v/v; The 1-monostearin and 1-monopalmitin were both treated at 0, 100, 250, 500, 750, 1000, 1250, 1500, 1750, 2000 and 5000 µM; whereas the 1-monoolein was treated at 0, 100, 250, 500, 750 and 1000 µM. Each of the four lipid treatments were added in a separate 96 well plate. In addition, a positive control group with 0.1% Triton X-100 was added onto each plate. Triton X-100 is a potent non-ionic detergent that disrupts cell membrane which leads to cell death. For each well, 100 µL of each lipid treatment (Peceol®, 1-monoolein, 1-monostearin, 1-monopalmitin) at various concentrations was added. For each experiment, there were three to six replicates for each concentration of the lipids. Afterward, the cells were incubated in a humidified Forma® incubator at 37°C, 5% CO_2 for 24 hours.

After the cells incubated with the monoglyceride treatment for 24 hours, 25 µL of the medium from each well was transferred to a new 96-well flat-bottomed plate. Then, 25 µL of the reconstituted substrate mix from the CytoTox96® Non-Radioactive Cytotoxicity Assay Kit was transferred to each well of the new 96-well plate containing the aliquots. The plate was covered with aluminum foil and incubated at room temperature for 15 minutes. Stop solution from the CytoTox96® assay kit was immediately added after the incubation time. Before any reading was taken, bubbles in the wells were eliminated using a syringe needle. The absorbance (A) was recorded at 492nm within 1 hour following the addition of stop solution using an Ascent® Multiskan spectrometer. The percentage cytotoxicity was determined in the following fashion: $(A_{sample} - A_{background}) / A_{Triton\ X\text{-}100}$.

3.3 Cell Viability Studies

3.3.1 Materials in Cell Viability Study

MTS CellTiter 96® AQueous One Solution Cell Proliferation Assay was purchased from Promega Corporation (Madison, WI, USA). All the other materials were identical as listed in section 3.2.1.

3.3.2 Equipment in Cell Viability Study

All the equipment used in this experiment were identical as listed in section 3.2.2.

3.3.3 24-hour Cell Viability Study (MTS Assay)

To ensure LDH cytotoxicity assay accurately captured the non-cytoxic range of these lipid treatments, the CellTiter 96® AQ_{ueous} One Solution assay (also called MTS assay) was also used to determine cell viability in response to these lipid treatments (122). The main advantages of CellTiter 96® AQ_{ueous} One Solution cell proliferation assay is that it is more convenient, faster and safer to use compared to other tetrazolium compounds, such as methylthiazol tetrazolium (MTT) or *p*-iodonitrotetrazolium (INT) (123, 124). The CellTiter 96® AQ_{ueous} Assay one solution contains both the novel tetrazolium compound 3-(4,5-dimethylthiazol-2-yl)-5-(3-carboxymethoxyphenyl)-2-(4-sulfophenyl)-2H-tetrazolium, inner salt (MTS) and an electron coupling reagent, phenazine methosulfate (PMS). PMS is used to enhance the chemical stability, which allows it to be combined with MTS to form a stable solution. The MTS tetrazolium compound can be bioreduced by metabolically active cells into a colored formazan product that is soluble in tissue culture medium. This conversion is accomplished by NADPH or NADH produced by dehydrogenase enzymes from metabolically active cells. The quantity of formazan product as measured by the absorbance at 492 nm is directly proportional to the number of living cells in culture.

Caco-2 cells were seeded and treated with different lipid treatments at various concentrations in 96-well plates as described in the cytotoxicity study. After 24-hour treatment, wells were washed with 100 µL PBS (pH 7.4) once. This

was followed by the addition of 100µL of CellTiter® 96 AQueous One Solution Reagent diluted with HBSS (1:5) was each well. The plate was covered with aluminum foil and incubated it at 37 ºC in a 5% CO_2 atmosphere for 1 hour. Any large bubbles in the wells were popped using a syringe needle, and absorbance was recorded at 492 nm using an Ascent® Multiskan 96-well plate reader. Triton X-100, 0.1%, was used as a positive control. Percentage cell viability was determined from readings in the following fashion: $(A_{Sample} - A_{Background}) / A_{Control}$

3.4 Rh123 Accumulation Study

3.4.1 Materials in Rh123 Accumulation Study

Rhodamine 123 (Rh123) and 2mg/mL BSA protein standard were purchased from Sigma-Aldrich (St. Louis, MO, USA). MK-571 was purchased from Alexis Biochemical® (San Diego, CA, USA). All the other tissue culture materials were listed in section 3.1.1. The BCA™ Protein Assay Kit was obtained from Pierce Biotechnology Inc. (Rockford, IL, USA).

3.4.2 Equipment in Rh123 Accumulation Study

The fluorimeter used in the study was a Perseptive Biosystems CytoFluor 4000 (Framingham, MA, USA). The spectrophotometer used was the Multiskan Ascent from Thermo Scientific, Inc. (Pittsburgh, PA, USA). All the other equipment used in the study were as listed in section 3.1.2.

3.4.3 Seeding 48-well Plates

Pelleted cells were re-suspended and counted in supplemented MEM media (with phenol red) as described in sections 3.1.5 and 3.1.6. The re-suspended Caco-2 cells were diluted to 200,000 cells per mL, and 200 µL of the diluted stock cell solution was added to each well in a 48-well plate. Thus, 40,000 Caco-2 cells were seeded per well in a 48-well plate. The medium was changed every other day. When the cells reached 90% confluency, the lipid-treatments could be added.

3.4.4 Fluorescence Measurement

For Rh123 accumulation study, cells were seeded on 48-well plates as described by in section 3.4.3. The following lipid treatments (Control: supplemented MEM; Peceol®: 0.1%, 0.25%, 1-monostearin: 500 and 1000 µM; 1-monopalmitin: 500 and 1000 µM; 1-monoolein: 500 µM; MK-571: 50 µM) were prepared as described 3.2.2. Ten micromolar Rh123 stock solution (supplemented with 10mM HEPES) was prepared. The Rh123 standards were prepared as shown in Table 5. After the seeded cells reached 90% confluency (~7 days), 200 µL of each lipid treatment was added per well. After 24 hours of treatment time, cells were washed once with PBS. Then, 200 µL of 10 µM Hanks' balanced salt solution (HBSS) diluted Rh123 solution was added to each well. After 2 hours of incubation with Rh123, the uptake was stopped by aspirating the Rh123/HBSS solution and washing the cells 3 times with ice-cold PBS. Cells were lysed in 200µL of 0.1% Triton X-100 for 30 minutes at room

temperature. The cell lysate from each well was transferred into a 1 mL Eppendorf tube and centrifuge at 16xg to remove the cell debris. Then, a 100 µL aliquot from each sample was transferred to a new 96-well plate. In the meantime, Rh123 standard curve was prepared in a 96-well plate as well. The Rh123 standards were prepared by serial dilutions of 10 µM Rh123 with 0.1% Triton X-100 ranging from 0 to 5 µM Rh123 (Table 5). The fluorescence in each sample was measured using a CytoFluor 4000 fluorimeter at excitation and emission wavelengths of 485 nm and 530 nm, respectively (gains=50, 3 scans per sample). The standard curve was plotted as Fluorescence vs. [Rh123] using Excel® and a linear equation was also generated. Lastly, the total Rh123 content was calculated by multiplying $[Rh123]_{sample}$ by the volume of cell lysate ($V_{cell\ lysate}$ = 0.2 mL).

Table 5. Dilution Scheme of Rh123 Stock Solution. $[Rh123]_{stock}$ =10 µM

Sample	$V_{Triton\ X\text{-}100}$ (µL)	V_{Rh123} (µL)	$[Rh123]_{Final}$ (µM)
1	200	100µL of Stock	5
2	100	100µL of Sample 1	2.5
3	100	100µL of Sample 2	1.25
4	100	100µL of Sample 3	0.625
5	100	100µL of Sample 4	0.3125
6	100	100µL of Sample 5	0.15625
7	100	100µL of Sample 6	0.078125
8	100	0	0

3.4.5 Protein Determination

After the fluorescence of each sample was measured, the protein concentration was determined. The BCA™ protein assay was used to normalize the Rh123 fluorescence data. The BCA™ protein assay is a detergent-compatible formulation based on bicinchoninic acid (BCA) for the colorimetric detection and quantitation of total protein. This method combines the well-known reduction of Cu^{2+} to Cu^{1+} by protein in an alkaline medium with the highly sensitive and selective colorimetric detection of Cu^{1+} by BCA (Figure 5). The first step is the chelation of copper with protein in an alkaline environment to form a blue colored complex. In the second step, BCA reacts with the cuprous cation (Cu^{1+}) that was formed in step 1. The purple-colored reaction product is formed by the chelation of two molecules of BCA with one cuprous ion. The water soluble BCA/copper complex is measured at 540nm (Figure 5).

$$\text{Protein} + Cu^{2+} \xrightarrow{OH^-} Cu^{1+}$$

$$Cu^{1+} + 2\ \text{BCA} \rightarrow 2\ \text{BCA-Cu Complex}$$

Figure 5. Schematic Reaction Mechanism of BCA Protein Assay

The BCA™ is not a true end-point method; that is, the final color continues to develop. However, following incubation, the rate of continued color development is sufficiently slow to allow large numbers of samples to be assayed

together. The macromolecular structure of protein, the number of peptide bonds and the presence of four particular amino acids (cysteine, cystine, tryptophan and tyrosine) are reported to be responsible for color formation with BCA.

For the BCA™ assay, 25µL cell lysate from each sample was added to a new 96-well plate. The protein concentrations for all samples were determined with reference to a protein standard curve, which was prepared by a commercially available 2.0 mg/mL bovine serum albumin (BSA) protein standard. The standards were prepared by serial dilution with 0.1% Triton X-100 solution (Table 6). For each standard, 25 µL was added per well. Three replicates were used at each concentration. The standard curve was prepared by plotting A_{540} vs. [BSA]. The best-fit line was drawn using Excel® program.

Table 6. Dilution Scheme of BSA Standards. BSA stock = 2 mg/mL

Sample	Volume of Triton X-100 (µL)	Volume of BSA (µL)	Final [BSA] (µg/µL)
1	0	50µL of BSA Stock	2000
2	25	25µL of Sample 1	1000
3	25	25µL of Sample 2	500
4	25	25µL of Sample 3	250
5	25	25µL of Sample 4	125
6	25	0	0

The total volume per well for standards and samples was 25 µL. The BCA™ working reagent was prepared by mixing the BCA™ Reagent A and Reagent B in a 50:1 ratio. Freshly prepared BCA™ working reagent (200 µL) was added to each well and mixed thoroughly on a plate shaker (Multiskan Ascent® spectrophotometer) for 30 seconds. Then the samples in the 96-well plate were incubated at room temperature for 30 minutes. The absorbance of these samples was read at 540 nm using a Multiskan Ascent® spectrophotometer. The protein concentration for each sample was extrapolated from absorbance reading using a linear equation generated by Excel®. Later, the total concentration was calculated by multiplying the protein concentration with the total volume of the cell lysate (0.2 mL).

3.4.6 Relative Rh123 Accumulation

The cellular accumulation of Rh123 was calculated in pmole and the total accumulation of Rh123 was obtained by doubling the Rh123 amount within the aliquot to adjust to the total cell lysate in each sample. The total Rh123 accumulated for each treatment group was normalized with respect to the total protein content (pmole/µg) as determined by the BCA™ assay. Subsequently, the normalized Rh123 content for each treatment was converted to percentage compared to the control group.

3.5 Rh123 Accumulation Dose-Response Study

The Rh123 accumulation dose-response studies were conducted for cells treated with monopalmitin, monostearin and monoolein for 24 hours. For these studies, all four lipids were measured within their non-cytotoxic ranges as determined in sections 3.2 and 3.3. The detailed procedure for Rh123 accumulation study was described in section 3.4.

3.6 $E_2$17βG Bidirectional Flux Study

3.6.1 Materials for the Transport Study

Tritium labeled $E_2$17βG was purchased from PerkinElmer, Inc. (Boston, MA, USA). The $E_2$17βG was labeled at the C6 and C7 positions of the estradiol. The specific activity of [^{3}H] $E_2$17βG was 47.1 Ci/mmol packed in 1.0mCi/mL ethanol:water (9:1) solution. CytoScint® scintillation cocktail was purchased from Fisher Scientific, Inc. (Ottawa, ON, CA). All the other materials were listed in section 3.1.1. The HBSS solution was buffered with HEPES to pH 7.4.

3.6.2 Equipment for the Transport Study

Costar® 12-well Transwell™ plates with collagen-coated PTFE membrane inserts (pore size of 0.4 μm, diameter of 1.2 cm) were purchased from Corning (NY, USA). A transepithelial electrical resistance (TEER) measurement device,

Millicell-ERS, was purchased from Millipore (Bedford, MA, USA). A liquid scintillation counter was purchased from Beckman Coulter, Inc. (Mississauga, ON, CA). All the other equipment for tissue culture were as listed in section 3.1.2.

3.6.3 Seeding and Maintaining Cells on 12-well Transwell® Plates

Caco-2 cells were trypsinized and counted as described in section 3.1.5. The cells were resuspended with completed MEM medium at a concentration of $0.6x10^6$ cells per mL. The first step was to 1.5mL of completed MEM medium with phenol red was transferred to a new 12-well plate. Next, a number of inserts (pore size of 0.4 μm, diameter of 1.2 cm) were placed in the 12-well cell culture plate to pre-wet the inserts for 5 minutes before seeding cells. Subsequently, 0.5mL (~300,000 Caco-2 cells) of the resuspended cell solution was dispensed on each insert. Thereafter, the plate was incubated in a humidified environment at 37 °C and 5% CO_2 overnight. On the next day, the apical medium in the insert was removed and replaced with 0.5 mL of supplemented MEM medium to remove non-adherent cells and reduce the risk of multilayer formation. The medium in each well was changed every other day. The medium was first aspirated from the basolateral side of all wells, and then the medium in the apical side was carefully and slowly decanted. The aspirated medium was replaced with fresh complete MEM medium. The cells were maintained for approximately 21 days before use.

3.6.4 Assessing Caco-2 Monolayer Integrity

TEER values were routinely measured with a Millicell-ERS after replacing the cell culture medium as well as before and after conducting the transport experiments. TEER can be used as a way to monitor monolayer development and evaluate tight junction formation of the cell monolayer. Once the TEER value exceeded 350 $\Omega \cdot cm^2$ (around 21 days post-seeding), the cell monolayer would be well-differentiated with the formation of tight junction. Only then, the cells were ready to be used for bidirectional flux experiments.

3.6.5 Experimental Protocol for Bidirectional Transport Study

The culture medium in the 12-well Transwell™ plate needed to be changed one day before the bidirectional transport study. The following treatments (Control completed MEM; Peceol®: 0.25% v/v, 1-monostearin: 1000 µM; 1-monopalmitin: 1000 µM; 1-monoolein: 500 µM; MK-571: 50 µM) were prepared with complete MEM as described in section 3.1.1. On the day of the experiment, all treatment solutions and media were pre-warmed to 37 °C. Cells were washed once with warmed PBS before adding the various treatments in duplicate. There were 0.5 mL and 1.5 mL of each lipid treatment loaded onto the apical and basolateral side, respectively. The Transwell™ plate was then stored in an incubator, providing a humidified, 37 °C and 5% CO_2 environment, for 24 hours. In the meantime, 10nM radioactive $E_2$17βG was prepared with 10mM HEPES buffered HBSS solution (pH 7.4). After a 24-hour incubation, the TEER

value in each well was measured. Then cells were washed twice with HBSS-HEPES solution before loading the radioactive 10 nM $E_2$17βG on the appropriate sides. For the apical-to-basolateral (ab) experiments, the washing solution was decanted by placing the insert to the edge of the filter support against the edge of the 12-well plate. Then the insert was moved to a new 12-well plate containing 1.5mL basolateral HBSS-HEPES solution in each well. After all the inserts for the apical to basolateral experiment were transferred to the new 12-well plate, a sample (C_0) was taken from the donor solution containing 10 nM $E_2$17βG. Immediately, 0.5mL of the donor solution containing 10 nM $E_2$17βG was added to the apical side of each well (t=0). For the basolateral-to-apical (ba) transport experiments, the washing solution was decanted as described for ab transport experiments. Then the inserts were transferred to a new 12-well plate containing 1.5 mL basolateral 10 nM $E_2$17βG donor solution. A sample from donor solution in the basolateral compartment was taken as the initial donor chamber concentration (C_0) immediately followed by the addition of 0.5mL HBSS-HEPES solution to the apical side of the inserts (t=0). The lid-covered plate with filter supports was then incubated at 37°C with a humidified 5% CO_2 environment for 30 minutes. Meanwhile, an $E_2$17βG standard curve was prepared by serial dilution of the 10 nM $E_2$17βG stock solution with HBSS-HEPES (0.3125, 0.625, 1.25, 2.5, 5, 10 nM). For the absorptive flux (A->B), 750 µL of $E_2$17βG was sampled on the basolateral compartment and replaced with buffered HBSS at 0, 30, 60 and 120 min; for secretory flux (B->A), 250 µL of $E_2$17βG was sampled on the apical compartment and replaced with buffered HBSS at 0, 30, 60 and 120

min. At the end of the experiment, the TEER value in each well was measured again to ensure the integrity of the monolayer had been maintained throughout the experiment. For each treatment, duplicate was used.

3.6.6 Scintillation Counting

Liquid scintillation counting is used for the measurement of beta emitting nuclides, such as, tritium and carbon-14. This technique involves dissolving the sample containing a radionuclide in a suitable scintillation solution and the use of a liquid scintillation counter. The solution normally consists of an aromatic organic solvent containing a fluor and a detergent to make the whole solution miscible when counting aqueous samples. The energy of the emitted beta particles is transferred via the solvent to the primary fluor and sometimes to a secondary fluor, which then emits energy as light photons. These photons are detected using a photomultiplier. Only a small proportion of the available energy is liberated as light. The residue is dissipated as vibrational and rotational energy in the solvent. In this case, liquid scintillation counting was used to measure the amount of [^{3}H] $E_2$17βG transported either in the direction from apical to basolateral or from basolateral to apical directions. Samples and standards were placed in 7mL scintillation vials. An aliquot of 5.4 mL CytoScint scintillation cocktail fluid was added to each vial and then the vial was vigorously mixed on a desk-top shaker. The samples were placed in a Beckman liquid scintillation counter. The signal was detected by the counter in disintegrations per minute (dpm) over three minutes.

3.6.7 Transport Study Data Analysis

To analyze the data obtained from the study, the standard curve of $E_2$17βG at different concentrations was plotted. From the equation generated from the best-fit line of the standard curve, the concentrations of $E_2$17βG from all samples were calculated. Then for each treatment group, a kinetic graph of [$E_2$17βG] (nM) vs. time (second) was plotted. The linear region in the graph was used to calculate the apparent permeability coefficient (P_{app}).

$$P_{app} = dQ/dt \cdot [1/(A \cdot C_0)]$$

Where dQ/dt is the steady-state flux (in μM /s), A is the surface area of the filter (in cm^2), and C_0 is the initial concentration in the donor chamber at each time interval (in μM). The net efflux ratio was calculated as the quotient of $P_{app, ba}$ to $P_{app, ab}$.

3.7 MRP2 Protein Expression Study

3.7.1 Materials for Western Blotting

Tween-20, protease inhibitor cocktail, Phenylmethylsulphonylfluoride (PMSF), Na-deoxycholate, isopropanol, ethylenediaminetetraacetic acid (EDTA) and NaCl were obtained from Sigma-Aldrich (St. Louis, MO, USA). MK-571 was purchased from Alexis Biochemical® (San Diego, CA, USA). The BCA™ Protein Assay Kit was obtained from Pierce Biotechnology Inc. (Rockford, IL, USA). NP-40 was purchased from Roche Applied Science (Laval, QC, CA). 30%

acrylamide, Laemmli sample buffer (1x), Tris buffered saline (TBS), 2% Bis solution N, N, N', N'-Tetra-methyl-ethelenediamine (TEMED), nitrocellulose membranes were purchased from Bio-Rad (Hercules, CA, USA). High range molecular weight markers, anti-MRP2 (M_2III-6), anti-Actin (I-19) primary antibodies and peroxidase-conjugated bovine anti-goat IgG for Western blotting were purchased from Santa Cruz Biotechnology, Inc. (Santa Cruz, CA, USA). Peroxidase-conjugated AffiniPure goat anti-mouse IgG (H+L) was purchased from Jackson ImmunoResearch Laboratory, Inc. (West Grove, PA, USA). Beta actin (human) recombinant protein was purchased from ProSci Incorporated (Poway, CA, USA).

3.7.2 Equipment for Western Blotting

The equipment for electrophoresis, such as the mini analytical protein electrophoresis cells, electrode apparatus, 1.5mm glass plates, 10-well comb, and plastic gel cassette were bought from BIO-RAD (San Francisco, CA, USA).

3.7.3 Seeding 6-well Plate for Protein Expression Study

Pelleted cells were re-suspended and counted in complete MEM media (with phenol red) as described in sections 3.1.5 and 3.1.6. The re-suspended Caco-2 cells were diluted to 200,000 cells per mL, and 2mL of the diluted stock cell solution was added to each well in a 6-well plate. Thus, 400,000 Caco-2 cells were seeded per well in a 6-well plate. On the next day, the medium in all wells was changed. Afterwards, the medium was changed every other day until the cells reached 90% confluency (~7 days).

3.7.4 Sample Preparation

3.7.4.1 Treatment of 6-well Plate

The cells in the 6-well plates were treated with 0.1% and 0.25% Peceol, 500μM monoolein, 500μM and 1000μM monopalmitin, 500μM and 1000μM monopalmitin. Then the 6-well plates were incubated in an incubator with a humidified, 37°C and 5% CO_2 environment for 24 hours. After the incubation period, the medium in each well was aspirated and the whole plate was washed twice with cold PSB. Then the plates were stored in -80°C freezer untill protein extraction.

3.7.4.2 Membrane Protein Extraction

During the protein extraction process, the plates were temporarily stored in an ice-containing bucket to minimize protein degradation. The cell lysing solution consisted of a mixture of protease inhibitor cocktail and phenylmethanesulphonylfluoride (PMSF) in radioimmunoprecipitation assay (RIPA) buffer (20mM HEPES [pH 7.0], 150mM NaCl, 1mM ethylenediaminetetraacetic acid, 1% NP-40, 1% deoxycholate, 0.1% sodium dodecyl sulfate) in 1:100 ratios. The cell lysing solution was added into each well of a 6-well plate. Cell scrapper was used to dislodge cells attached to the plate. Subsequently, cell lysates were pipetted into 1.5mL Eppendorfs and incubated on ice for 20 minutes. Then they were centrifuged at 12,850xg for 30 minutes at 4°C. After the centrifugation, the supernatant was carefully extracted and the pellet was discarded.

3.7.4.3 Protein Concentration Determination

The protein content in each sample was quantified by BCA™ assay as described in section 3.4.3.4. A BSA standard curve was also prepared at the same time. The protein assay was used to ensure equal amount of protein contents will be loaded to a sodium dodecyl sulfate-polyacrylamide electrophoresis (SDS-PAGE) gel. The protein extracts were stored at -80 °C before running SDS-PAGE.

3.7.5 Electrophoresis

The glass plates were first cleaned with methanol and distilled water before placing them in the casting apparatus. The SDS-PAGE gel had two components to it, resolving and stacking gels. The 7% resolving gel (pH 8.8) was prepared as follows:

Distilled H2O.....15.3 mL

1.5M Tris-HCl pH 8.8 .....7.5 mL

10% (w/v) SDS.....300 µL

Acrylamide/Bis-acrylamide (30%/0.8% w/v).....6.9 mL

10% (w/v) ammonium persulfate .....150 µL

TEMED.....15 µL

Total Volume.....30.165 mL

Once the resolving gel solution was poured between the glass plates, 300µL of isopropanol was added to immediately afterward. After leave the gel to

solidify for 1 hour, the residual isopropanol was decanted and rinsed away with distilled water. Then, the residual distilled water was removed using Kimwipes®. The stacking gel was poured and a 10-well comb inserted. The 4% resolving gel (pH 6.8) could be prepared as follows:

Distilled H2O	9.225 mL
1.5M Tris-HCl pH 6.8	3.75 mL
10% (w/v) SDS	150 μL
Acrylamide/Bis-acrylamide (30%/0.8% w/v)	2.01 mL
10% (w/v) ammonium persulfate	75 μL
TEMED	15 μL
Total Volume	15 mL

To prepare the loading sample, 60 μg protein lysate from each sample was first added to a 1 mL Eppendorf tube. Then, RIPA buffer was added to each sample so that all samples had a same final volume in the Eppendorf tubes. Subsequently, an equal volume of Laemmli buffer (with β-mercaptoethanol) was added to each adjusted protein lysate in a 1:1 ratio. Twelve micro litres of molecular marker was added. The gel was separated by electrophoresis with a 7% SDS-PAGE gel at 100 V for 120 minutes. The gel was then transferred to a nitrocellulose membrane at 0.07 A constant current for 90 minutes. A pre-stained high range molecular marker was used to identify the MRP2 at 200 kD and β-actin at 42 kD.

3.7.6 Western Blotting

After the proteins were transferred to the nitrocellulose membrane, the membrane was blocked with 5% non-fat milk (in 1x TBS-T) for 2 hours. Mouse anti-human MRP2 (M_2III-6) primary antibody was added in 1:200 dilution with 5% non-fat milk to detect MRP2; goat anti-human actin (I-19) was added in 1:500 dilution with 5% non-fat milk to detect β-actin as an internal control. The membranes were washed 4 times with TBS-Tween (1% Tween-20). The membrane was incubated for 90 minutes in a 1:3000 dilution of goat anti-mouse IgG-HRP and bovine anti-goat IgG-HRP secondary antibodies for MRP2 and β-actin, respectively, followed by four washes with TBS-T. Bands were visualized using ECL Western blotting detection reagent from Amersham Biosciences (Piscataway, NJ, USA), exposed to an X-Omat film from Kodak™ and quantified with UVP-Labworks software. The optimal range of the densitometer was determined by using a commercially available beta actin standard.

3.8 Statistical Analysis

One Way Analysis of Variance (ANOVA) was used to analyze the data sets from cell viability, toxicity, and accumulation and bidirectional transport studies. The Student's t-test was used to analyze MRP2 protein expression data. Statistically significant differences between multiple treatment groups versus control group were assessed using Tukey post test method with a predetermined alpha value of 0.05. A difference was considered significant if P value was less

than 0.05. All statistical analysis was performed using SigmaStat version 3.5 from Systat Inc. Data were expressed as mean ± standard deviation (SD).

CHAPTER 4

RESULTS

4.1 Toxicity and Viability Studies in Caco-2 Cells

4.1.1 Effects of Peceol® on Toxicity and Viability

To assess the non-cytotoxic range of Peceol® in Caco-2 cells accurately, two different enzymatic assays were performed to ascertain the data obtained. LDH is used as an indirect measure of cell membrane integrity, and it is used to measure the cytotoxicity range when cells were treated with different concentrations of Peceol®. As shown in Figure 6 A), there was no significant toxicity associated with Peceol® treatment when its concentration was equal or less than 1% v/v compared to the control group. The approximately 15% toxicity associated with treatments within the non-cytotoxic range (ie. ≦ 1% Peceol®) was the result of the basal cell turnover. To ensure the accuracy of the data obtained from the LDH cytotoxicity assay, a MTS assay was used to determine the cell viability in response to Peceol® treatments. The MTS assay is an indirect measure of cells' metabolic activities. As shown in Figure 6 B), the data were in agreement with what had been observed for toxicity associated with Peceol® treatment. Cells treated with equal or less than 1% v/v Peceol® showed no observable reduction in their viability compared to the control group. However, there was a drastic decrease in cell viability and a drastic increase in cell toxicity when the Peceol® concentration was greater than 1%. Therefore, taking toxicity and viability data together, a conservative estimation of the non-cytotoxic range would fall within 1% v/v Peceol®.

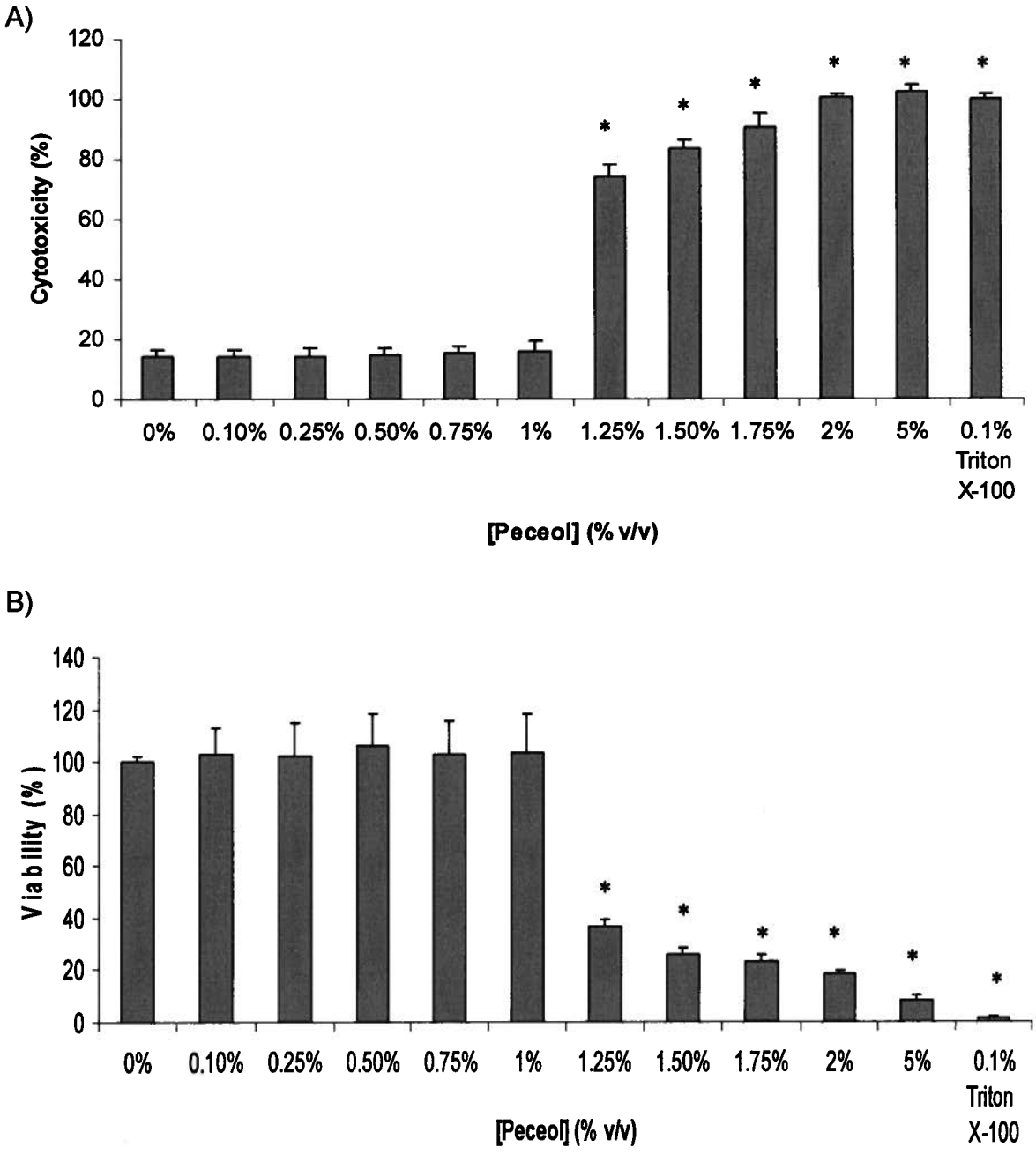

Figure 6. Effects of Peceol® on Cell Viability and Cytotoxicity in Caco-2 cells. A) The 24-hour toxicity profile of Caco-2 cells treated with Peceol® measured by LDH assay. The positive control group was the one treated with 0.1% Triton X-100. (n=6; *p<0.05, Peceol® treated groups vs. Triton X-100 treated group). B) The 24-hour viability profile of Caco-2 cells treated with Peceol® measured by MTS assay. The control group was the one treated with medium alone. Six replicates were used per treatment group in one experiment (n=6; *p<0.05, Peceol® treatment group vs. the negative control group without treatment). The values were expressed as mean ± SD.

4.1.2 Effects of Monoglycerides on Toxicity and Viability

Both LDH and MTS assays were also used to assess the non-cytotoxic ranges of mono-palmitin, -stearin, -olein in Caco-2 cells. Figure7 shows that there was neither increased toxicity nor decreased viability associated with 24-hour monoolein incubation compared to the control when the concentration was equal or less than 500 μM. The non-cytotoxic concentration range of cells treated with monostearin and monopalmitin was within 1000 μM (Figure 8 and 9). In summary, the cytotoxic profiles generated by LDH and MTS assays for each monoglyceride were in agreement with each other.

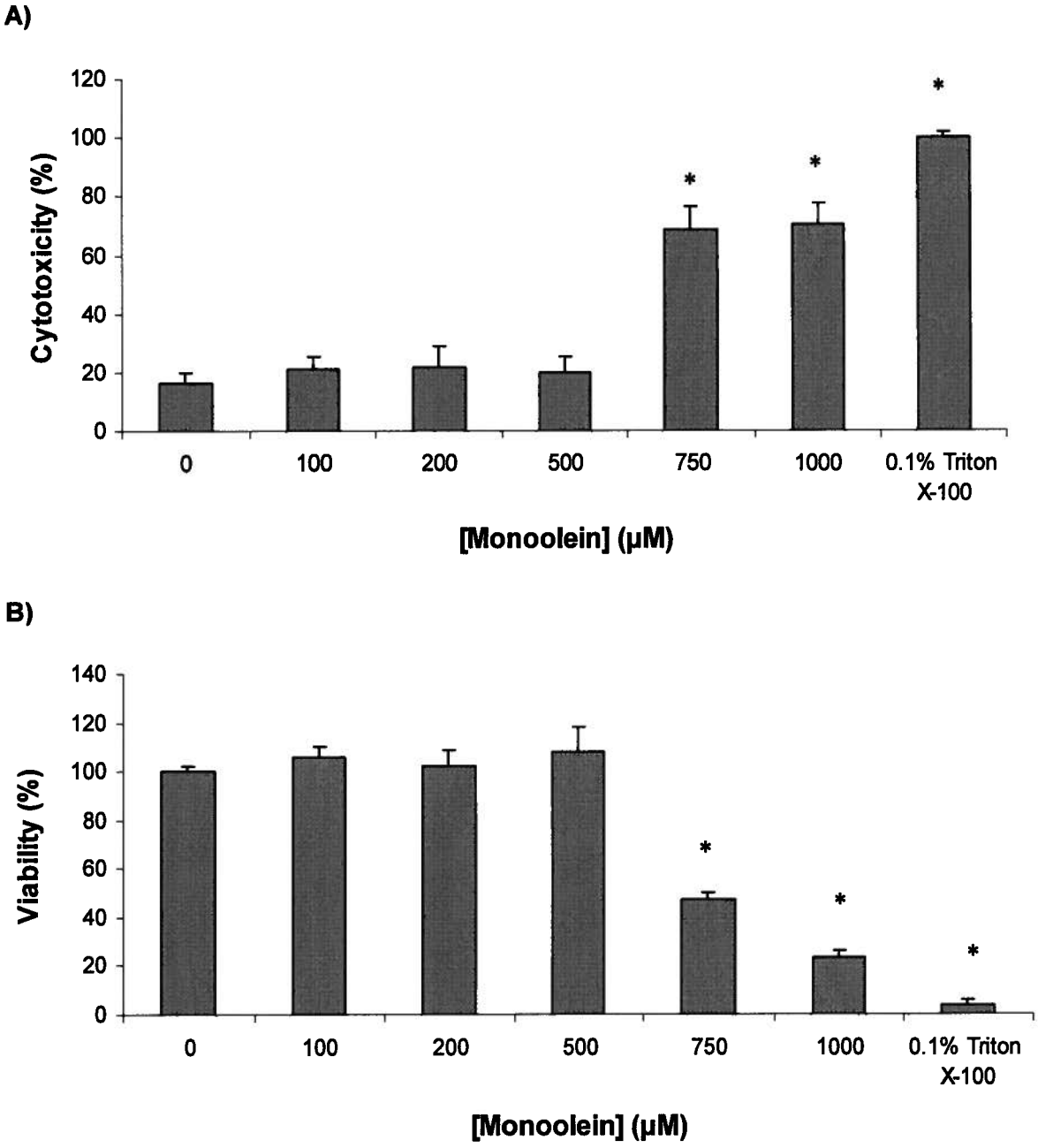

Figure 7. Effects of Monoolein on Cell Viability and Cytotoxicity in Caco-2 Cells. A) The 24-hour toxicity profile of Caco-2 cells treated with 1-monoolein measured by LDH assay. The positive control group was the one treated with 0.1% Triton X-100. (n=6; *p<0.05, 1-monoolein treated groups vs. Triton X-100 treated group). B) The 24-hour viability profile of Caco-2 cells treated with 1-monoolein measured by MTS assay. The control group was the one treated with media alone. Six replicates were used per treatment group in each experiment. (n=6; *p<0.05, treatment group vs. the negative control group without treatment). Values were expressed as mean ± SD.

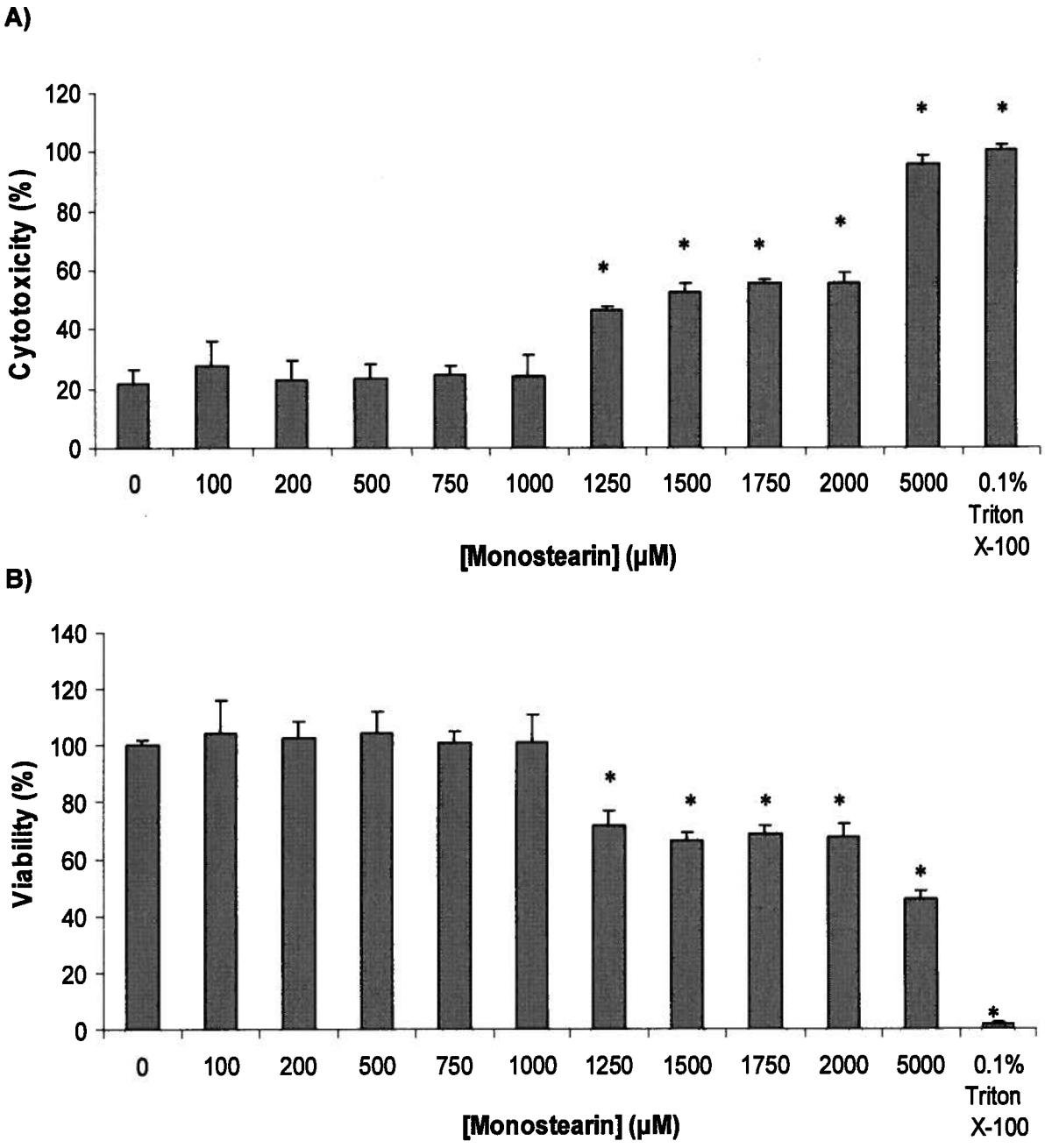

Figure 8. Effects of Monostearin on Cell Viability and Cytotoxicity in Caco-2 Cells. A) The 24-hour toxicity profile of Caco-2 cells treated with 1-monostearin measured by LDH assay. The positive control group was the one treated with 0.1% Triton X-100. (n=6; *p<0.05, 1-monostearin treated groups vs. Triton X-100 treated group). B) The 24-hour viability profile of Caco-2 cells treated with 1-monostearin measured by MTS assay. The control group was the one treated with media alone. Six replicates were used per treatment group in each experiment. (n=6; *p<0.05, treatment group vs. the negative control group without treatment). Values were expressed as mean ± SD.

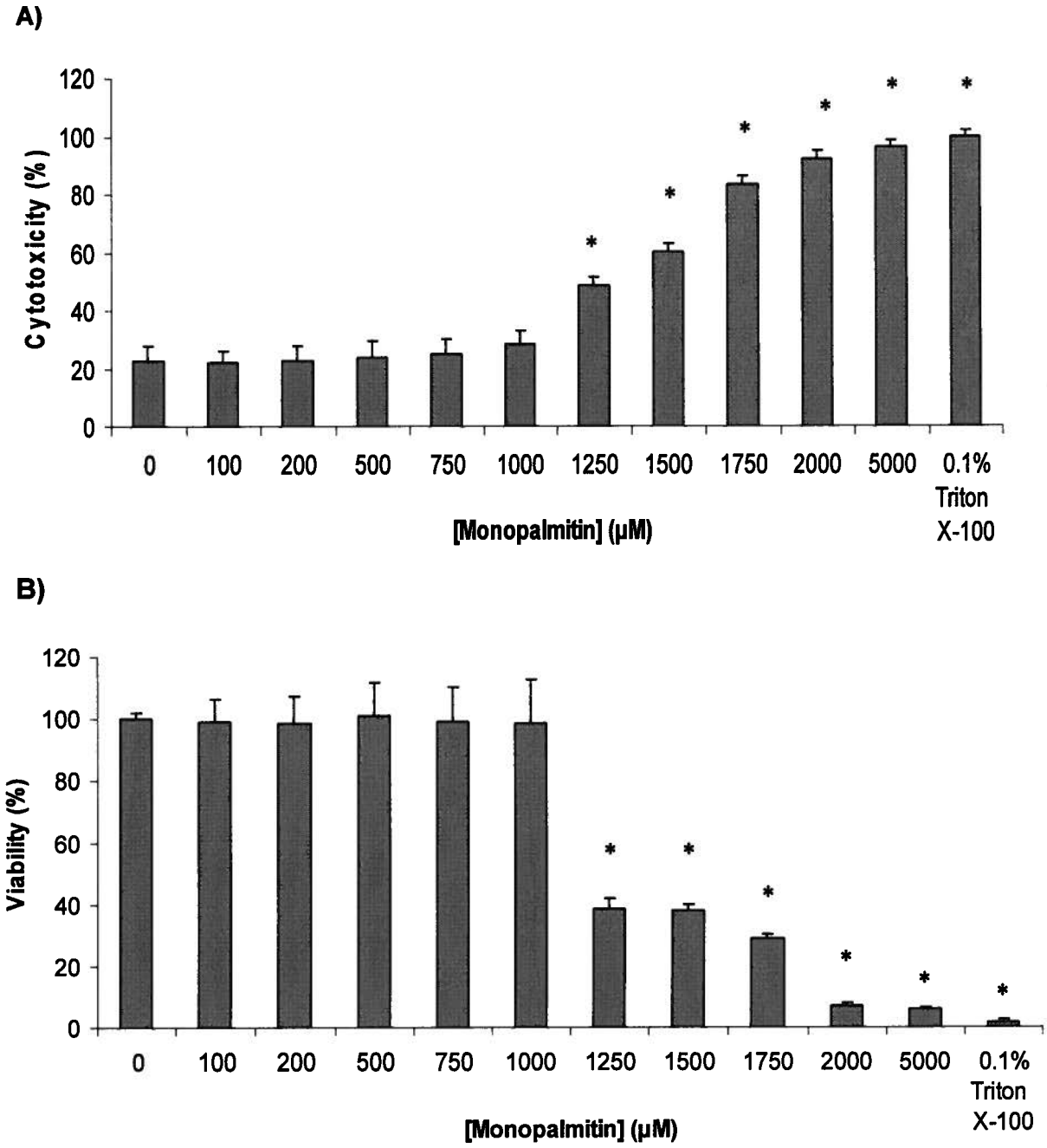

Figure 9. Effects of Monopalmitin on Cell Viability and Cytotoxicity in Caco-2 cells. A) The 24-hour toxicity profile of Caco-2 cells treated with 1-monopalmitin measured by LDH assay. The positive control group was the one treated with 0.1% Triton X-100. (n=6; *p<0.05, 1-monopalmitin treated groups vs. Triton X-100 treated group). B) The 24-hour viability profile of Caco-2 cells treated with 1-monopalmitin measured by MTS assay. The control group was the one treated with media alone. Six replicates were used per treatment group in each experiment, (n=6; *p<0.05, treatment group vs. the negative control group without treatment). Values were expressed as mean ± SD.

4.2 Effects of Peceol® on MRP2 Activity

4.2.1 Effects of Peceol® on Rh123 Accumulation

To determine the relative Rh123 accumulation in Peceol® treated Caco-2 cells, the Rh123 standard curve needs to be plotted as shown in Figure 10. The equation derived from the best fit line in the standard curve was used to quantify the amount of Rh123 accumulated in Caco-2 cells after treatment with 0.25% v/v Peceol®.

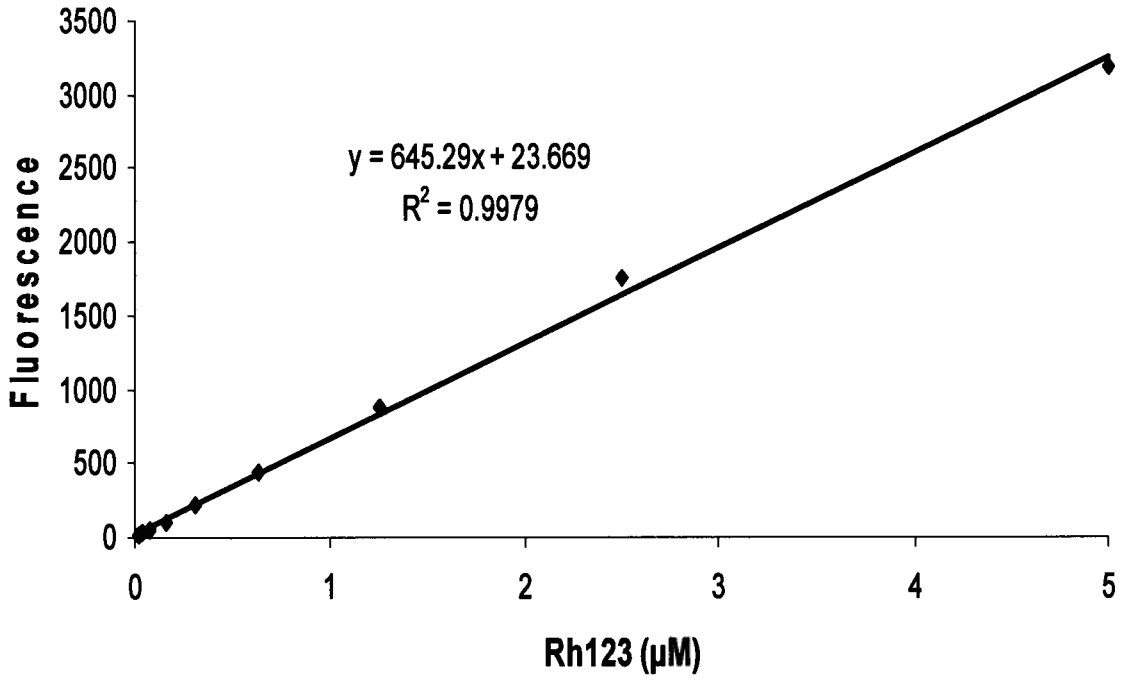

Figure 10. The Rh123 Standard Curve of Fluorescence versus Rh123 Concentration. This is a representative graph from one independent experiment (n=5). The excitation and emission wavelengths used were 485nm and 530nm, respectively. [y=645.29x+23.669, R^2=0.9979]

After the amount of Rh123 in each sample was determined, the amount of protein in each sample was measured to normalize the Rh123 accumulation data. This step was necessary to minimize possible variations derived from the different number of cells in each well. The BSA standard curve was plotted as shown in Figure 11. The equation derived from the best fit line in the standard curve was used to quantify the amount of protein in each well after treatment with 0.25% v/v Peceol®.

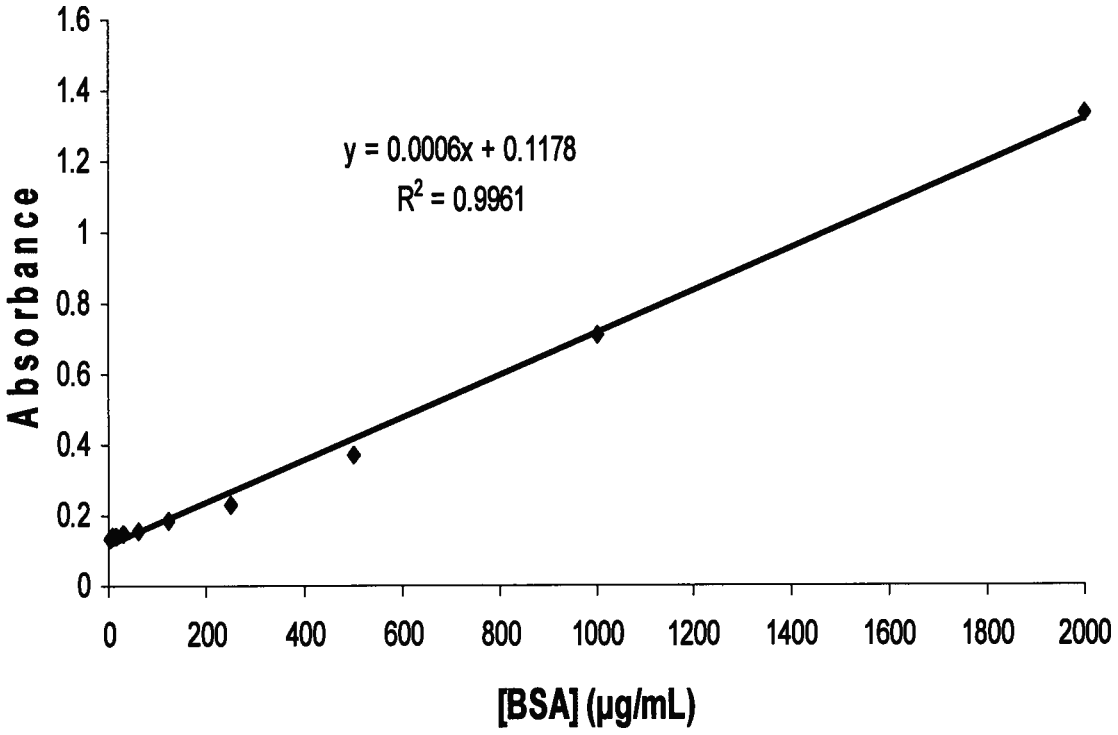

Figure 11. BSA Standard Curve for Protein Determination. The absorbance was measured at 540nm. This was a representative graph from an independent experiment. (n=5). [y=0.0006x+0.1178, R^2=0.9961]

After both protein content and Rh123 were determined, the relative Rh123 accumulation was calculated. In Table 7, 0.25% v/v Peceol® treated cells had an 84% increase in the accumulation of Rh123, a non-specific MRP2 substrate, compared to the negative control. The positive control used in the accumulation study was 50μM MK571 which is a specific MRP inhibitor. Following this treatment, cells had a 112% increase in Rh123 accumulation.

Table 7. 2-hour Accumulation of Rh123 in 24-hour Peceol® and MK-571 treated Caco-2 Cells. The absolute accumulation of Rh123 in each well was first normalized with protein content by dividing the amount of Rh123 by protein content in pmole/μg. The relative Rh123 accumulation with each treatment was then compared in % with the control group. The negative control group was treated with medium alone. MK-571, a specific inhibitor of MRP, was used as a positive control. Data expressed as mean ± SD (n=5, *P<0.05, each monoglyceride group vs. the control; n=3, *P<0.05, Peceol® and MK-571 vs. the control). There were three replicates per treatment in one experiment.

Treatment Group	Relative Rh123 Accumulation (%)
Control	100 ± 9
0.25% v/v Peceol®	184 ± 30 *
50 μM MK-571	212 ± 50 *

4.2.2 Effects of Peceol® on Bi-directional Transport of $E_2$17βG

To monitor the transport of $E_2$17βG across Caco-2 cell monolayer, it was crucial to ensure the tight junction of the monolayer maintaining intact throughout the experiment. One way to estimate the formation of tight junction was using the TEER value. As shown in Table 8, all TEER values were higher than 350 $\Omega*cm^2$, and there was no change in TEER values before and after the experiment for all

treatment groups in either apical to basolateral or basolateral to apical directions. These data suggested that the Caco-2 cell monolayer had maintained its integrity during the experiment. In other words, the transport of $E_2$17βG across Caco-2 cell monolayer was restricted to the transcellular route.

Table 8. Effects of Peceol® and MK571 on Transepithelial Electrical Resistance (TEER) Values in Caco-2 Cells. TEER values of Caco-2 cells monolayer were measured before and after the bi-directional transport of $E_2$17βG in the A→B (apical-to-basolateral) and B→A (basolateral-to-apical) directions in the presence of 0.25% v/v Peceol®.

	TEER ($\Omega \cdot cm^2$)			
Treatment Group	**A→B Before**	**A→B After**	**B→A Before**	**B→A After**
Control	386 ± 12	384 ± 10	390 ± 10	382 ± 14
0.25% v/v Peceol®	379 ± 12	376 ± 11	381 ± 14	379 ± 11

To calculate the efflux ratio or evaluate the rate of transport of $E_2$17βG in either direction, the apparent permeability coefficient (P_{app}) needs to be determined as described in 3.6.7. The linear region in the graph was used to calculate the apparent permeability coefficient (P_{app}). P_{app} was calculated using the equation:

$$P_{app} = dQ/dt \cdot [1/ (A \cdot C_0)]$$

One important component in determining P_{app} is finding the steady-state flux which could be obtained by plotting [$E_2$17βG] versus time as shown in Figures 12 and 13. In both figures, best fit linear lines could be drawn. The steady state flux is the slope of the best fit line.

A)

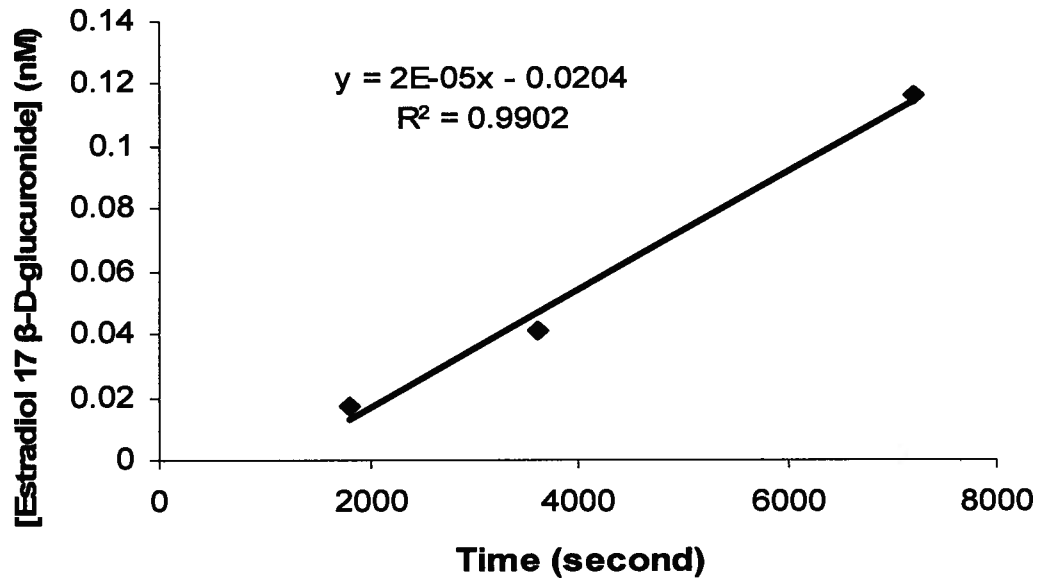

B)

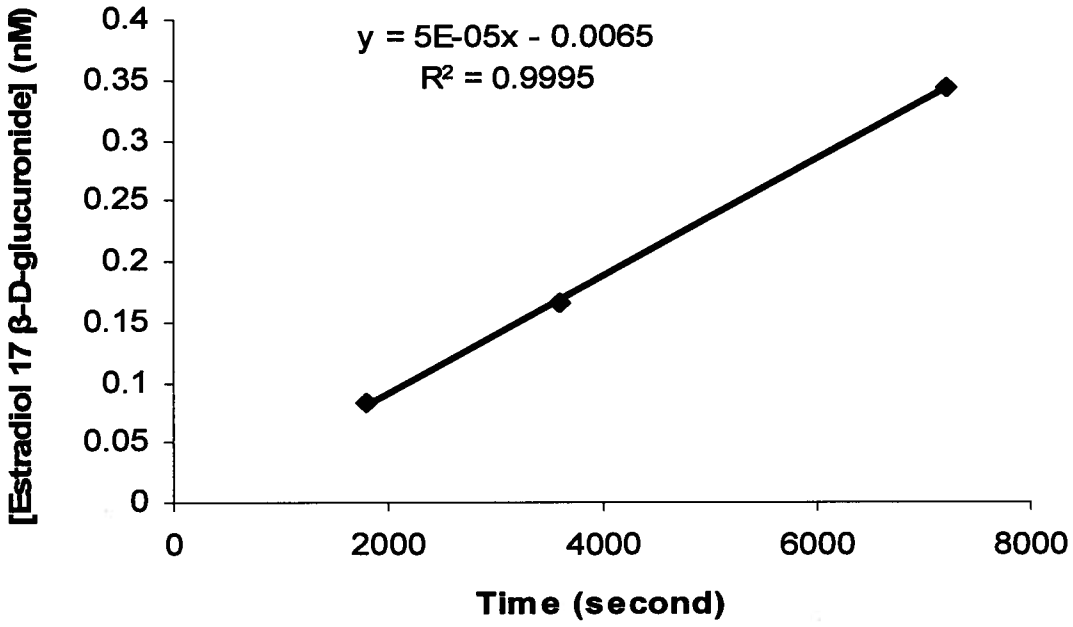

Figure 12. The 2-hour $E_2$17βG Bi-directional Transport Profiles of Medium Treated Caco-2 Cell Monolayers. A) Apical to basolateral; B) Basolateral to apical. The plots shown above were representative ones from one independent experiment (n=6).

A

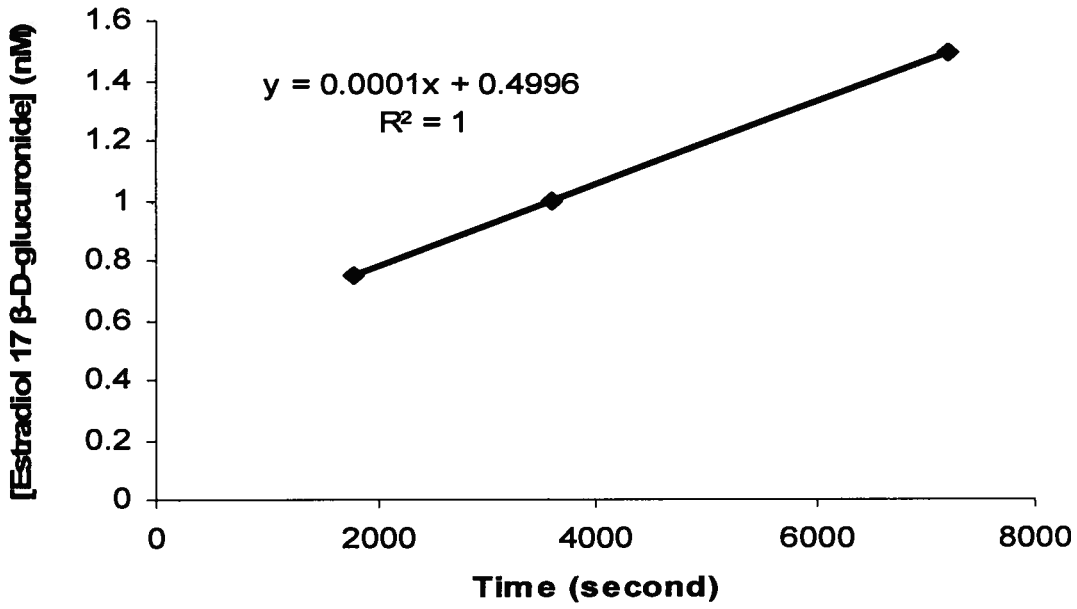

B

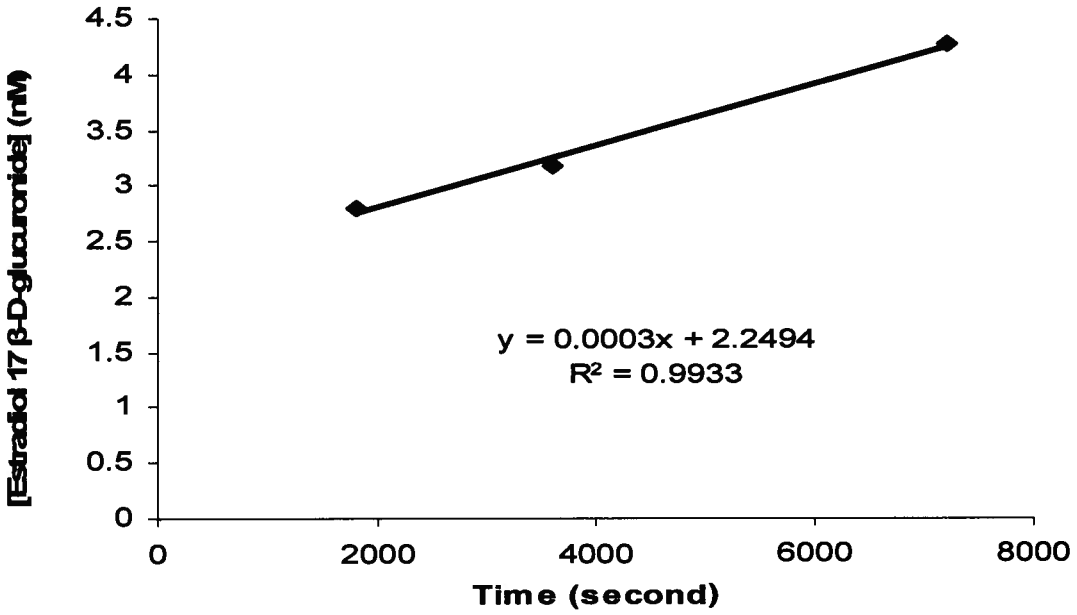

Figure 13. The 2-hour $E_2$17βG Bi-directional Transport Profiles of Peceol® Treated Caco-2 Cell Monolayers. A) Apical to basolateral; B) Basolateral to apical. The plots shown above were representative ones from one independent experiment (n=6).

In Figure 14, the $P_{app,ab}$ for the $E_2$17βG transport of 0.25% v/v Peceol® treated group was (10.6 ± 5.9) $x10^{-6}$ cm/s, while the $P_{app,ab}$ for the control group was (3.2 ± 1.7) $x10^{-6}$ cm/s. There was a statistically significant difference in apparent permeability in the absorptive direction. Yet, there was no significant difference in $P_{app,ba}$ between the control and 0.25% v/v Peceol® treated groups [Control: (31.1 ± 13.9) $x10^{-6}$ cm/s; Peceol®: (26.5 ± 18.4) $x10^{-6}$ cm/s] (Figure 14).

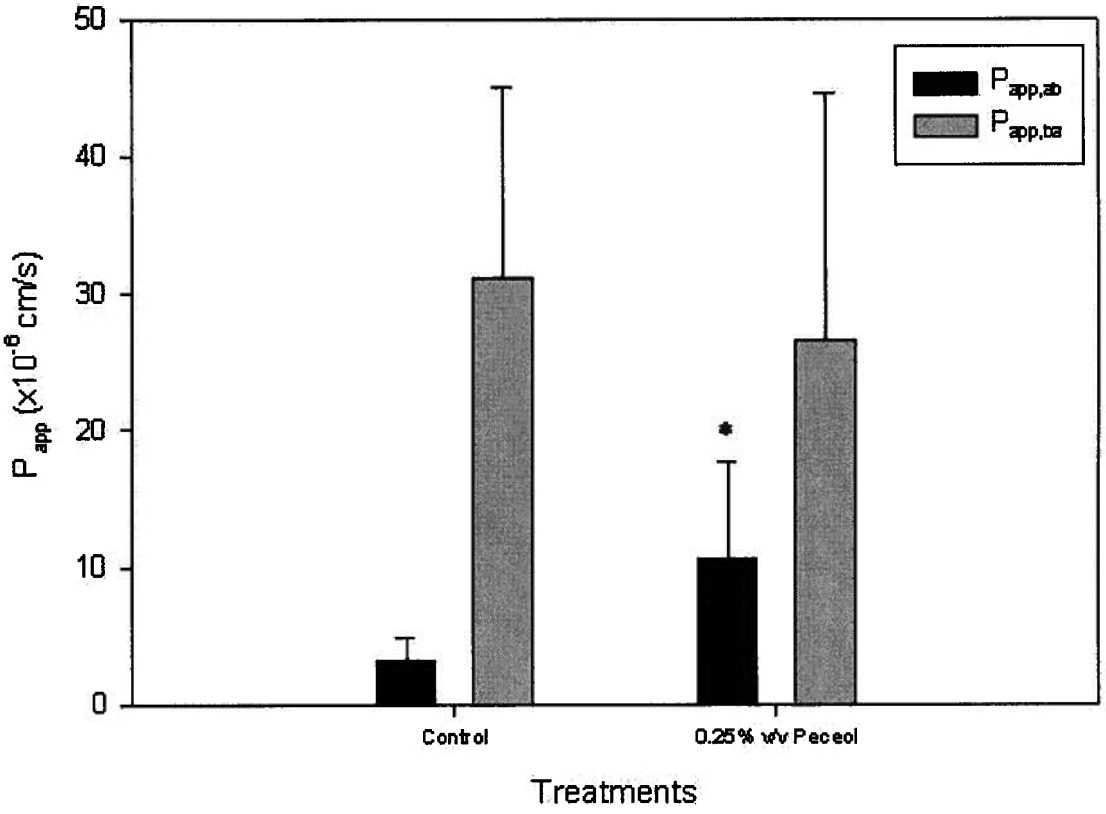

Figure 14. Apparent Permeability Coefficients (P_{app}) for Bi-directional Transfer of $E_2$17βG across Peceol® Treated Caco-2 Cell Monolayers. The control group was treated with medium alone which used as the negative control. Data were expressed as mean ± SD (n=6, *P<0.05, $P_{app,\ ab}$ for each lipid treatment vs. $P_{app,\ ab}$ for the control; $P_{app,\ ba}$ for each lipid treatment vs. $P_{app,ba}$ for the control).

In Table 9, the efflux ratio was calculated for the control and 0.25% v/v Peceol® treated groups. There was a 4-fold reduction in efflux ratio for Peceol® treated cells compared to the control.

Table 9. Apparent Permeability Coefficients (P_{app}) for Bi-directional Transfer of $E_2$17βG across Caco-2 Cell Monolayer in Peceol® Treated Caco-2 Cells. The apparent permeability coefficient (P_{app}) was calculated with the following equation: $P_{app} = dQ/dt \cdot [1/(A \cdot C_0)]$, where C_0 the initial $E_2$17βG concentration in the donor compartment at t=0, A is the surface area of the monolayer (in cm^2), dQ/dt the drug permeation rate. The net efflux (P_{app} ratio) is expressed as the quotient of P_{app}(B→A) to P_{app}(A→B). The control group was treated with medium alone and used as the negative control. MK-571, a specific MRP inhibitor, was used as a positive control. Data expressed as mean ± SD (n=6, ***P<0.001, each lipid treatment group vs. the control).

Treatment Group	Efflux Ratio
Control	10.1 ± 1.0
0.25% v/v Peceol®	2.5 ± 0.6 ***

4.3 Effects of Peceol® on MRP2 Protein Expression

The optimal intensity range for densitometer reading was first determined using commercially available beta actin (Figure 15). For optical density within 2000 to 8000 OD, the amount of proteins can correlate well with the readings. The MRP2 protein expression was first normalized to the expression of beta actin, which acted as the house-keeping protein. For each treatment group, its MRP2 protein expression was compared to MRP2 expression from the control group. When the cells were treated with 0.1% and 0.25% v/v Peceol®, there was 29% reduction in the MRP2 protein expression treated with 0.25% v/v Peceol® while no change was observed for 0.1% v/v Peceol® treated cells (Figure 16).

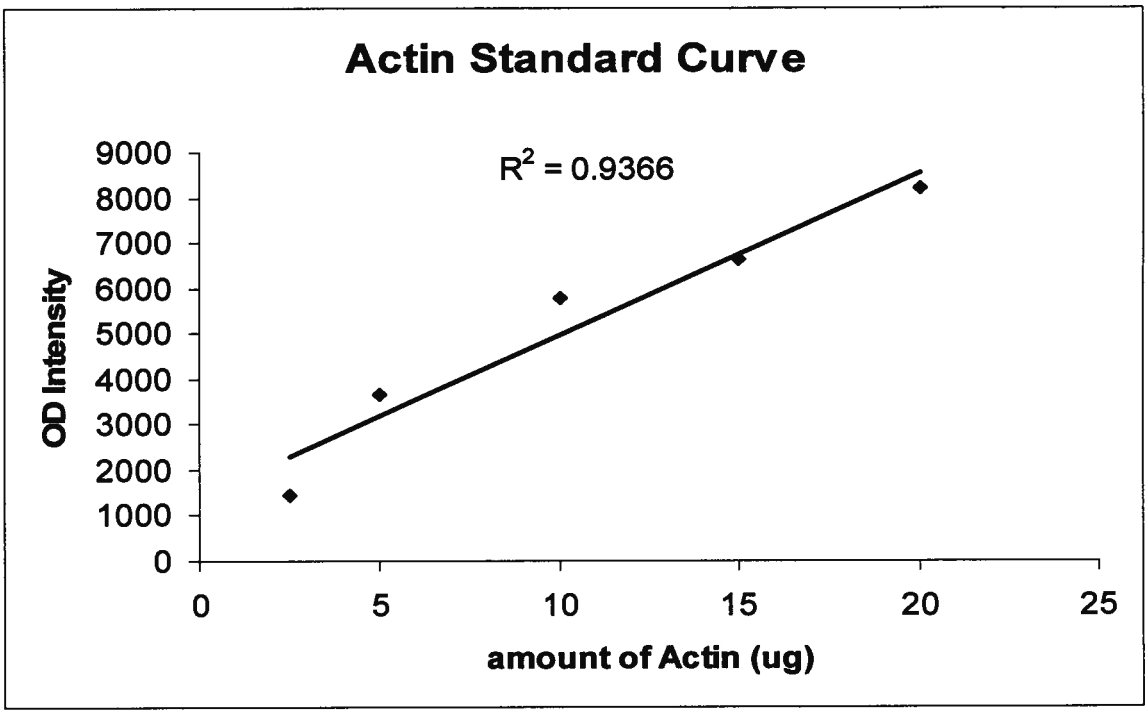

Figure 15. The Optimal Density Range of Densitometer using Beta Actin as the Standard. The primary antibody used to probe against β-actin was goat anti-human β-actin (I-19). The molecular weight of β-actin is around 42 kDa. The beta actin standards were prepared at 2.5, 5, 10, 15 and 20 μ per sample. (n=1)

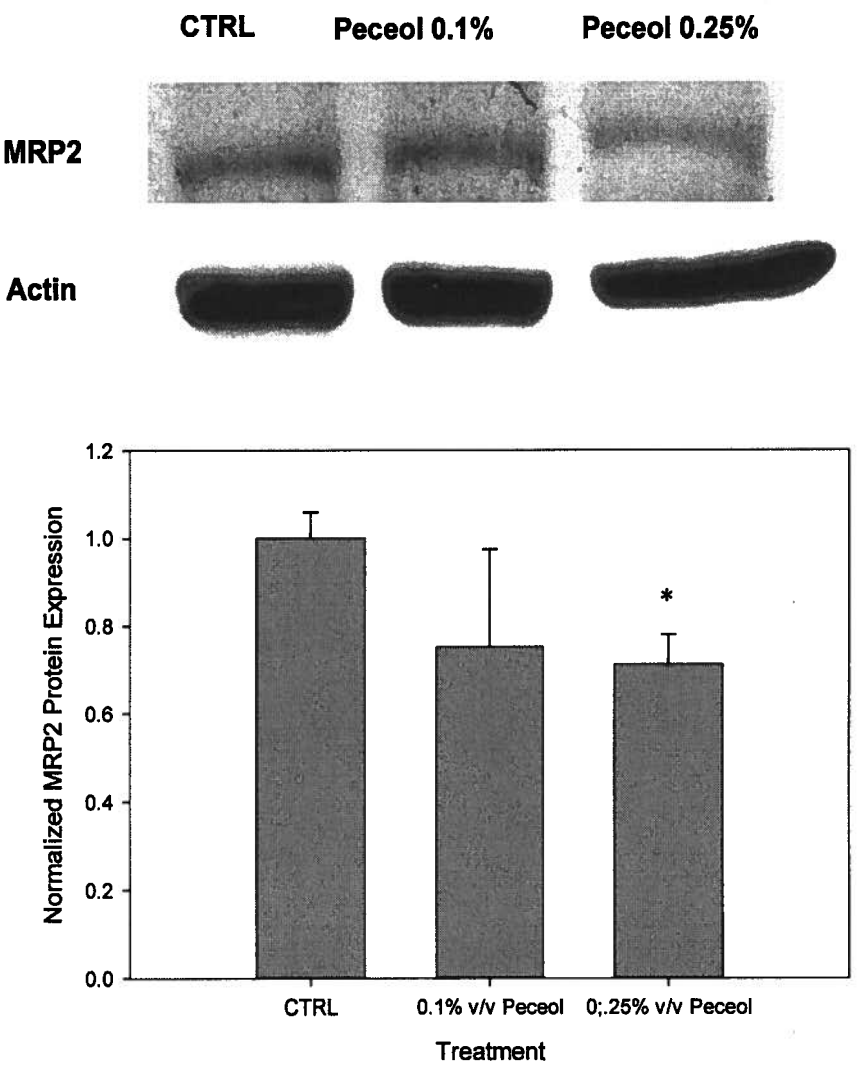

Figure 16. The 24-hour Peceol® Effect on MRP2 Protein Expression in Caco-2 Cells. The primary antibodies used to probe against MRP2 and β-actin were mouse anti-human MRP2 (M_2III-6) and goat anti-human β-actin (I-19), respectively. The molecular weight of MRP2 is around 200kDa; whereas the molecular weight of β-actin is around 42kDa. The insert shown was an image of a representative blot. Lane 1 was the control group; lane 2 was the cells treated with 0.1% v/v Peceol®; lane 3 was the cells treated with 0.25% Peceol®. Each bar value was presented as mean ± SD of MRP2 protein expression normalized by β-actin expression. MRP2 protein expression in treatment groups were compared with the untreated control group. (n=5, *P<0.05).

4.4 Effect of Monoglycerides on MRP2 Functional Activity

4.4.1 Rh123 Accumulation Study

To assess the effect of these lipid treatments on MRP2 activity, a non-MRP2 specific fluorescent substance Rh123 was first used. The positive control used in the accumulation study was 50μM MK-571, a specific MRP inhibitor. In Table 10, cells treated with mono-olein, -palmitin and -stearin had 22%, 19% and 23% increases, respectively, while 50μM MK-571 treatment has resulted in a 81% increase in the accumulation of Rh123 compared to the control.

Table 10. Accumulation of Rh123 in 24-hour Monoglycerides and MK-571 Treated Caco-2 Cells. The accumulation was measured after 2-hour incubation of the cells with the substrate, Rh123. The absolute accumulation of Rh123 in each well was first normalized by using protein content divided by the amount of Rh123 in pmole/μg. The relative Rh123 accumulation with each treatment was then compared in % with the control group. The negative control group was treated with medium alone. MK-571, a specific inhibitor of MRP, was used as a positive control. Data expressed as mean ± SD (n=5, *P<0.05, each monoglyceride group vs. the control; n=3, *P<0.05, MK-571 vs. the control). There were three replicates per treatment in each independent experiment.

Treatment Group	Relative Rh123 Accumulation (%)
Control	100 ± 9
500 μM 1-monoolein	122 ± 6 *
1000 μM 1-monopalmitin	119 ± 2 *
1000 μM 1-monostearin	123 ± 6 *
50 μM MK-571	181 ± 3 *

4.4.2 Rh123 Dose-Response Study

Following Rh123 accumulation study conducted at a single maximum non-cytotoxic concentration for each monoglyceride, a dose-response study was performed to determine whether the increase in Rh123 was a gradual process or not. As seen in Figure 17, Rh123 accumulation was only significant when cells were treated with 500 μM of monoolein.

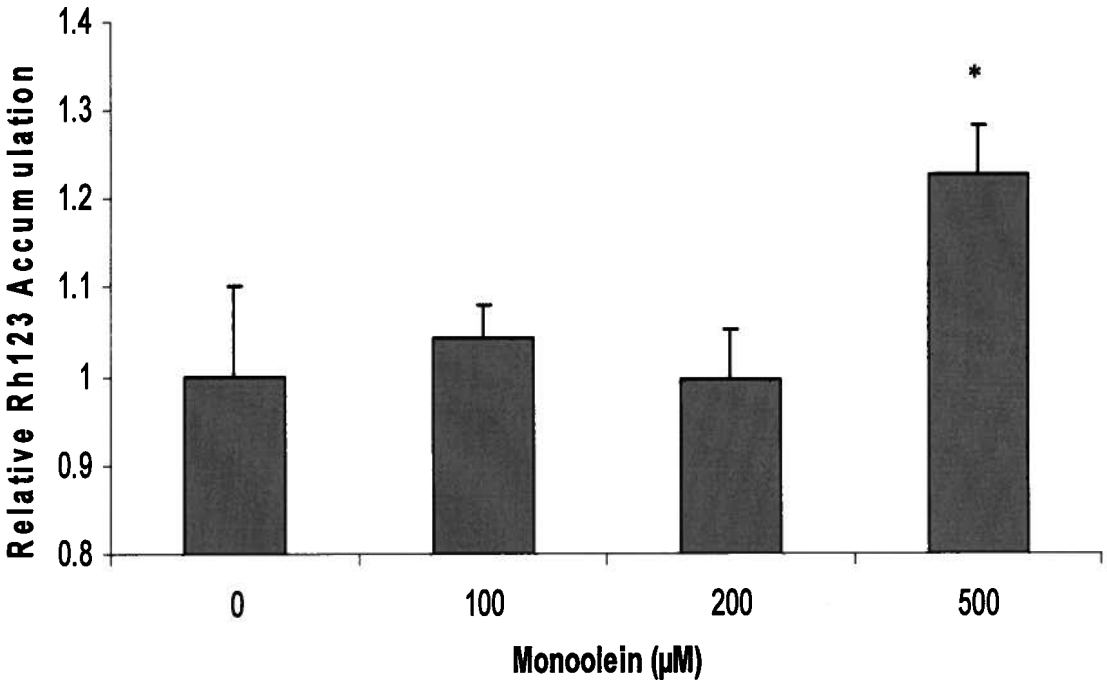

Figure 17. Dose-Response Study of Rh123 Accumulation in Cells Treated with Monoolein for 24 Hours. The accumulation was measured after 2-hour incubation of the cells with the substrate, Rh123. The absolute accumulation of Rh123 in each well was first normalized by using protein content divided by the amount of Rh123 in pmole/μg. The relative Rh123 accumulation with each treatment was then compared in % with the control group. Each bar value was presented as mean ± SD. (n=4, *P<0.05, each monoolein treatment group vs. the control)

In Figure 18, Rh123 accumulation was significant when cells were treated with 750 μM and 1000 μM of monopalmitin. At concentrations less than 750 μM monopalmitin, there was no difference in Rh123 accumulation.

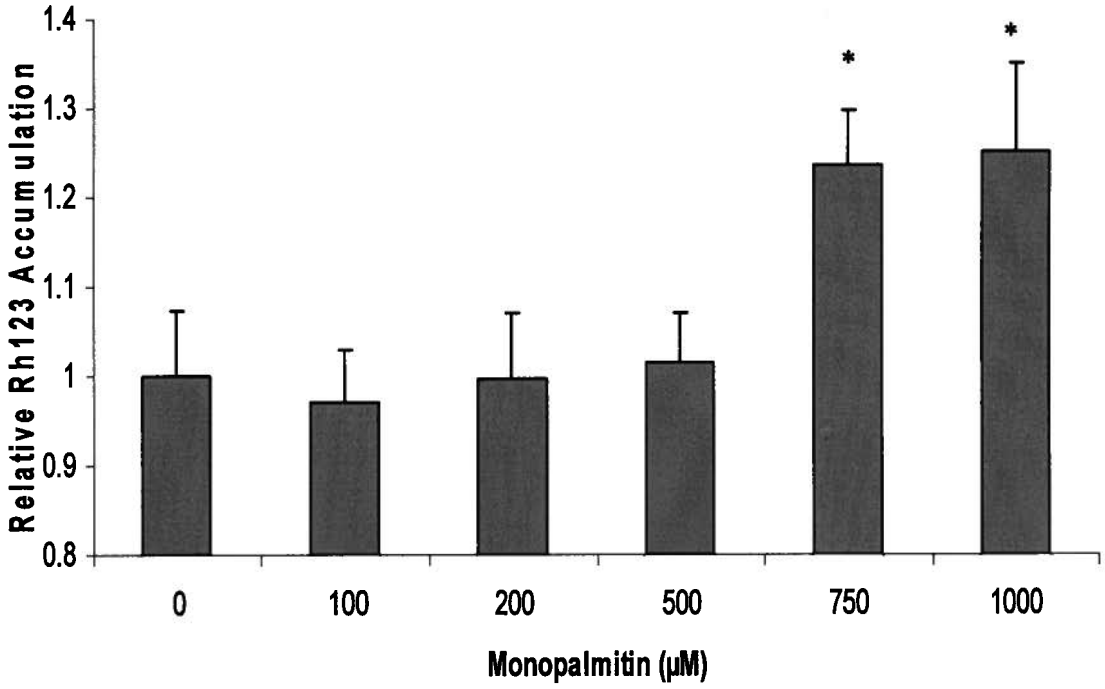

Figure 18. Dose-Response Study of Rh123 Accumulation in Cells Treated with Monopalmitin for 24 Hours. The accumulation was measured after 2-hour incubation of the cells with the substrate, Rh123. The absolute accumulation of Rh123 in each well was first normalized by using protein content divided by the amount of Rh123 in pmole/μg. The relative Rh123 accumulation with each treatment was then compared in % with the control group. Each bar value was presented as mean ± SD. (n=4, *P<0.05, each monopalmitin treatment group vs. the control)

In Figure 19, Rh123 accumulation was significant when cells were treated with 750 μM and 1000 μM of monostearin. At concentrations less than 750 μM monopalmitin, there was no difference in Rh123 accumulation.

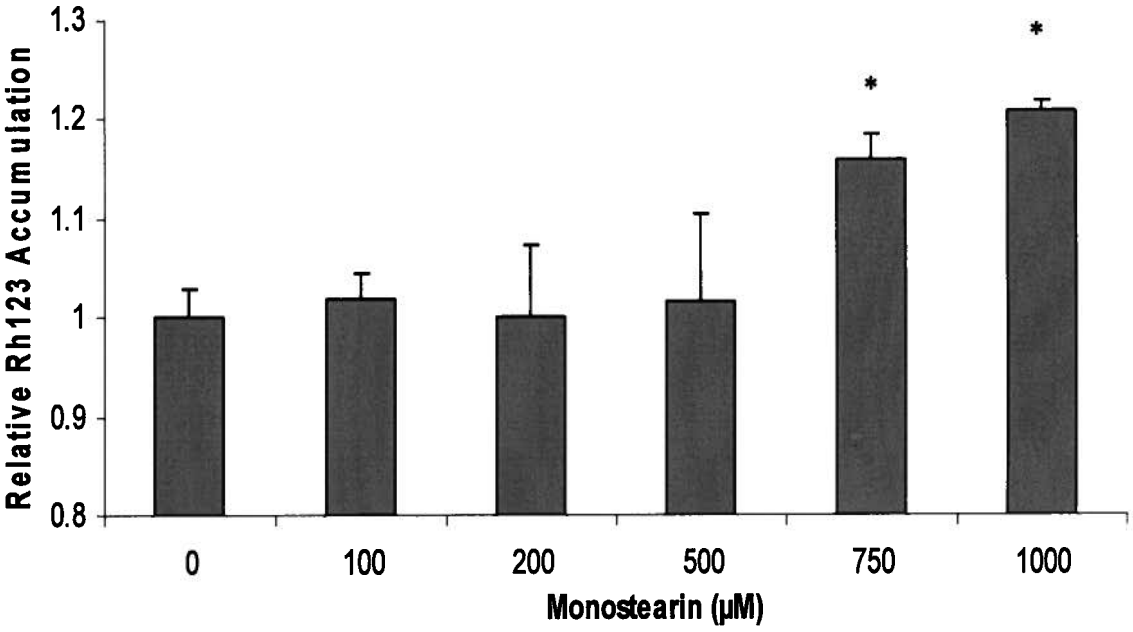

Figure 19. Dose-Response Study of Rh123 Accumulation in Cells Treated with Monostearin for 24 Hours. The accumulation was measured after 2-hour incubation of the cells with the substrate, Rh123. The absolute accumulation of Rh123 in each well was first normalized by using protein content divided by the amount of Rh123 in pmole/μg. The relative Rh123 accumulation with each treatment was then compared in % with the control group. Each bar value was presented as mean ± SD. (n=4, *P<0.05, each monostearin treatment group vs. the control)

4.4.3 $E_2$17βG Bidirectional Flux Study

To monitor the transport of $E_2$17βG across Caco-2 cell monolayer, the monolayer must maintain its integrity throughout the experiment. As shown in Table 11, all TEER values were higher than 350 Ω^*cm^2, and there was no change in TEER values before and after the experiment for all treatment groups (control, monopalmitin, monostearin, monoolein and MK-571) in either apical to basolateral or basolateral to apical directions.

Table 11. Effects of Monoglycerides (mono-olein, -stearin, -palmitin) and MK571 on TEER Values in Caco-2 Cells. TEER values of Caco-2 cells monolayer were measured before and after the bi-directional transport of $E_2$17βG in the A→B and B→A directions in the presence of medium only, 500 μM monoolein, 1000 μM monopalmitin, 1000 μM monostearin and 50 μM MK-571.

	TEER ($\Omega \cdot cm^2$)			
Treatment Group	**A→B Before**	**A→B After**	**B→A Before**	**B→A After**
Control	386 ± 12	384 ± 10	390 ± 10	382 ± 14
500μM monoolein	386 ± 21	380 ± 24	381 ± 14	374 ± 9
1000μM monopalmitin	383 ± 10	378 ± 17	381 ± 23	379 ± 21
1000μM monostearin	381 ± 16	382 ± 16	384 ± 15	382 ± 14
50μM MK-571	380 ± 23	376 ± 22	384 ± 8	379 ± 8

To calculate the P_{app}, the steady state flux can be found from the slope of the best fit line in the graph with [$E_2$17βG] versus time shown in Figure 20-23 (monoolein, monostearin, monopalmitin and MK-571).

A

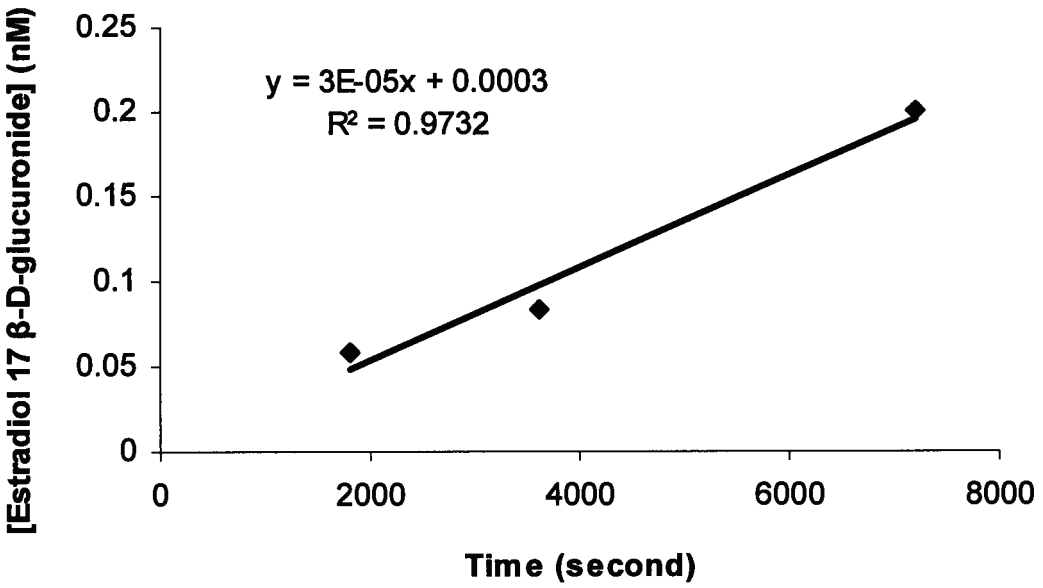

B

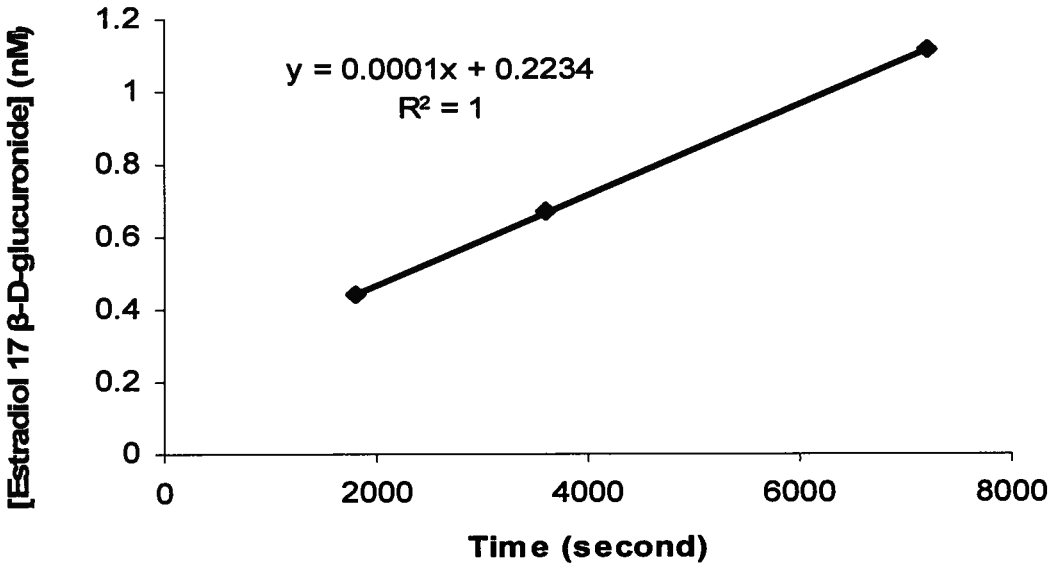

Figure 20. The 2-hour $E_2$17βG Bi-directional Transport Profiles of 500μM Monoolein Treated Caco-2 Cell Monolayers. (A) Apical to basolateral; B) Basolateral to apical. The plots shown above were representative ones from one experiment. (n=6)

A

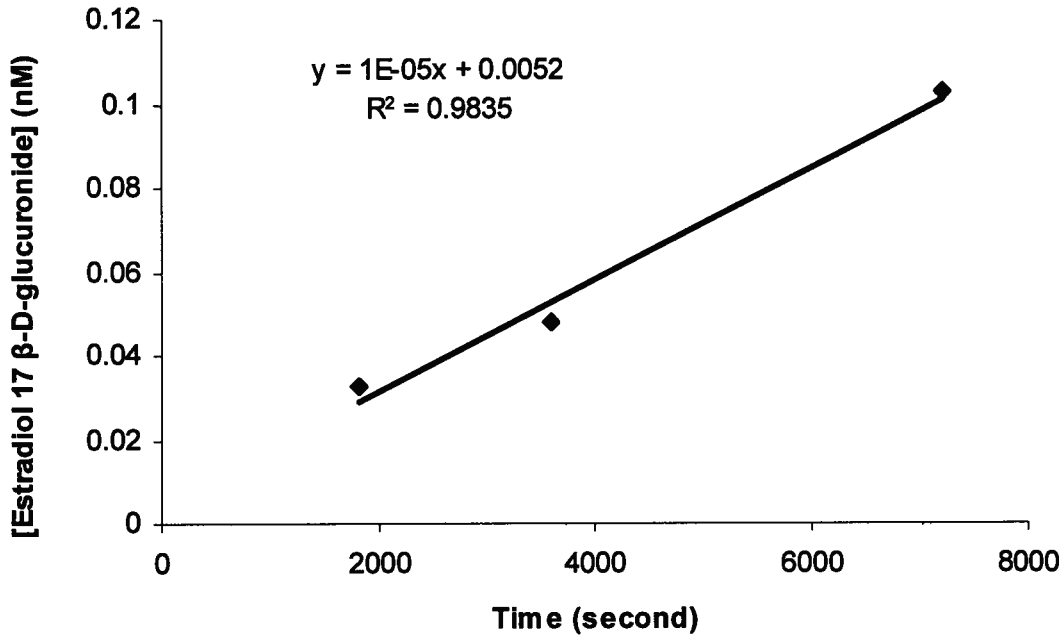

B

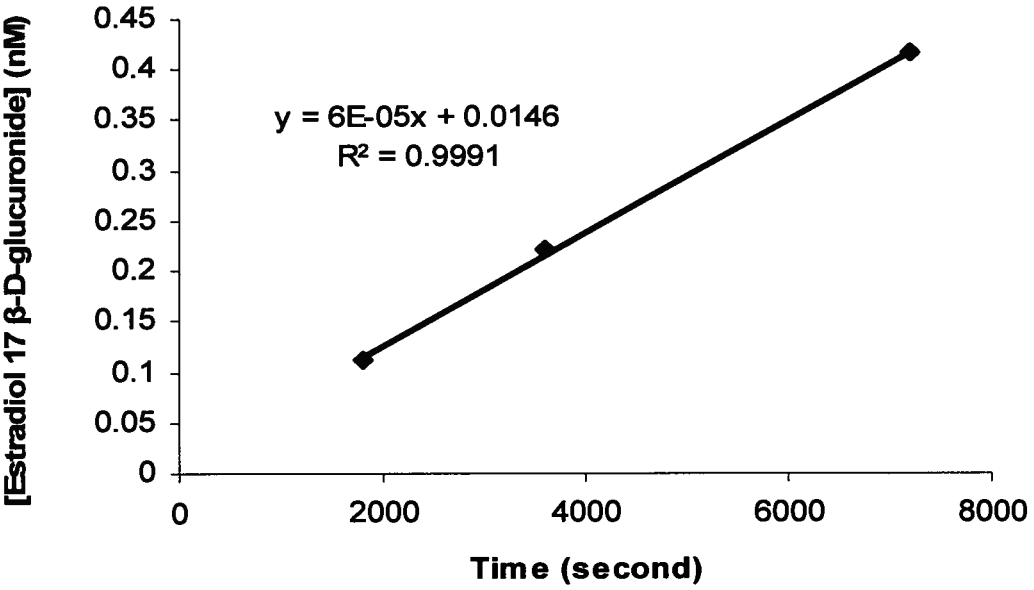

Figure 21. The 2-hour $E_2$17βG Bi-directional Transport Profiles of 1000μM Monostearin Treated Caco-2 Cell Monolayers. A) Apical to basolateral; B) Basolateral to apical. The plots shown above were representative ones from one experiment. (n=6)

A

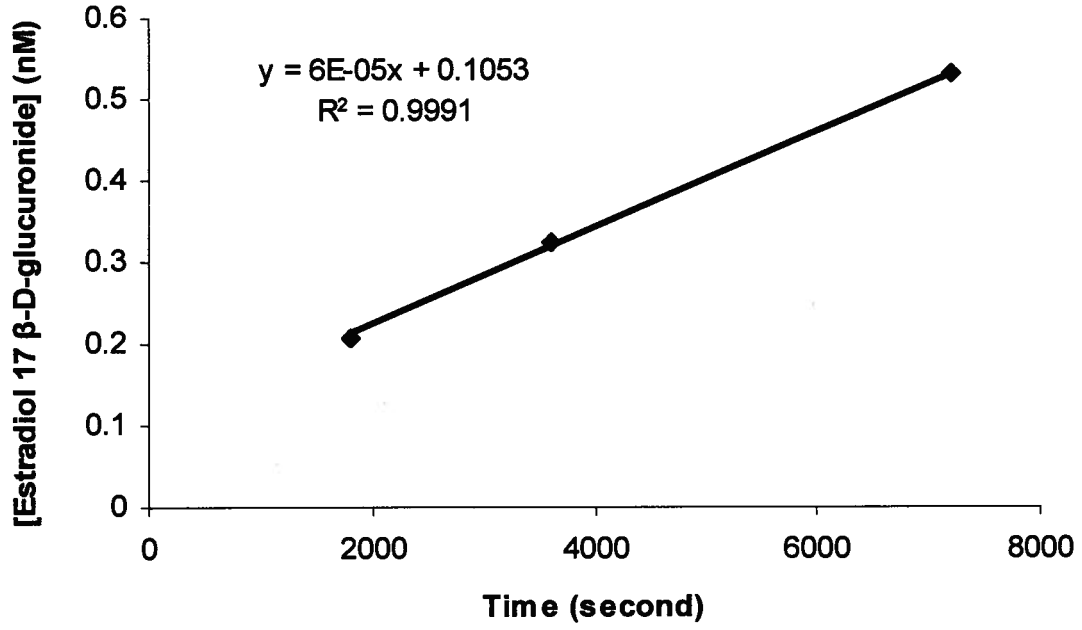

B

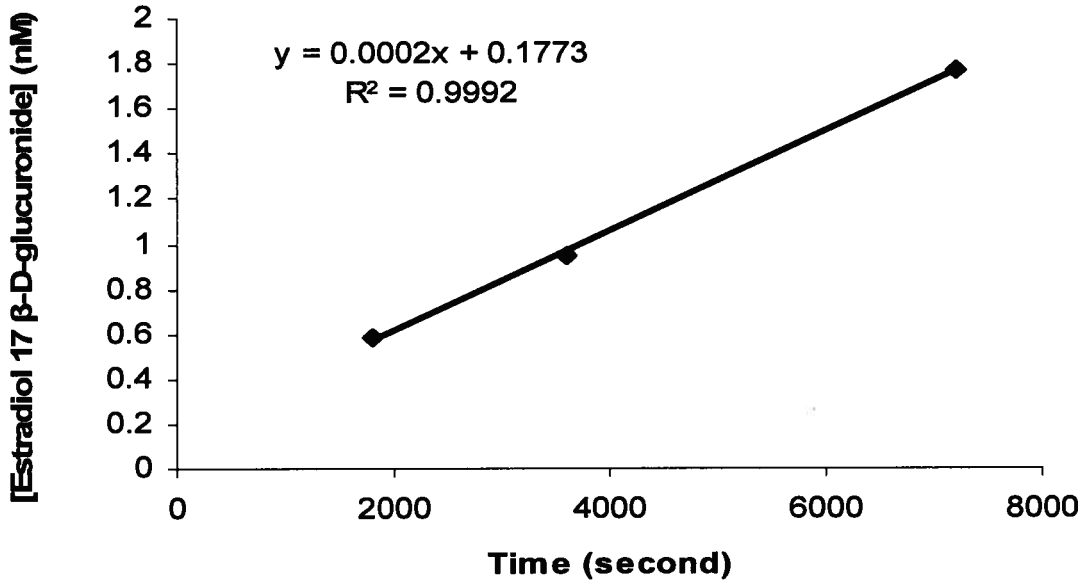

Figure 22. The 2-hour $E_2$17βG Bi-directional Transport Profiles of 1000μM Monopalmitin Treated Caco-2 Cell Monolayers. A) Apical to basolateral; B) Basolateral to apical. The plots shown above were representative ones from one experiment. (n=6)

.

A

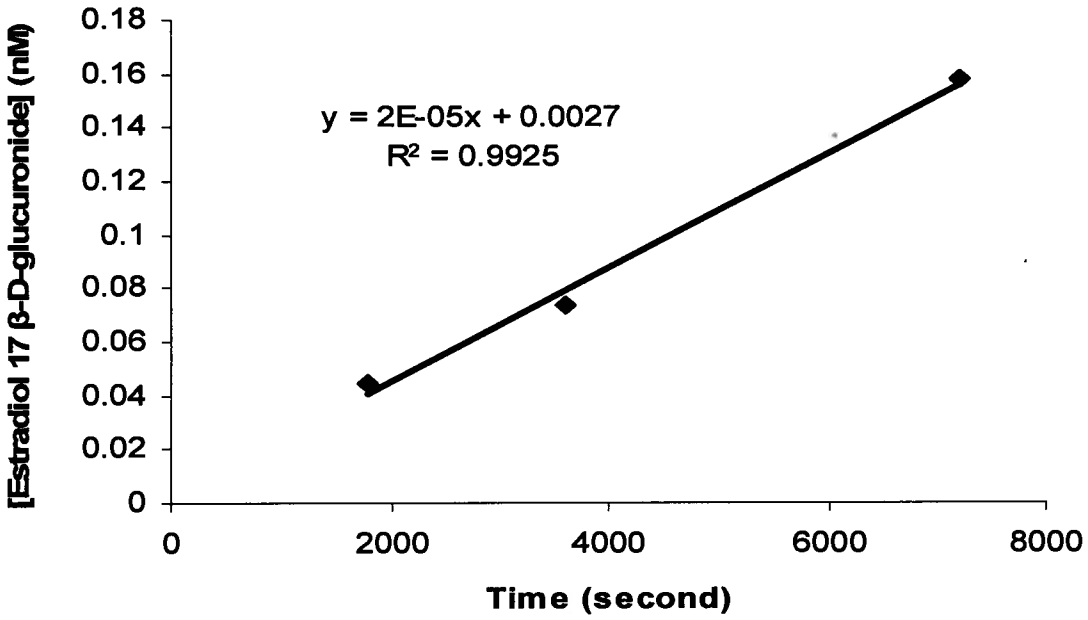

B

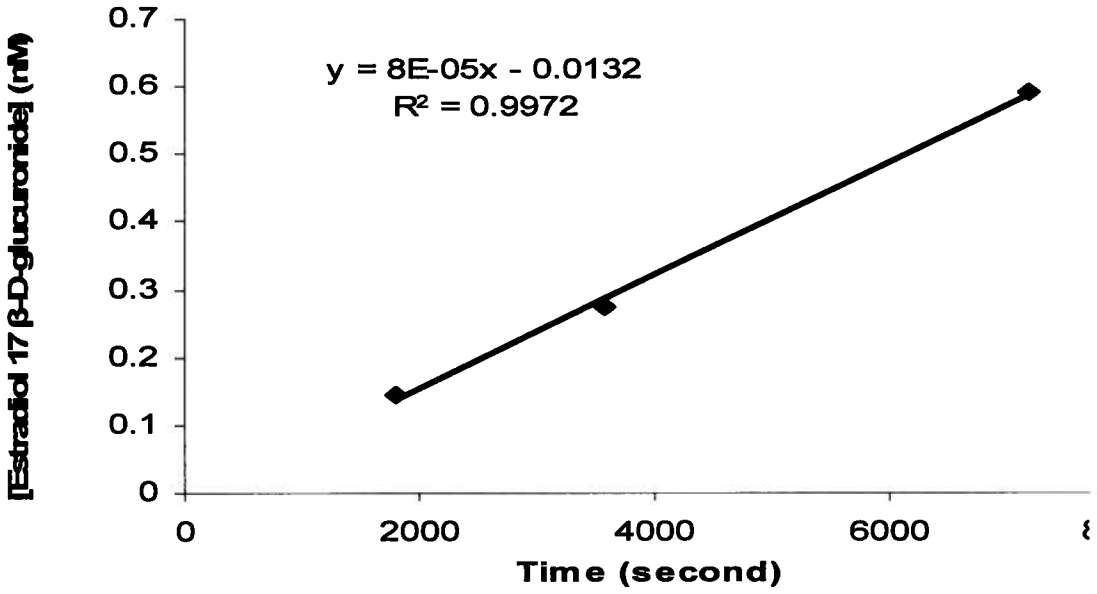

Figure 23. The 2-hour $E_2$17βG Bi-directional Transport Profiles of 50μM MK-571 Treated Caco-2 Cell Monolayers. A) Apical to basolateral; B) Basolateral to apical. The plots shown above were representative ones from one experiment. (n=6)

In Figure 24, $P_{app,ab}$ (from apical to basolateral side) for the $E_2$17βG transport of 500 μM monoolein, 1000 μM monostearin and 1000 μM monopalmitin treated groups were (3.8 ± 2.1), (5.0 ± 1.8) and (6.1 ± 1.4) $x10^{-6}$ cm/s, respectively; while the $P_{app, ab}$ for the control and 50μM MK-571 (a specific MRP1 and MRP2 inhibitor) treated groups were (3.2 ± 1.7) and (3.6 ± 1.4) $x10^{-6}$ cm/s, respectively. The apparent permeabilities in the absorptive direction for 500 μM monoolein, 1000 μM monostearin and 50 μM MK-571 treated groups were not statistically significant different from the control group (treated with medium only), with the exception of 1000μM monopalmitin treated group which had its apparent permeability in the absorptive direction almost doubled compared to the control. For the basolateral to apical $E_2$17βG transport, 500μM monoolein [$P_{app,ba}$: (13.2 ± 4.5) $x10^{-6}$ cm/s], 1000 μM monostearin [$P_{app,ba}$: (11.5 ± 3.6) $x10^{-6}$ cm/s] and 50 μM MK-571 [$P_{app,ba}$: (10.3 ± 3.3)] $x10^{-6}$ cm/s] treated groups had statistically significant decreases in their apparent permeability coefficients compared to the control group [$P_{app,ba}$: (31.1 ± 13.9) $x10^{-6}$ cm/s], with the exception of 1000 μM monopalmitin treated group [$P_{app,ba}$: (31.5 ± 14.9) $x10^{-6}$ cm/s] which showed no change in $P_{app,ba}$ compared to the control. Thus, the apparent permeability of transporting $E_2$17βG in the effluxing direction (basolateral to apical) was greatly reduced in cells treated with either 500 μM monoolein, 1000 μM monostearin or 50 μM MK-571; in contrast, the apparent permeability in the absorptive direction (apical to basolateral) did not change for any of these three treatments. The only exception observed for the transport of $E_2$17βG was the 1000 μM monopalmitin treated group which had an increased

apparent permeability from the apical to basolateral direction, while the apparent permeability in the reverse direction remained unchanged compared to the control.

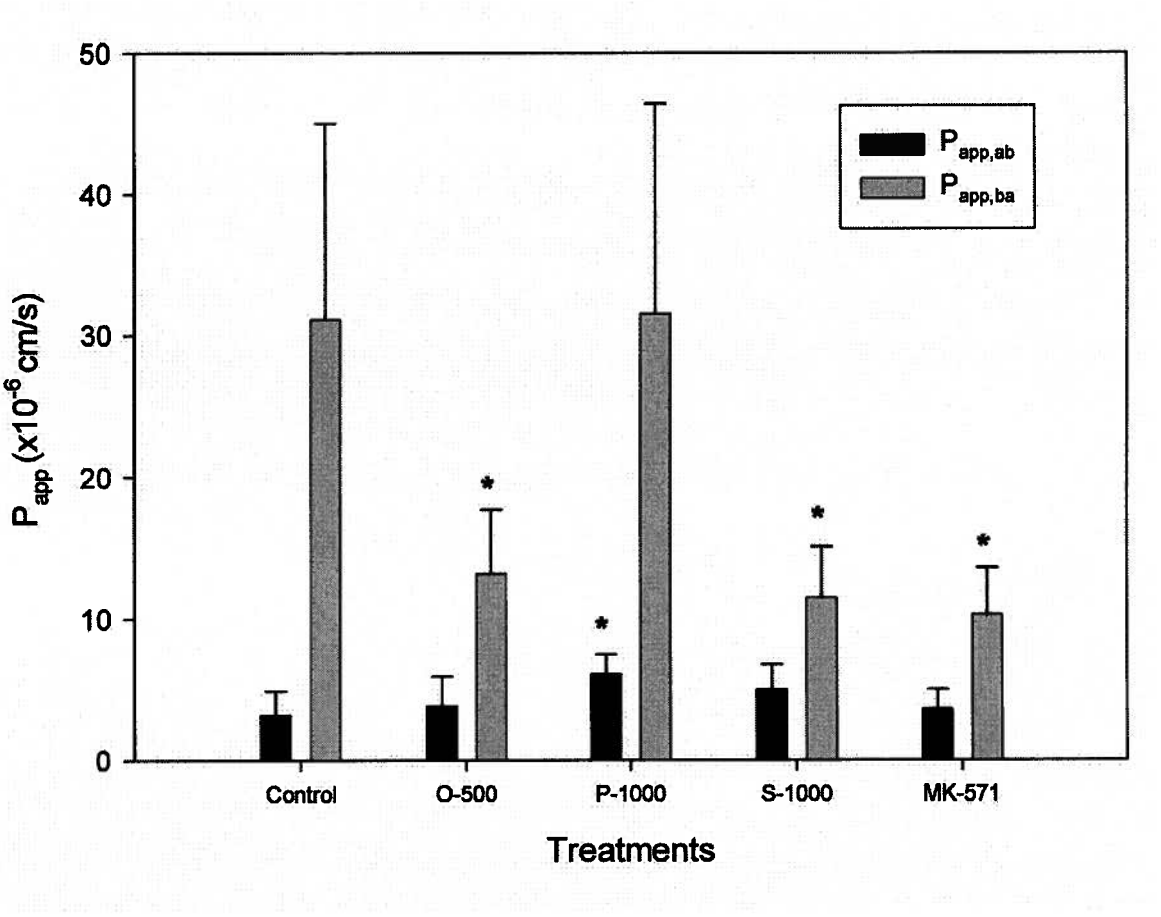

Figure 24. Apparent Permeability Coefficients (P_{app}) for Bi-directional transfer of $E_2$17βG across Monoglycerides Treated Caco-2 Cell Monolayers. The apparent permeability coefficient (Papp) was calculated with the following equation: Papp = $dQ/dt \cdot [1/(A \cdot C_0)]$, where C_0 is the initial $E_2$17βG concentration in the donor compartment at t=0, A is the surface area of the monolayer (in cm2), dQ/dt is the drug permeation rate. The control group was treated with medium alone which used as the negative control. MK-571 (50 μM), a specific MRP inhibitor, was used as a positive control. O-500, P-1000, S-1000 were the three monoglyceride treatments which were 500 μM monoolein, 1000 μM monopalmitin and 1000 μM monostearin, respectively. Data were expressed as mean ± SD (n=6, *P<0.05, $P_{app,\ ab}$ for each lipid treatment vs. $P_{app,\ ab}$ for the control; $P_{app,\ ba}$ for each lipid treatment vs. $P_{app,ba}$ for the control).

In Table 12, the efflux ratios for each treatment were tabulated, and all treatment groups (500 μM monoolein, 1000 μM monostearin, 1000 μM monopalmitin and 50 μM MK-571) had shown statistically significant reductions in the efflux of $E_2$17βG, a typical substrate for MRP2, compared to the control group. The rank order from the most significant to the least reduction in efflux ratios was listed as following: 1000 μM monostearin > 500 μM monoolein > 1000 μM monopalmitin.

Table 12. The Efflux Ratio of Caco-2 Cell Monolayer Treated with Monoglycerides and MK-571 Treated Caco-2 Cell Monolayer The calculated efflux ratio was the quotient of $P_{app,ba}$ over $P_{app,\ ab}$, where $P_{app,ba}$ was apparent permeability coefficient from basolateral to apical side, $P_{app,\ ab}$ was of the apparent permeability coefficient from the apical to basolateral side. The control group was treated with medium alone which was used as the negative control. MK-571, a specific MRP inhibitor, was used as a positive control. Data were expressed as mean ± SD (n=6, ***P<0.001, each lipid treatment group vs. the control).

Treatment Group	Efflux Ratio
Control	10.1 ± 1.0
500 μM monoolein	3.8 ± 1.0 ***
1000 μM monopalmitin	5.6 ± 3.2 ***
1000 μM monostearin	2.4 ± 0.5 ***
50 μM MK-571	3.4 ± 0.8 ***

4.5 Effects of Monoglycerides on MRP2 Protein Expression

The MRP2 protein expression in response to each monoglyceride treatment was evaluated by Western blotting technique. The relative MRP2 protein content was normalized using β-actin as the house-keeping protein. As shown in Figure 25 and 26, there were 35 % and 19 % decrease of the relative MRP2 protein expression in cells treated with 500 μM monoolein and 1000 μM monopalmitin, respectively, as compared to the control group (medium treated only). However, there was no change in the relative MRP2 protein expression of cells treated with 1000 μM monostearin compared to the control group (Figure 27).

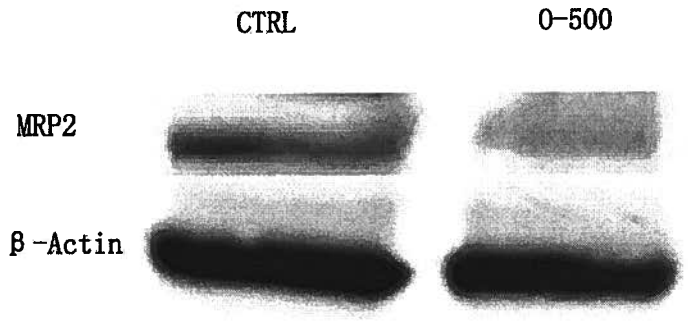

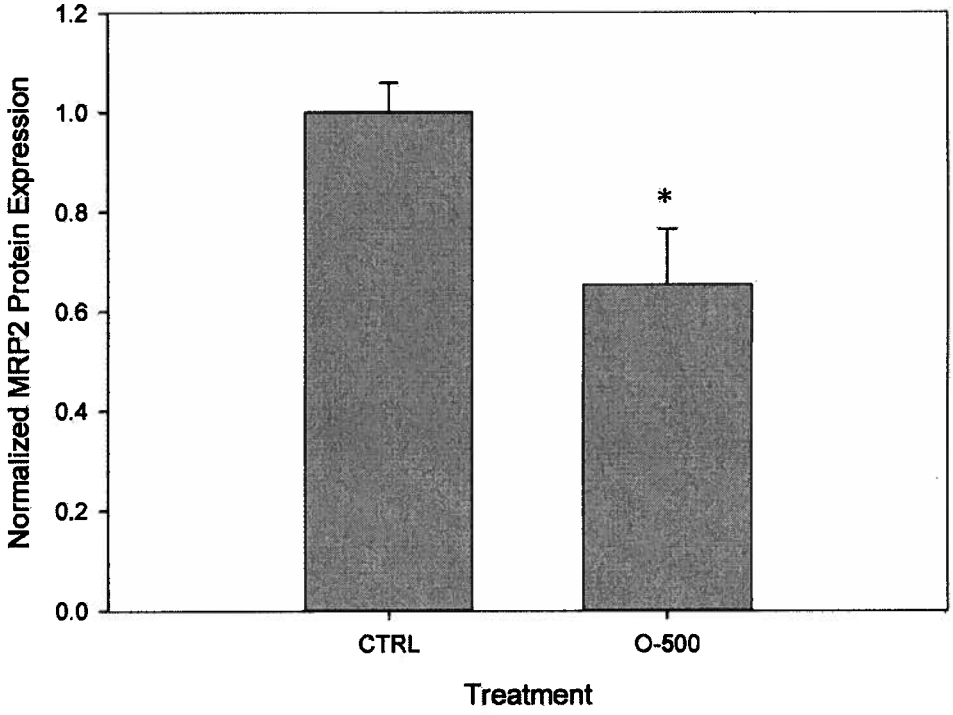

Figure 25. The 24-hour 1-Monoolein Effect on MRP2 Protein Expression in Caco-2 Cells. The primary antibodies used to probe against MRP2 and β-actin were mouse anti-human MRP2 (M_2III-6) and goat anti-human β-actin (I-19), respectively. The molecular weight of MRP2 is around 200kDa; whereas the molecular weight of β-actin is around 42kDa. The insert shown was an image of a representative blot. Each bar value was presented as mean ± SD of MRP2 protein expression normalized by β-actin expression. MRP2 protein expression in treatment groups were compared with the untreated control group. (n=5, *P<0.05).

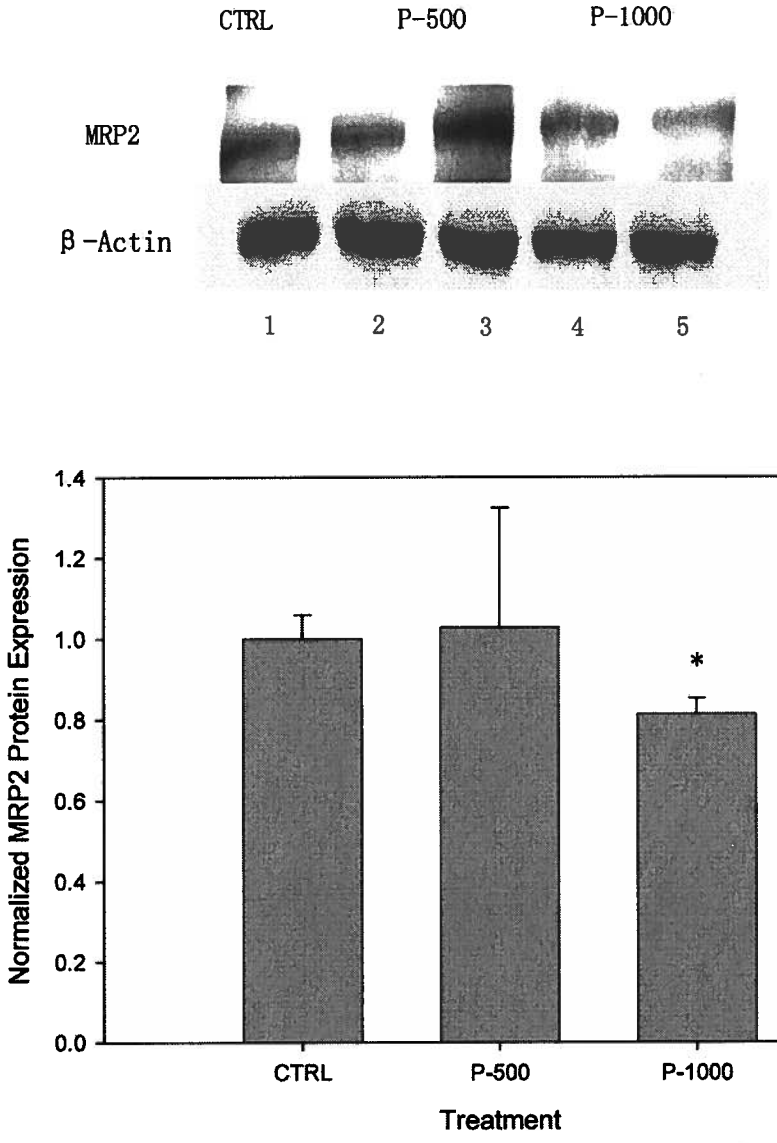

Figure 26. The 24-hour 1-Monopalmitin Effect on MRP2 Protein Expression in Caco-2 Cells. The primary antibodies used to probe against MRP2 and β-actin were mouse anti-human MRP2 (M_2III-6) and goat anti-human β-actin (I-19), respectively. The molecular weight of MRP2 is around 200kDa; whereas the molecular weight of β-actin is around 42kDa. The insert shown was an image of a representative blot. Lane 1 was the control group; lane 2 and 3 were the cells treated 500μM of monopalmitin; lane 4 and 5 were the cells treated with 1000μM of monopalmitin. Each bar value was presented as mean ± SD of MRP2 protein expression normalized by β-actin expressionMRP2 protein expression in treatment groups were compared with the untreated control group. (n=5, *P<0.05).

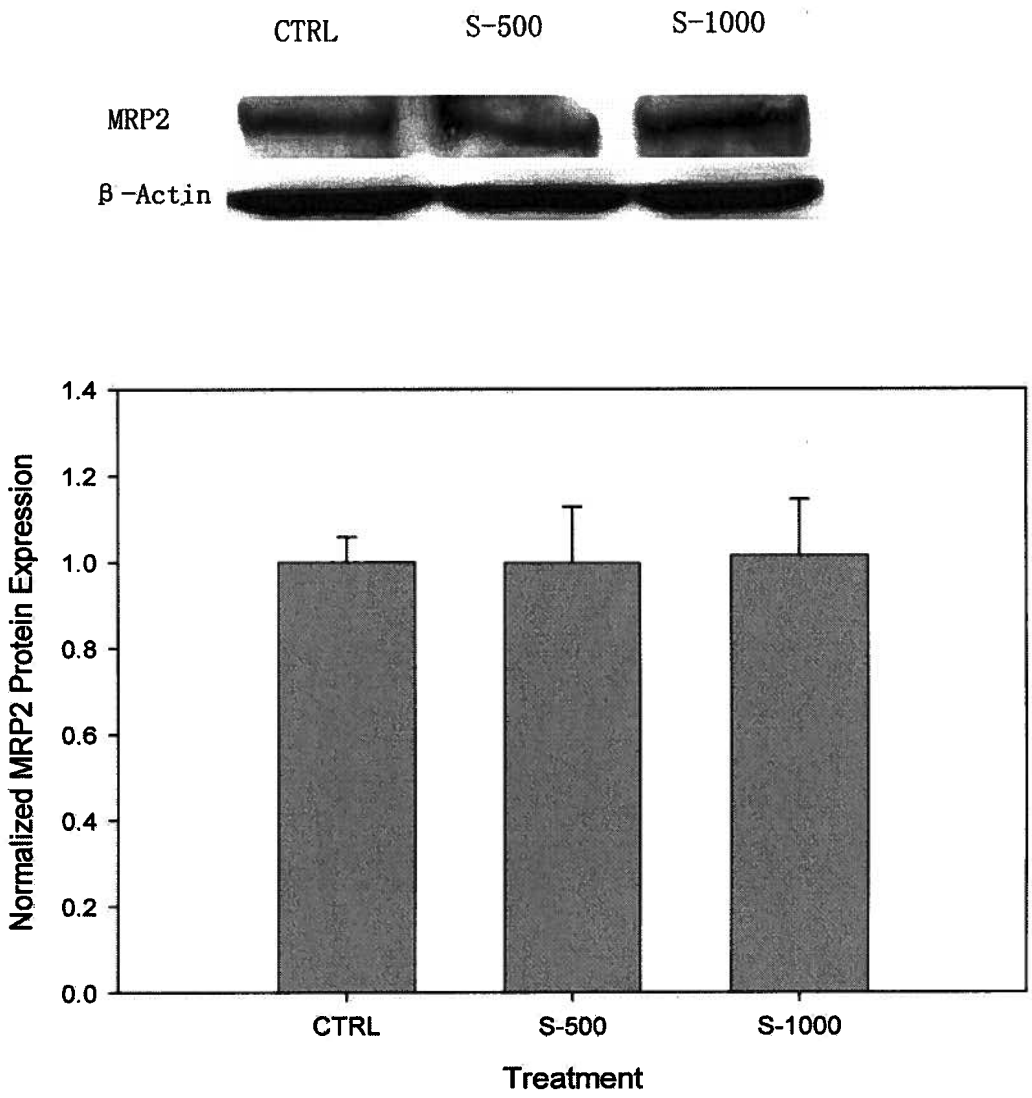

Figure 27. The 24-hour 1-Monostearin Effect on MRP2 Protein Expression in Caco-2 Cells. The primary antibodies used to probe against MRP2 and β-actin were mouse anti-human MRP2 (M_2III-6) and goat anti-human β-actin (I-19), respectively. The molecular weight of MRP2 is around 200 kDa; whereas the molecular weight of β-actin is around 42 kDa. The insert shown was an image of a representative blot. Each bar value was presented as mean ± SD of MRP2 protein expression normalized by β-actin expression. Lane 1 was the control group; lane 2 was the cells treated 500μM of monostearin; lane 3 was the cells treated with 1000μM of monostearin. MRP2 protein expression in treatment groups were compared with the untreated control group. (n=5).

CHAPTER 5

DISCUSSION

5.1 Cytotoxicity and Viability Ranges of Peceol® and Monoglycerides

For each lipid treatment, the non-cytotoxic concentration range was first determined before proceeding to any transporter activity or protein expression studies to eliminate factors, such as cell necrosis and apoptosis, which could alter the normal physiology of Caco-2 cells (124, 125). Two different colorimetric methods were employed to determine the non-cytotoxic ranges for Peceol® and monoglycerides, which provided some confidence in the accuracy of the results. The MTS assay is a measure of the mitochondrial respiration; whereas, the LDH assay is an assessment of the cell membrane integrity (126).

The CellTiter 96® MTS assay used in the study requires a minimum of 1000 cells/well for an accurate determination; on the other hand, the CytoTox 96® LDH assay can detect as few as 150 cells/well under serum-free conditions (126). Therefore, the LDH assay is a more sensitive assay compared to the MTS assay. In the CytoTox 96® LDH Assay, formazan concentrations in the medium are determined by measuring optical absorbance at 492 nm (127). Medium free of phenol red is necessary to accurately measure the red formazan product in LDH and MTS assays (126). One major advantage of MTS assay over LDH assay is that one can monitor cell viabilities at multiple time points instead of one.

Interestingly, a MTS study conducted by Barta *et al.* has shown an increase in the viability for cells treated with monoglycerides compared with the control (29). It was reasoned that the MTS assay skewed the results because the testing compounds were inhibitors of efflux transporters. However, one major drawback of that MTS study is that phenol-red containing cell medium was used, which could ultimately account for the large standard deviations to the cell viabilities data. The LDH assay was also conducted in Barta *et al*'s study which measured the release of LDH by damaged or nonviable cells into the media (29). The discrepancies between the MTS and LDH data from that study have shown the importance of using two colorimetric assays to avoid potential pitfalls.

The non-cytotoxic ranges obtained from both MTS and LDH studies for each type of monoglyceride were in agreement with each other. The 24-hour non-cytotoxic ranges of Peceol®, 1-monoolein, 1-monostearin and 1-monopalmitin in Caco-2 cells were equal or less than 1% v/v, 500 µM, 1000 µM and 1000 µM, respectively (Figure 6-9). The toxicity of MK-571 at 50 µM was also assessed using MTS and LDH assays (data not shown), and there was no increased toxicity associated with this treatment compared to the control group after 24 hours.

5.2 Peceol®: Rh123 Accumulation & $E_2$17βG Transport Studies

A study conducted by Sachs-Barrable *et al.* had shown that 24-hour Peceol® treatment reduced the activity of Pgp (15). Therefore, Peceol®, a mixture of mono- and di-glycerides, was used in the preliminary study before screening for the possible effects of specific monoglycerides on MRP2 activity and expression. The functional activities of MRP2 were assessed by both the accumulation study and bi-directional transport study.

Rh123 is a well known Pgp substrate, and the Michaelis-Menton constant (K_m) value of Pgp for Rh123 is 13.5 μM (128). Besides Pgp, MRP2 and BCRP are the two principal apically located efflux transporters in intestinal epithelial cells. Rh123 is also a substrate for MRP1 and MRP2 to a lesser degree (129-131). However, Rh123 is not a substrate for the wild-type form of BCRP (132). Due to the low expression level and the basolateral cellular location of MRP1, the Rh123 accumulation study was used to assess the functional activities of Pgp and MRP2 on the apical side.

There was an 84% increase in Rh123 accumulation in 0.25% v/v Peceol® treated cells (Table 7). Since Rh123 is a non-specific substrate for both Pgp and MRP2, it is imperative to have a positive control MK571, a specific MRP1 and MRP2 inhibitor, in the study (133). IC_{50} represents the concentration of a compound that is required for 50% inhibition of a biological process. MK571 has

an IC_{50} value of 5.2 μM against the transport of Rh123 by MRP1 and MRP2 (134). The concentration of MK571 used in the Rh123 accumulation was 50 μM, which was approximately 10 times higher than its IC_{50} value. Therefore, there should be a complete inhibition of MRP2 in the cells. The data has shown a 112% increase in Rh123 accumulation when Caco-2 cells were treated with 50 μM MK571 (Table 7).

To further assess the vectorial transport of substances by MRP2, $E_2$17βG bidirectional efflux study was conducted. $E_2$17βG is a natural cholestatic metabolite of estradiol which excreted into the bile via cMOAT/MRP2 (12). $E_2$17βG is a well-known substrate for the study of MRPs (such as MRP1, MRP2, MRP3, MRP4 and MRP7). The Michaelis-Menton constants (K_m) for MRP1, MRP2 and MRP3 are 1 μM, 7 μM and 27 μM, respectively (135-138). K_m is used to describe the binding affinity of an enzyme for a substrate. The K_m value is inversely proportional to the binding affinity of the enzyme for that substrate. Therefore, MRP1 has the highest affinity toward $E_2$17βG than both MRP2 and MRP3. $E_2$17βG has a much lower affinity for other MRPs besides MRP1-3. Despite the high affinity of $E_2$17βG with MRP1, there is a considerably lower expression level of MRP1 compared to MRP2 in Caco-2 cells (139). As for MRP3, it localizes on the basolateral side of Caco-2 cells. In addition, MRP2 relative expression level was about 4-fold higher than MRP3 (140). Thus, $E_2$17βG could be considered as a relatively specific MRP2 substrate in this study (141,142).

One major advantage of the bi-directional transport study over the accumulation study was the polarization and tight junction formation of these Caco-2 cells, which provided the best possible *in vitro* simulation of intestinal epithelial cells. The unchanged TEER values before and after each experiment ensured that the observed reduced transport activity was not caused by cell damage, death or monolayer leakage. In Table 11, it had shown that there was no change in TEER values before and after the experiment which implies that the transport of compounds was through the transcellular route. The reported TEER values ranges from 150 to 800 $\Omega \cdot cm^2$. This variation in TEER values of Caco-2 monolayers might be resulted from differences arise from cell types, the number of post-seeding days, the passage number, the material of the filter support, and the culture conditions. In Hubatsch *et al.* group, their standard TEER value for a differentiated and intact cell monolayer was set at 260 ± 65 $\Omega \cdot cm^2$. Cell monolayer that has a TEER value below 165 $\Omega \cdot cm^2$ was discarded (143). The TEER value is highly dependent on the temperature which may explain some of the erroneously high TER reported in literature (143). When the Caco-2 cells were initially seeded on the 12-well inserts, the TEER values were all below 100 $\Omega \cdot cm^2$. Tracking the growth of the cells, the TEER values peaked around 350 $\Omega \cdot cm^2$ post-seeding on day 18, and the values maintained stable after reaching the plateau.

The interaction between MRP2 and $E_2$17βG are quite complex and require more than one distinct binding site on MRP2 (144). $E_2$17βG can first bind

to a transport site, and then it can bind to an allosteric site that increases its own transport (144). In Table 9, it has shown that 0.25% v/v Peceol® decreased the $E_2$17βG efflux ratio by 4-fold, which suggested a decrease in efflux activity of MRP2. However, this decrease in efflux ratio should be interpreted with caution. In Figure 14, the apparent permeability coefficient in the secretory direction ($P_{app, ba}$) did not change in 0.25% v/v Peceol® treated group compared to the control; yet, the apparent permeability coefficient in the absorptive direction ($P_{app, ab}$) for the 0.25% v/v Peceol® treated group increased close to 3-fold compared to the control. Both P_{app} values have large standard deviations. This could result from the numerous ingredients within Peceol® exerting opposing forces on the transport process.

Taking together the data from the Rh123 accumulation and $E_2$17βG bi-directional transport studies, they suggested that Peceol® might attenuate the efflux activity of MRP2.

5.3 Peceol®: MRP2 Protein Expression

One possible explanation for the decreased MRP2 activity is the reduction of MRP2 protein expression. A previous study done by Sachs-Barrable *et al.* has shown that 24-hour 0.25% v/v Peceol® treatment can reduce the protein expression of Pgp by 62% after seeing the functional activity of Pgp was reduced (15). In this study, I had seen close to 30% reduction of MRP2 protein expression

after 24-hour 0.25% v/v Peceol® treatment as shown in Figure 16. This demonstrated that Peceol® at 0.25% v/v could affect the protein expression of both Pgp and MRP2. Peceol® might be able to modulate the expressions of these two major efflux transporters by either transcriptional or translational regulation. Transcriptional regulation confers the ability to regulate expression over a longer period of time; translational regulation enables a more rapid response to physiological, pharmacological or toxicological stress (145).

5.4 Monoglycerides: Rh123 Accumulation & Dose Response Study

Peceol® was composed of mono- and di-glycerides. Although Peceol® has shown to reduce Pgp and MRP2 activities, the specific components in Peceol® that caused this were still under investigation. A study conducted by Konisihi *et al.* had shown monoglycerides (in particularly, monopalmitin) not diglycerides could reduce Pgp activities (38). Another study published by Barta *et al.* has shown monoolein and monostearin could decrease Pgp activity and protein expression (29). Therefore, monoolein, monopalmitin and monostearin were chosen in this study to investigate their effects on MRP2 activity and expression in Caco-2 cells.

For the accumulation study, Rh123 was used to monitor the changes of the functional activities of Pgp and MRPs (131, 146-150). Rh123 is a cationic fluorescent dye that accumulates selectively in the mitochondria of eukaryotic

cells, and it could be transported by Pgp and MRPs but not BCRP (151,152). Although studies had shown that both Pgp and MRP could transport Rh123 via direct bindings, a recent study had indicated that MRPs contributed to a lesser degree on Rh123 efflux compared to Pgp (153-155). MK571, a MRP1 and MRP2 inhibitor was used in this study as a positive control. There was about 20% increase in Rh123 accumulation for each monoglyceride treatment (Table 10) which implied that efflux activities of Pgp and MRPs were affected.

The dose response studies conducted for all three monoglycerides had indicated that they did not accumulate Rh123 in a dose dependent matter (Figure 17-19). For monostearin and monopalmitin treated studies, there were drastic increases in Rh123 accumulation when the concentrations were equal or above 750 μM; for monoolein treated cells, there was only a sharp increase in Rh123 accumulation when the comconcentration was at 500 μM.

5.5 Monoglycerides: $E_2$17βG Bi-directional Transport

Vectorial transport is an asymmetrical transport across a monolayer of polarized cells, and it plays a major role in the intestinal absorption of drugs from the viewpoint of drug absorption and disposition (1). After screened the effect of these monoglycerides on Pgp and MRP using Rh123, the bi-directional transport study was conducted using $E_2$17βG as the substrate to assess the transport activity of MRP2.

In the $E_2$17βG bi-directional transport study, it had shown that all three monoglycerides treatments lowered their efflux ratios compared to the control (Table 12). However, efflux ratios should be interpreted with caution as they could not indicate which side of the cell membrane was affected by the treatments. In Figure 24, Caco-2 cells treated with monopalmitin increased the absorptive (the apical to basolateral) transport while maintained its efflux transport (basolateral to apical) compared to the control; on the contrary, cells treated with monoolein and monostearin decreased their secretory transport without changing their absorptive transport (apical to basolateral) compared to the control. Therefore, these suggested that there may not be a generalized mechanism applying to all monoglycerides on how they affecting transporters' activities.

The unchanged basolateral to apical flux and enhanced apical to basolateral flux of $E_2$17βG in monopalmitin treated cells suggested that monopalmitin may not affect the functional activities of efflux transporter like MRP2 on the apical side of the monolayer, instead it may affect apical to basolateral transport of $E_2$17βG by stimulating uptake activity of absorptive transporters on the apical side in Caco-2 cells. In recent years, studies had shown that $E_2$17βG is also the substrate for a major intestinal absorptive transporter, organic anion transporting polypeptide (OATP) (156).

Another possibility that could account for the increased permeability in the absorptive direction for monopalmitin treated cells was the critical micelle concentration (CMC) issue. The critical micelle concentration is defined as the concentration of surfactants above which micelles are spontaneously formed. Since the CMC for monopalmitin is at 850 μM, the concentration used in the study (ie. 1000 μM) was greater than its CMC value (157). When concentrations of monoglycerides are above their CMC values, micelles will form, which facilitate permeation across the thick unstirred water layer above Caco-2 cells.

As for the other two monoglycerides, the CMC values of monostearin and monoolein are 610 μM and 820 μM, respectively (157). Since the actual concentrations of monostearn and monoolein are 1000 μM and 500 μM, respectively, monoolein is the only monoglyceride has a concentration below its CMC value. The permeability coefficient in absorptive direction for monolein treated cells is closest to the control value. As for monostearin, although it didn't exhibit a significant difference in its apparent permeability coefficient in the absorptive direction due to a large standard deviation, its mean value of the $P_{app,ab}$ is much higher than that of the control.

For monostearin and monoolein treated cells, the basolateral to apical transports of $E_2$17βG were reduced while apical to basolateral transports remained unchanged compared to control (Figure 24). Thus, the decrease in

efflux transport of $E_2$17βG in cells treated with monostearin and monoolein might be partially accounted by the attenuation of the functional activity of MRP2.

Furthermore, it was noticed that monopalmitin has a 16-carbon saturated acyl chain attached to the glycerol backbone; whereas monostearin and monoolein have one saturated and another unsaturated 18-carbon acyl chains, respectively, attached to the glycerol backbone. It was speculated that the chain lengths of the monoglycerides might play a role in selectively affecting the functional activities of enterocyte based efflux/uptake transporters.

5.6 Monoglycerides: MRP2 Protein Expression

A possible explanation for the reduced activity of MRP2 upon treatments of monoglycerides is the observed decrease in MRP2 protein expression. A study done by Barta *et al.* has partially linked the reduction in Pgp activity with the attenuation of Pgp protein expression when treated with 500 μM of monoolein and monostearin (29). In this study, I investigated whether attenuation of MRP2 protein expression could be partially accounted for the decrease in MRP2 activity caused by monoglycerides. Our data had indicated monopalmitin and monoolein treated cells has shown decreased MRP2 protein expression while monostearin had shown no change in MRP2 protein expression in Caco-2 cells (Figure 25-27).

Although monostearin has shown the greatest reduction in MRP2 transport activity, it did not affect the MRP2 protein expression level (Table 12 and Figure 27). Hence, monostearin must attenuate the functional activity of MRP2 through other mechanisms. It might act in a similar fashion to the Pluronic block copolymers on Pgp by either depleting intracellular ATP or inhibiting the ATPase activity of the efflux transporters (120,158). The reduction in MRP2 activity may also be the result of conformational changes of the efflux transporters due to monostearin caused changes in membrane fluidity and/or nonspecific steric hindrance of the drug-binding sites. Monostearin might accumulate in the cytosolic compartment of Caco-2 cells which directly inhibit the MRP2-mediated transport.

Monopalmitin treated cells had shown a lesser degree of MRP2 down-regulation at a much higher concentration compared to the monoolein treated cells. Since it mostly affected the apical to basolateral transport, monopalmitin may not have a significant impact on MRP2 activity. Although MRP2 protein expression was downregulated as the result of monopalmitin treatment, the permeability coefficient in the efflux direction didn't change (Table 12 and Figure 26). Monopalmitin may have stimulated the activity of other efflux transporters, such as BCRP, which acts as compensatory mechanism for the reduced number of MRP2 available.

For monoolein treated cells, there was a significant reduction in MRP2 protein expression compared to the control. Thus, the down-regulation of MRP2 protein expression by monoolein treatment might be partially accounted for the accumulation of Rh123 and reduction of $E_2$17βG efflux. The monoglycerides had already shown to effect the protein expression of another major ABC efflux transporter, Pgp. A membrane fluidity study by Barta *et al.* has shown that monoglycedie could change membrane fluidity (29). This is not surprising because that monoolein has an unsaturated fatty acid attached to its glycerol backbone. Degrees of unsaturation have been previously noted to alter the packing order of phospholipid bilayers (159). The kink in the hydrocarbon chain might have an effect on fluidity of the cell membrane.

The decrease in MRP2 protein expression caused by the 24-hour monoglyceride treatment is believed to occur at the transcriptional level. A study done by Risovic et al. has shown that the decrease in Pgp protein expression caused by Peceol was resulted from the downregulation of MDR1 gene (14). Transcriptional regulation confers the ability to regulate expression over a longer period of time. The MRP2 protein has a half life of 27 hours. Thus, 24-hour incubation with the monoglyceride could be considered as a prolonged exposure.

This is the first study to our knowledge that has shown a specific monoglyceride could reduce the activity of MRP2, a major enterocyte efflux transporter, by down-regulating its protein expression in Caco-2 cells.

5.7 Limitations

The small intestine is a very dynamic environment; in contrast, Caco-2 cell model is a relatively static model consisting of one single cell type with a thicker unstirred water layer than *in vivo* situation (160). Thus, the exact concentrations of monoglycerides that the intestinal cells might be exposed to in an *in vivo* situation were difficult to assess and correlate with the concentrations used in the cell studies.

Another major limitation of this study was that there is no specific substrate for MRP2. However, this concern was partially accounted for by using two different types of substrates to assess the activity of MRP2.

5.8 Conclusions

In conclusion, these findings suggested that monoolein, monostearin and monopalmitin could attenuate the efflux activities partially by modulation of enterocyte-based efflux transporters, such as MRP2, in Caco-2 cells. Furthermore, the reduction of MRP2 efflux activity in monoolein treated cells could be partially accounted by the down-regulation of MRP2 protein expression.

5.9 Future Research

Treatment groups used in this study were incubated with these three monoglyceride for 24 hours. Since many lipid-formulated oral drugs were

administered on a relatively long-term basis, the effect of longer exposure of these monoglycerides in Caco-2 cells could be explored in the future. Some preliminary studies of cells treated with monoglycerides for 48-hour and 72-hour had already shown a greater percentage of Rh123 accumulation than they were when treated for 24-hour in Caco-2 cells (data not shown).

Results from our lab has pointed out that monoolein could downregulate Pgp protein expression as well (29). Thus, it was speculated that monoolein might have some indirect interplays with nuclear receptors at the transcriptional level to exert a non-specific downregulation on ABC efflux transporters. Recently, a number of nuclear receptors, such as retinoic acid receptor (RAR), steroid-activated receptor (SXR), farnesoid receptor (FXR), and constitutive androstane receptor (CAR) have been implicated in the transcriptional control of transport proteins (161-163). A number of studies have shown these nuclear receptors could exert global transcriptional control over MRP2 and Pgp in response to rifampin treatment (164, 165). Therefore, the effect of monoglycerides on protein expression of nuclear receptors should also be pursued.

Since this project was conducted using a cell-based model, the effects of these monoglycerides on ABC efflux transporters in enterocytes need to be determined in a more physiologically relevant system, for instance, an MRP2 knock-out mouse model.

The mRNA levels of MRP2 and other major efflux transporters as well as some nuclear receptors could be determined to assess the effects of monoglycerides at the transcriptional level. If lipids or lipid excipients indeed influence efflux transporters' expressions, pharmaceutical industry and the regulatory agencies need to address the concerns in drug formulation development.

Although Rh123 was not a specific substrate, the relative expression level of MRP2 comparing to other ABC transporters in Caco-2 cells makes it somewhat reflective of the efflux activity of MRP2. The four majorly ABC transporters expressed in Caco-2 cells are MRP2, BCRP, MRP3 and Pgp. MRP2 relative expression level was about 2-fold higher than BCRP and 4-fold higher than MRP3 and Pgp (140). Since Rh123 is not a substrate for BCRP in Caco-2 cells, the increase in accumulation of Rh123 at least could partially contribute to the attenuation of the MRP2 activity.

REFERENCES

1. L.L. Buxton. Pharmacokinetics and Pharmacodynamics: The Dynamics of Drug Absorption, Distribution, Action, and Elimination. In LL. Brunton, JS. Lazo and K. Parker (eds.), Goodman & Gilman's the Pharmacological Basis of Therapeutics, 11th ed., McGraw-Hill Companies, Inc, USA, 2006, pp 1-40.

2. C.J.H. Porter, N. L. Trevaskis, and W.N. Charman. Lipids and lipid-based formulations: optimizing the oral delivery of lipophilic drugs. Nat Rev Drug Discov. 6:231-248 (2007).

3. R.N. Gursoy and S. Benita. Self-emulsifying drug delivery systems (SEDDS) for improved oral delivery of lipophilic drugs. Biomed Pharmacother. 58:173-182 (2004).

4. C.A. Lipinski. Drug-like properties and the causes of poor solubility and poor permeability. J Pharmacol Toxicol Methods. 44:235-249 (2000).

5. P.P. Constantinides and K.M. Wasan. Advances in lipid-based drug solubilization and targeting. Adv Drug Deliv Rev. 56:1239-1240 (2004).

6. K.S. Pang. Modeling of intestinal drug absorption: roles of transporters and metabolic enzymes. Drug Metab Dispos. 31:1507-1519 (2003).

7. C.W. Pouton. Formulation of self-emulsifying drug delivery systems. Adv Drug Deliv Rev. 25:47-58 (1997).

8. A. J. Humberstone and W. N. Charman. Lipid-based vehicles for the oral delivery of poorly water soluble drugs. Adv Drug Deliv Rev. 25:103-128 (1997).

9. T. H. Liao, P. Hamosh, and M. Hamosh. Fat digestion by lingual lipase: mechanism of lipolysis in the stomach and upper small intestine. Pediatr Res. 18:402-409 (1984).

10. M. Hamosh, J. W. Scanlon, D. Ganot, M. Likel, K. B. Scanlon, and P. Hamosh. Fat digestion in the newborn: characterization of lipase in gastric aspirates of premature and term infants. J Clin Invest. 67:838-846 (1981).

11. W.N. Charman, C.J.H. Porter, S. Mithani, and J.B. Dressman. Physiochemical and physiological mechanisms for the effects of food on drug absorption: the role of lipids and pH. J Pharm Sci. 86:269-282 (1997).

12. A. J. Humberstone and W. N. Charman. Lipid-based vehicles for the oral delivery of poorly water soluble drugs. Adv Drug Deliv Rev. 25:103-128 (1997).

13. C.J.H. Porter and W.N. Charman. Intestinal Lymphatic Drug Transport: an Update. Adv Drug Deliv Rev, 50:61-80 (2001).

14. V. Risovic, K. Sachs-Barrable, M. Boyd, and K.M. Wasan. Potential mechanisms by which Peceol increases the gastrointestinal absorption of Amphotericin B. Drug Dev Ind Pharm. 30:767-774 (2004).

15. K. Sachs-Barrable, A. Thamboo, S.D. Lee, and K.M. Wasan. Lipid excipients Peceol and Gelucire 44/14 decrease P-glycoprotein mediated efflux of rhodamine 123 partially due to modifying P-glycoprotein protein expression within Caco-2 cells. J Pharm Pharm Sci. 10:319-331 (2007).

16. B.K. Nordskog, C.T. Phan, D.F. Nutting, and P. Tso. An examination of the factors affecting intestinal lymphatic transport of dietary lipids. Adv Drug Deliv Rev. 50: 21–44 (2001).

17. J. Borovicka, W. Schwizer, C. Mettraux, C. Kreiss, B. Remy, K. Asal, J.B.M.J Jansen, I. Douchet, R. Verger, and M. Fried. Regulation of gastric and pancreatic lipase secretion by CCK and cholinergic mechanisms in humans. Am J Physiol. 273: 374-380 (1997).

18. H. Moreau, A. Bernadac, Y. Gargouri, F. Benkouka, R. Laugier, and R. Verger. Immunocytolocalization of human gastric lipase in chief cells of the fundic mucosa. Histochemistry. 91: 419–423 (1989).

19. A.B.R. Thomson, M. Keelan, M.L. Garg, and M.T. Clandinin. Intestinal aspects of lipid absorption: in review. Can J Physiol Pharmacol. 67: 179–191 (1989).

20. W.C. Duane, R.L. Ginsberg, and L.J. Bennion. Effects of fasting on bile acid metabolism and biliary lipid composition in man. J Lipid Res. 17:211–219 (1976).

21. A.B. Thomson, C. Schoeller, M. Keelan, L. Smith, and M.T. Clandinin. Lipid absorption: passing through the unstirred layers, brush-border membrane, and beyond. Can J Physiol Pharmacol. 71: 531–555 (1993).

22. P. Artursson, A.L. Ungell, and J.E. Lofroth. Selective paracellular permeability in two models of intestinal absorption, cultured monolayers of human intestinal epithelial cells and rat intestinal segments. Pharm Res. 10: 1123-1129 (1993).

23. V. Pade and S. Stavchansky. Estimation of the relative contribution of the transcellular and paracellular pathway to the transport of passively absorbed drugs in the Caco2 cell culture model. Pharm Res. 14: 1210-1215 (1997).

24. Y. Huang, P. Anderle, K.J. Bussey, C. Barbacioru, U. Shankavaram, Z. Dai, W.C. Reinhold, A. Papp, J.N. Weinstein, and W. Sadée. Membrane transporters and channels: role of the transportome in cancer chemosensitivity and chemoresistance. Cancer Res. 64: 4294-4301 (2004).

25. A. Tsuji and I. Tamai. Carrier-mediated intestinal transport of drugs. Pharm Res. 13: 962-977 (1996).

26. B. Steffansen, C.U. Nielsen, B. Broden, A.H. Eriksson, R. Andersen, and S. Frokjaer. Intestinal solute carriers: an overview of trends and strategies for improving oral drug absorption. Eur J Pharm Sci. 21: 3-16 (2004).

27. C.F. Higgins. ABC transporters: from microorganisms to man. Annu Rev Cell Biol. 8:67-113 (1992).

28. T. Konishi, H. Satsu, Y. Hatsugai, K. Aizawa, T. Inakuma, S. Nagata, S. H. Sakuda, H. Nagasawa, and M. Shimizu. A bitter melon extract inhibits the P-glycoprotein activity in intestinal Caco-2 cells: monoglyceride as an active compound. Biofactors. 22: 71-74 (2004).

29. C. A. Barta, K. Sachs-Barrable, F. Feng, and K. M. Wasan. Effects of Monoglycerides on P-Glycoprotein: Modulation of the Activity and Expression in Caco-2 Cell Monolayers. Mol Pharm. (2008).

30. E.D. Hugger, B.L. Novak, P.S. Burton, K.L. Audus, R.T. Borchard, and T. Ronald. A Comparison of Commonly Used Polyethoxylated Pharmaceutical Excipients on Their Ability to Inhibit P-glycoprotein Activity In Vitro. J Pharm Sci. 91:1991-2002 (2002).

31. B.D. Rege, J.P.Y. Kao, and J.E. Polli. Effects of nonionic surfactants on membrane transporters in Caco-2 cell monolayers. Eur J Pharm Sci. 16:237-246 (2002).

32. Y. Lo. Phospholipids as multidrug resistance modulators of the transport of epirubicin in human intestinal epithelial Caco-2 cell layers and everted gut sacs of rats. Biochem Pharmacol. 60:1381-1390 (2000).

33. N. L. Trevaskis, W. N. Charman, and C. J. H. Porter. Lipid-based delivery systems and intestinal lymphatic drug transport: A mechanistic update. Adv Drug Delivery Rev. 60:702-716 (2008).

34. L.V. Leak. The structure of lymphatic capillaries in lymph formation. Fed Proc. 35:1863-1871 (1976).

35. S.M. Sieber, V.H. Cohn, and W. T. Wynn. The entry of foreign compounds into the thoracic duct lymph of the rat. Xenobiotica. 4:265-284 (1974).

36. M. P. Mcintosh, C. J. H. Porter, K. M. Wasan, M. Ramaswamy, and K. M. Wasan. Differences in the lipoprotein binding profile of halofantrine in fed and fasted human or beagle plasma are dictated by the respective masses of core apolar lipoprotein lipid. J Pharm Sci. 88:378-384 (1999).

37. K. Sachs-Barrable, S. D. Lee, E. K. Wasan, S. J. Thornton, and K. M. Wasan. Enhancing drug absorption using lipids: a case study presenting the development and pharmacological evaluation of a novel lipid-based oral amphotericin B formulation for the treatment of systemic fungal infections. Adv Drug Deliv Rev. 60:692-701 (2008).

38. S.M. Khoo, D.M. Shackleford, C.J.H. Porter, G.A. Edwards, and W.N. Charman. Intestinal lymphatic transport of Halofantrine occurs after oral administration of a unit-dose lipid-based formulation to fasted dogs. Pharm Res. 20: 1460-1465 (2003).

39. D.M. Shackleford, W.A. Faassen, N. Houwing, H. Lass, G.A. Edwards, C.J.H. Porter, and W.N. Charman. Contribution of lymphatically transported testosterone undecanoate to the systemic exposure of testosterone after oral administration of two andriol formulations in conscious lymph duct-cannulated dogs. J Pharmacol Exp Ther. 306: 925-933 (2003).

40. G.L. Amidon, H. Lennernas, V.P. Shah, and J.R. Crison. A theoretical basis for a biopharmaceutics drug classification: the correlation of in vitro drug product dissolution and in vivo bioavailability. Pharm Res. 12: 413-420 (1995)

41. Waiver of in vivo bioavailability and bioequivalence studies for immediate-release solid oral dosage forms based on a biopharmaceutics classification system. http://www.fda.gov/cder/guidance/3618fnl.htm (accessed 7/15/08), part of Food and Drug Administration: Guidance for Industry: http://www.fda.gov/cder/guidance/index.htm (accessed 07/15/08).

42. C.Y. Wu and L.Z. Benet. Predicting drug disposition via application of BCS: transport/absorption/elimination interplay and development of a biopharmaceutics drug disposition classification system. Pharm Res. 22: 11-23 (2005).

43. C.A. Lipinski, F. Lombardo, B.W. Dominy, and P.J. Feeney. Experimental and computational approaches to estimate solubility and permeability in drug discovery and development settings. Adv Drug Deliv Rev. 46: 3-26 (2001).

44. M.H. Stipanuk. Digestion and absorption of macronutrients. In M. H. Stipanuk (ed.), Biochemical and Physiological Aspects of Human Nutrition, WB Saunders Company, Philadelphia, 2000, pp 75-152.

45. W.F. Ganong. Review of Medical Physiology 22nd ed., McGraw-Hill Companies, Inc., USA, 2005.

46. K. S. Pang, L. Liu, and H. Sun. Interaction of Drug Transporters with Excipients. In K. Wasan (ed.), Role of Lipid Excipients in Modifying Oral and Parenteral Drug Delivery, John Wiley & Sons, Inc., US, 2006, pp. 1-31.

47. E.W. Strauss. Electron microscopic study of intestinal fat absorption in vitro from mixed micelles containing linolenic acid, monoolein, and bile salt. J Lipid Res. 7: 307-323 (1966).

48. W. Stremmel. Uptake of fatty acids by jejunal mucosal cells is mediated by a fatty acid binding membrane protein. J Clin Invest. 82:2001-2010 (1988).

49. N.L. Trevaskis, M.L. Chun, Y.M. Li, P. Tso, H.R. Irving, C.J.H. Porter, and W.N. Charman. An acute and coincident increase in FABP expression and lymphatic lipid and drug transport occurs during intestinal infusion of lipid-based drug formulations to rats. Pharm Res. 23:1786-1796 (2006).

50. M. Dean, Y. Hamon, and G. Chimini. The human ATP-binding cassette (ABC) transporter superfamily. J Lipid Res. 42:1007-1017 (2001).

51. S. Choudhuri and C. D. Klaassen. Structure, function, expression, genomic organization, and single nucleotide polymorphisms of human ABCB1 (MDR1), ABCC (MRP), and ABCG2 (BCRP) efflux transporters. Int J Toxicol. 25:231-259 (2006).

52. A. Aleksandrov, L. Aleksandrov, and J. Riordan. CFTR (ABCC7) is a hydrolyzable-ligand-gated channel. Pflügers Arch Euro J Physiol. 453: 693-702 (2007).

53. S.C. Hyde, P. Emsley, M.J. Hartshorn, M. M. Mimmack, U. Gileadi, S. R.Pearce, M.P. Gallagher, D.R. Gill, R.E. Hubbard, and C.F. Higgins. Structural model of ATP-binding proteins associated with cystic fibrosis, multidrug resistance and bacterial transport. Nature. 346: 362–365 (1990).

54. J.F. Oram. Tangier disease and ABCA1. Mol Cell Biol Lipids. 1529: 321-330 (2000).

55. C. Gerth, M. Andrassi-Darida, M. Bock, M.N. Preising, B.H. Weber, and B. Lorenz. Phenotypes of 16 Stargardt macular dystrophy/fundus flavimaculatus patients with known ABCA4 mutations and evaluation of

genotype-phenotype correlation. Graefe's Arch Clin Exp Ophthalm. 240:628-638 (2002).

56. V. Keitel, A. T. Nies, M. Brom, J. Hummel-Eisenbeiss, H. Spring, and D. Keppler. A common Dubin-Johnson syndrome mutation impairs protein maturation and transport activity of MRP2 (ABCC2). Am J Physiol Gastrointest Liver Physiol. 284: 165-174 (2003).

57. A.S. Plomp, R.J. Florijn, J.T. Brink, B. Castle, H. Kingston, A. Martin-Santiago, T.G. Gorgels, P.T. de Jong, and A. A. Bergen. ABCC6 mutations in pseudoxanthoma elasticum: an update including eight novel ones. Mol Vis. 14:118-124 (2008).

58. C.F. Higgins and K.J. Linton. The ATP switch model for ABC transporters. Nat Struct Mol Biol. 11: 918–926 (2004).

59. E.M. Leslie, R.G. Deeley, and S.P. Cole. Multidrug resistance proteins: Role of P-glycoprotein, MRP1, MRP2, and BCRP (ABCG2) in tissue defense. Toxicol Appl Pharmacol. 204: 216–237 (2005).

60. M.M. Gottesman, T. Fojo, and S.E. Bates. Multidrug resistance in cancer: role of ATP-dependent transporters. Nat Rev Cancer. 2: 48-58 (2002).

61. R.G. Deeley, C. Westlake, and S.PC. Cole. Transmembrane transport of endo- and xenobiotics by mammalian ATP-binding cassette multidrug resistance proteins. Physiol Rev. 86: 849-899 (2006).

62. G. Chang and C.B. Roth. Structure of MsbA from E. coli: A Homolog of the Multidrug Resistance ATP Binding Cassette (ABC) Transporters. Science. 293:1793-1800 (2001).

63. P. Ramakrishnan. The Role of P-glycoprotein in the blood-brain barrier. Einstein Quart J Biol Med. 19: 160–165 (2003).

64. P. Borst and A.H. Schinkel. Genetic dissection of the function of the mammalian P-glycoproteins. Trends Genet. 13: 217–222 (1997).

65. K. M. Wasan, K. Sachs-Barrable, and S. D. Lee. Potential mechanisms by which lipid excipients increase the oral gastrointestinal absorption of drugs: A case study using amphotericin B. Bulletin technique Gattefossé. 99: 31-42 (2006).

66. J.E. Walker, M. Saraste, M.J. Runswick, and N.J. Gay. Distantly related sequences in the alpha- and beta-subunits of ATP synthase, myosin, kinases and other ATP-requiring enzymes and a common nucleotide binding fold. EMBO J. 1: 945-951 (1982).

67. C.F. Higgins and M.M. Gottesman. Is the multidrug transporter a flippase? Trends Biochem Sci. 17: 18–21 (1992).

68. E. Teodori, S. Dei, C. Martelli, S. Scapecchi, and F. Gualtieri. The functions and structure of ABC transporters: implications for the design of new inhibitors of Pgp and MRP1 to control multidrug resistance (MDR). Curr Drug Targets. 7: 893-909 (2006).

69. E.M. Leslie, R.G. Deeley, and S.P.C. Cole. Multidrug resistance proteins: role of P-glycoprotein, MRP1, MRP2, and BCRP (ABCG2) in tissue defense. Toxicol Appl Pharmacol. 204: 216-237 (2005).

70. A. Geick, M. Eichelbaum, and O. Burk. Nuclear receptor response elements mediate induction of intestinal mdr1 by rifampin. J Biol Chem. 276: 14581–14587 (2001).

71. S. Choudhuri and L.G. Valerio. Usefulness of studies on the molecular mechanism of action of herbals/botanicals: The case of St. John's wort. J Biochem Mol Toxicol. 19: 1–11 (2005).

72. G.D. Kruh and M.G. Belinsky. The MRP family of drug efflux pumps. Oncogene. 22: 7537-7552 (2003).

73. G.D Kruh, M.G Belinsky, J. Gallo, and K. Lee. Physiological and pharmacological functions of Mrp2, Mrp3 and Mrp4 as determined from recent studies on gene-disrupted mice. Cancer Metastasis Rev. 26: 5-14 (2007).

74. Ulrike Gradhand and Richard B. Kim. Pharmacogenomics of MRP Transporters (ABCC1-5) and BCRP (ABCG2). Drug Metabolism Reviews. 40:317 - 354 (2008).

75. S.P. Cole, G. Bhardwaj, J.H. Gerlach, J.E. Mackie, C.E. Grant, K.C. Almquist, A.J. Stewart, E.U. Kurz, A.M. Duncan, and R.G. Deeley. Overexpression of a transporter gene in a multidrug-resistant human lung cancer cell line. Science. 258:1650-1654 (1992).

76. I. Leier, G. Jedlitschky, U. Buchholz, M. Center, S.P. Cole, R.G. Deeley, and D. Keppler. ATP-dependent glutathione disulphide transport mediated by the MRP gene-encoded conjugate export pump. Biochem J. 314: 433–437 (1996).

77. I. Leier, G. Jedlitschky, U. Buchholz, M. Center, S.P. Cole, R.G. Deeley, and D. Keppler. The MRP gene encodes an ATP-dependent export pump for leukotriene C4 and structurally related conjugates. J Bio Chem. 269:27807 -27810 (1994).

78. S. Conrad, H.M. Kauffmann, K.I. Ito, E.M. Leslie, R.G. Deeley, D. Schrenk, and S.P.C. Cole. A naturally occurring mutation in MRP1 results in a selective decrease in organic anion transport and in increased doxorubicin resistance. Pharmacogenetics. 12:321-330 (2002).

79. O. Janneh, A. Owen, B. Chandler, R.C. Hartkoorn, C.A. Hart, P.G. Bray, S.A. Ward, D.J. Back, and S.H. Khoo. Modulation of the intracellular accumulation of saquinavir in peripheral blood mononuclear cells by inhibitors of MRP1, MRP2, P-gp and BCRP. AIDS. 19:2097-2102 (2005).

80. M.M. Gottesman and I. Pastan. Biochemistry of multidrug resistance mediated by the multidrug transporter. Annu Rev Biochem. 62: 385–427 (1993).

81. S. Ryu, T. Kawabe, S. Nada, and A. Yamaguchi. Identification of Basic Residues Involved in Drug Export Function of Human Multidrug Resistance-associated Protein 2. J Biol Chem. 275: 39617-39624 (2000).

82. K. Taniguchi, M. Wada, K. Kohno, T. Nakamura, T. Kawabe, M. Kawakami, K. Kagotani, K. Okumura, S. Akiyama, and M. Kuwano. A Human Canalicular Multispecific Organic Anion Transporter (cMOAT) Gene Is Overexpressed in Cisplatin-resistant Human Cancer Cell Lines with Decreased Drug Accumulation. Cancer Res. 56: 4124-4129 (1996).

83. U. Hoffmann and H.K. Kroemer. The ABC transporters MDR1 and MRP2: multiple functions in disposition of xenobiotics and drug resistance. Drug Metab Rev. 36:669-701 (2004).

84. Y. Cui, J. Konig, U. Buchholz, H. Spring, I. Leier, and D. Keppler. Drug Resistance and ATP-Dependent Conjugate Transport Mediated by the Apical Multidrug Resistance Protein, MRP2, Permanently Expressed in Human and Canine Cells. Mol Pharmacol. 55: 929-937 (1999).

85. O. Fardel, E. Jigorel, M. LeVee, and L. Payen. Physiological, pharmacological and clinical features of the multidrug resistance protein 2. Biomed Pharmacother. 59:104-114 (2005).

86. I.F. Faneyte, P.M. Kristel, and M.J. Vijver. Multidrug resistance associated genes MRP1, MRP2 and MRP3 in primary and anthracycline exposed breast cancer. Anticancer Res. 24:2931-2939 (2004).

87. G. Jedlitschky, I. Leier, U. Buchholz, J. Hummel-Eisenbeiss, B. Burchell, and D. Keppler. ATP-dependent transport of bilirubin glucuronides by the multidrug resistance protein MRP1 and its hepatocyte canalicular isoform MRP2. Biochem J. 327:305-310 (1997).

88. G.L. Scheffer, M. Kool, M. de Haas, J.M. Vree, A.C.L.M. Pijnenborg, D. K. Bosman, R.P.J.O. Elferink, P. van der Valk, P. Borst, and R. J. Scheper. Tissue distribution and induction of human multidrug resistant protein 3. Lab Invest. 82:193-201 (2002).

89. D.W. Zhang, H.M Gu, M. Vasa, M. Muredda, S.P.C. Cole, S.P.C. Cole, and Deeley G.R. Characterization of the role of polar amino acid residues within predicted transmembrane helix 17 in determining the substrate specificity of multidrug resistance protein 3. Biochem. 42:9989-10000 (2003).

90. M.J. Zamek-Gliszczynski, K. Nezasa, X. Tian, A.S. Bridges, K. Lee, M.G. Belinsky, G.D. Kruh, and K.L.R. Brouwer. Evaluation of the Role of Multidrug Resistance-Associated Protein (Mrp) 3 and Mrp4 in Hepatic Basolateral Excretion of Sulfate and Glucuronide Metabolites of Acetaminophen, 4-Methylumbelliferone, and Harmol in Abcc3-/- and Abcc4-/- Mice. J Pharmacol Exp Ther. 319: 1485-1491 (2006).

91. N. Zelcer, K. van de Wetering, M. Hillebrand, E. Sarton, A. Kuil, P. Wielinga, T. Tephly, A. Dahan, J. Beijnen, and P.H. Borst. Mice lacking multidrug resistance protein 3 show altered morphine pharmacokinetics and morphine-6-glucuronide antinociception. Proc. Natl. Acad. Sci. USA 102:7274-7279 (2005).

92. D. van der Kolk, E. de Vries, J. Koning, E. van den Berg, M. Muller, and E. Vellenga. Activity and expression of the multidrug resistance proteins MRP1 and MRP2 in acute myeloid leukemia cells, tumor cell lines, and normal hematopoietic CD34+ peripheral blood cells. Clin Cancer Res. 4:1727-1736 (1998).

93. A.W. Torky, E. Stehfest, K. Viehweger, C. Taege, and H.Foth. Immuno-histochemical detection of MRPs in human lung cells in culture. Toxicology. 207: 437-450 (2005).

94. M. Rius, A.T. Nies, J. Hummel-Eisenbeiss, G. Jedlitschky, and D. Keppler. Cotransport of reduced glutathione with bile salts by MRP4 (ABCC4) localized to the basolateral hepatocyte membrane. Hepatology. 38:374-384 (2003).

95. L. Kun, A.J.P. Klein-szanto, and G.D. Kruh. Analysis of the MRP4 drug resistance profile in transfected NIH3T3 cells. J Natl Cancer Inst. 92:1934-1940 (2000).

96. A.T Nies, G. Jedlitschky, J. König, C Herold-Mende, H.H. Steiner, H.P Schmitt, and D. Keppler Expression and immunolocalization of the

multidrug resistance proteins, MRP1-MRP6 (ABCC1-ABCC6), in human brain. Neuroscience. 129:349-360 (2004).

97. J. Konig, M. Hartel, A.T. Nies, M.E. Martignoni, J.C. Guo, M.W. Buchler, H. Friess, and D.Keppler. Expression and localization of human multidrug resistance protein (ABCC) family members in pancreatic carcinoma. Int J Cancer. 115:359-367 (2005).

98. P.R. Wielinga, I. Van der Heijden, G. Reid, J.H. Beijnen, J. Wijnholds, and P. Borst. Characterization of the MRP4- and MRP5-mediated transport of cyclic nucleotides from intact cells. J Biol Chem. 278:17664-17671 (2003).

99. A.A.B. Bergen, A.S. Plomp, E.J. Schuurman, S. Terry, M. Breuning, H. Dauwerse, J. Swart, M. Kool, S. van Soest, F. Baas, J.B. ten Brink and P.T.V.M. de Jong. Mutations in ABCC6 cause pseudoxanthoma elasticum. Nature Genetics. 25:228-231 (2000).

100. M. Kool, M. v. d. Linden, M. de Haas, F. Baas, and P. Borst. Expression of Human MRP6, a Homologue of the Multidrug Resistance Protein Gene MRP1, in Tissues and Cancer Cells. Cancer Res. 59:175-182 (1999).

101. Z. S. Chen, E. Hopper-Borge, M. G. Belinsky, I. Shchaveleva, E. Kotova, and G. D. Kruh. Characterization of the transport properties of human multidrug resistance protein 7 (MRP7, ABCC10). Mol Pharmacol. 63:351-358 (2003).

102. Y. Guo, E. Kotova, Z. Chen, K. Lee, E. Hopper-Borge, M.G. Belinsky, and G. D. Kruh. MRP8 (ABCC11) is a cyclic nucleotide efflux pump and a resistance factor for fluoropyrimidines, 2'3'-dideoxycytidine and 9'-(2'-phosphonylmethoxyethyl)-adenine. J Biol Chem. 278:29509-29514(2003).

103. N. Zelcer, M.T. Huisman, G. Reid, P. Wielinga, P. Breedveld, A. Kuil, P. Knipscheer, J.H.M. Schellens, and A.H. Schinkel. Evidence for two interacting ligand binding sites in human multidrug resistance protein 2 (ATP binding cassette C2), J Biol Chem. 278: 23538–23544 (2003).

104. S.B.M. Fernández, Z. Holló, A. Kern, É. Bakos, P.A. Fischer, P. Borst, and R. Evers. Role of the N-terminal transmembrane region of the multidrug resistance protein MRP2 in routing to the apical membrane in MDCKII cells. J Biol Chem. 277: 31048–31055 (2002).

105. L. L. Brunton, J. S. Lazo, and K. Parker. Membrane Transporters and Drug Response. In Goodman & Gilman's the Pharmacological Basis of Therapeutics, 11th Edition, McGraw-Hill Companies, Inc., USA, 2006.

106. S. Choudhuri and C.D. Klaassen. Structure, function, expression, genomic organization, and single nucleotide polymorphisms of human ABCB1

(MDR1), ABCC (MRP), and ABCG2 (BCRP) efflux transporters. Int J Toxicol. 25:231-259 (2006).

107. H.R. Horton, L.A. Moran, R.S.R.D. Ochs, and K. G. Scrimgeour. Principles of Biochemistry, Prenhall Inc., USA, 2002.

108. R.M.C. Dawson. Data for Biochemical Research, 3rd ed., Oxford University Press, New York, 1986.

109. M. F. Horster and M. Stopp. Transport and metabolic functions in cultured renal tubule cells. Kidney Int. 29: 46-53 (1986).

110. M. Horio, K. Chin, S. Currier, S. Goldenberg, C. Williams, I. Pastan, M. Gottesman, and J. Handler. Transepithelial transport of drugs by the multidrug transporter in cultured Madin-Darby canine kidney cell epithelia. J Biol Chem. 264:14880-14884 (1989).

111. J. D. Irvine, L. Takahashi, K. Lockhart, J. Cheong, J.W. Tolan, H.E. Selick, J.R. Grove. MDCK (Madin-Darby canine kidney) cells: A tool for membrane permeability screening. J Pharm Sci. 88: 28-33 (1999).

112. A. Braun, S. Hammerle, K. Suda, B. Rothn-Ruthishauer, M. Guthert, S.D. Kramer, and H. Wunderli-Allenspach. Cell cultures as tools in biopharmacy. Eur J Pharm Sci. 11: S51-S60 (2000).

113. R. Evers, M. Kool, L. van Deemter, H. Janssen, J. Calafat, L.C. Oomen, C.C. Paulusma, R.P.O. Elferink, F. Baas, A.H. Schinkel, and P. Borst. Drug Export Activity of the Human Canalicular Multispecific Organic Anion Transporter in Polarized Kidney MDCK Cells Expressing cMOAT (MRP2) cDNA. J Clin Invest. 101: 1310-1319 (1998).

114. F. Tang, K. Horie, and R.T. Borchardt. Are MDCK cells transfected with the human MRP2 gene a good model of the human intestinal mucosa? Pharm Res. 19: 773-779 (2002).

115. P.V. Balimane, S. Chong, and R.A. Morrison. Current methodologies used for evaluation of intestinal permeability and absorption. J Pharmacol Toxicol Methods. 44: 301-312 (2000).

116. J. Taipalensuu, H. Törnblom, G. Lindberg, C. Einarsson, F. Sjöqvist, H. Melhus, P. Garberg, B. Sjöström, B. Lundgren, and P. Artursson. Correlation of gene expression of ten drug efflux proteins of the ATP-binding cassette transporter family in normal human jejunum and in human intestinal epithelial Caco-2 cell monolayers. J Pharmacol Exp Ther. 299: 164-170 (2001).

117. P. Artursson, K. Palm, and K. Luthman. Caco-2 monolayers in experimental and theoretical predictions of drug transport. Adv Drug Deliv Rev. 46: 27-43 (2001).

118. G. Englund, F. Rorsman, A. Rönnblom, U. Karlbom, L. Lazorova, J. Gråsjö, A. Kindmark, and P. Artursson. Regional levels of drug transporters along the human intestinal tract: co-expression of ABC and SLC transporters and comparison with Caco-2 cells. Eur J Pharm Sci. 29: 269-277 (2006).

119. D.J. Hauss, S.E. Fogal, J.V. Ficorilli, C.A. Price, T. Roy, A.A. Jayaraj, and J.J. Keirns. Lipid-based Delivery Systems for Improving the Bioavailability and Lymphatic Transport of a Poorly Water-soluble LTB4 Inhibitor. J Pharm Sci. 87: 164-169 (1998).

120. I.V. Batrakova, S. Li, Y. Li, V.Y. Alakhov, and A.V. Kabanov. Effect of Pluronic P85 on ATPase activity of drug efflux transporters. Pharm Res. 21: 2226-2233 (2004).

121. R. Regev, Y.G. Assaraf, and G.D. Eytan. Membrane fluidization by ether, other anesthetics, and certain agents abolishes P-glycoprotein ATPase activity and modulates efflux from multidrug-resistant cells. Eur J Biochem. 259: 18-24 (1999).

122. I. Bondesson, B. Ekwall, S. Hellberg, L. Romert, K. Stenberg, and E. Walum. MEIC-a new international multicenter project to evaluate the relevance to human toxicity of in vitro cytotoxicity tests. Cell Biol Toxicol. 5: 331-347 (1989).

123. G. Malich, B. Markovic, and C. Winder. The sensitivity and specificity of the MTS tetrazolium assay for detecting the in vitro cytotoxicity of 20 chemicals using human cell lines. Toxicology. 124: 179-192 (1997).

124. A.H. Cory, T.C. Owen, J.A. Barltrop, and J.G. Cory. Use of an aqueous soluble tetrazolium/formazan assay for cell growth assays in culture. Cancer Commun. 3: 207-212 (1991).

125. W.J. Welch. Mammalian stress response: cell physiology, structure /function of stress proteins, and implications for medicine and disease. Physiol Rev. 72: 1063-1081 (1992).

126. R. Rhodes. CellTiter 96® Non-Radioactive Cell Proliferation Assays and CytoTox 96® Non-Radioactive Cytotoxicity Assay. Promega Notes Magazine. 59:50-51 (1996).

127. Allen, M.S. and Rushton, N. Use of the CytoTox 96(TM) Assay in Routine Biocompatibility Testing In Vitro. Promega Notes Magazine.45:7-11 (1994).

128. A.B. Shapiro and V. Ling. Positively Cooperative Sites for Drug Transport by P-Glycoprotein with Distinct Drug Specificities. European Journal of Biochemistry. 250:130-137 (1997).

129. R. Daoud, C. Kast, P. Gros, and E. Georges. Rhodamine 123 Binds to Multiple Sites in the Multidrug Resistance Protein (MRP1). Biochemistry. 39:15344-15352 (2000).

130. J. Lee, K. Paull, M. Alvarez, C. Hose, A. Monks, M. Grever, A. Fojo, and S. Bates. Rhodamine efflux patterns predict P-glycoprotein substrates in the National Cancer Institute drug screen. Mol Pharmacol. 46:627-638 (1994).

131. G. Kroemer, B. Dallaporta, and M. Resche-Rigon. The mitochondrial death/life regulator in apoptosis and necrosis. Annu Rev Physiol, 60: 619-642 (1998).

132. C. Ozvegy, A. Varadi, and B. Sarkadi. Characterization of Drug Transport, ATP Hydrolysis, and Nucleotide Trapping by the Human ABCG2 Multidrug Transporter: Modulation of substrate specificity by a point mutation. J Biol Chem. 277:47980-47990 (2002).

133. C. Loetchutinat, C. Saengkhae, C. Marbeuf-Gueye, and A. Garnier-Suillerot. New insights into the P-glycoprotein-mediated effluxes of rhodamines. Eur J Biochem. 270:476-485 (2003).

134. R. Zaja, R. S. Klobučar, and T. Smital. Detection and functional characterization of Pgp1 (ABCB1) and MRP3 (ABCC3) efflux transporters in the PLHC-1 fish hepatoma cell line. Aqua Tox. 81:365-376 (2007).

135. L. Huang, T. Hoffman, and M. Vore. Adenosine triphosphate-dependent transport of Estradiol-17β (β-*d*-glucuronide) in membrane vesicles by MDR1 expressed in insect cells. Hepatology. 28: 1371-1377 (1998).

136. N. Yoshida, T. Takada, Y. Yamamura, I. Adachi, H. Suzuki, and Junichi Kawakami. Inhibitory effects of terpenoids on Multidrug Resistance-Associated Protein 2- and Breast Cancer Resistance Protein-mediated Transport. Drug Metab Dispos. 36: 1206-1211 (2008).

137. H. Kusuhara and Y. Sugiyama. Active efflux across the blood-brain barrier: role of the solute carrier family. NeuroRx. 2: 73-85 (2005).

138. C. Hilgendorf, G. Ahlin, A. Seithel, P.Artursson, A.L Ungell, and J. Karlsson. Expression of thirty-six drug transporter genes in human intestine, liver, kidney, and organotypic cell lines. Drug Metab Dispos. 35: 1333-1340 (2007).

139. R.A.M.H. Aubel, M.A. Kuijck, J.B. Koenderink, P.M.T. Deen, C. H. Os, and F.G.M. Russel. Adenosine triphosphate-dependent transport of anionic conjugates by the rabbit multidrug resistance-associated protein Mrp2 expressed in insect cells. Mol Pharmacol. 53:1062-1067 (1998).

140. C. Hilgendorf, G. Ahlin, A. Seithel, P. Artursson, A. Ungell, and J. Karlsson. Expression of Thirty-six Drug Transporter Genes in Human Intestine, Liver, Kidney, and Organotypic Cell Lines. Drug Metab Dispos. 35:1333-1340 (2007).

141. H. Takikawa, R. Yamazaki, N. Sano, and M. Yamanaka. Biliary Excretion of Estradiol-17 beta-glucuronide in the Rat. Hepatology. 23:607-613 (1996).

142. A.D. Mottino, T. Hoffman, F.A. Crocenzi, E.J.S. Pozzi, M.G. Roma, and M. Vore. Disruption of function and localization of tight junctional structures and Mrp2 in sustained estradiol-17beta-D-glucuronide-induced cholestasis. Am J Physiol Gastrointest Liver Physiol. 293: G391-402 (2007).

143. I. Hubatsch, E. G. Ragnarsson, and P. Artursson. Determination of drug permeability and prediction of drug absorption in Caco-2 monolayers. Nat Protoc. 2:2111-2119 (2007).

144. P. M. Gerk, W. Li, and M. Vore. Estradiol 3-glucuronide is transported by the multidrug resistance-associated protein 2 but does not activate the allosteric site bound by estradiol 17-glucuronide. Drug Metab Dispos. 32:1139-1145 (2004).

145. B.R. Jones, W. Li, J. Cao, A. Hoffman, P.M. Gerk, and M. Vore. The Role of Protein Synthesis and Degradation in the Post-Transcriptional Regulation of Rat Multidrug Resistance-Associated Protein 2 (Mrp2, Abcc2). Mol Pharmacol. 68: 701-710 (2005).

146. P.R. Twentyman, T. Rhodes, and S. Rayner. A comparison of rhodamine 123 accumulation and efflux in cells with P-glycoprotein-mediated and MRP-associated multidrug resistance phenotypes. Eur J Cancer. 9: 1360-1369 (1994).

147. M. Webb, C.L. Raphael, H. Asbahr, W.N. Erber, and B.F. Meyer. The detection of rhodamine 123 efflux at low levels of drug resistance. Br J Haematol. 93: 650-655 (1996).

148. S. Miyauchi, M. Komatsubara, and N. Kamo. In Archaebacteria, there is a doxorubicin efflux pump similar to mammalian P-glycoprotein. Biochim Biophys Acta. 1110: 144-150 (1992).

149. M.D. Troutman and D.R. Thakker. Rhodamine 123 requires carrier-mediated Influx for its activity as a P-glycoprotein Substrate in Caco-2 Cells. Pharm Res. 20: 1192-1199 (2003).

150. L.V. Johnson, M.L. Walsh, and L.B. Chen. Localization of mitochondria in living cells with rhodamine 123. Proc Natl Acad Sci. 77: 990-994 (1980).

151. O. Alqawi, S. Bates, and E. Georges. Arginine482 to threonine mutation in the breast cancer resistance protein ABCG2 inhibits rhodamine 123 transport while increasing binding. Biochem J. 382: 711-716 (2004).

152. B. Nare, R.K. Prichard, and E. Georges. Characterization of rhodamine 123 binding to P-glycoprotein in human multidrug-resistant cells. Mol Pharmacol. 45: 1145-1152 (1994).

153. R. Daoud, C. Kast, P. Gros, and E. Georges. Rhodamine 123 binds to multiple sites in the multidrug resistance protein (MRP1). Biochem. 39: 15344-15352 (2000).

154. L.A. Doganab, O. Legrandb, A.M. Faussatb, J.Y. Perrotb, and J.P. Marieb. Evaluation and comparison of MRP1 activity with three fluorescent dyes and three modulators in leukemic cell lines. Leuk Res. 28: 619–622 (2004).

155. Z.S. Chen, E. Hopper-Borge, M.G. Belinsky, I. Shchaveleva, E. Kotova, and G.D. Kruh. Characterization of the transport properties of human multidrug resistance protein 7 (MRP7, ABCC10). Mol Pharmacol. 63: 351-358 (2003).

156. H. Kusuhara and Y. Sugiyama. Role of transporters in the tissue-selective distribution and elimination of drugs: transporters in the liver, small intestine, brain and kidney. J Controlled Release. 78:43-54 (2002).

157. M. V. Flores, E. C. Voutsas, N. Spiliotis, G. M. Eccleston, G. Bell, D. P. Tassios, and P. J. Halling. Critical Micelle Concentrations of Nonionic Surfactants in Organic Solvents: Approximate Prediction with UNIFAC. J Colloid Interface Sci. 240:277-283 (2001).

158. A.V. Kabanov, E.V. Batrakova, and V.Y. Alakhov. An essential relationship between ATP depletion and chemosensitizing activity of Pluronic® block copolymers. J Controlled Release. 91:75-83 (2003).

159. The Pharmacological Effect of Lipids III: Role of Lipids in Cancer Research. In Kabara, J.J., ed., The American Oil Chemists Society, Phoenix, AZ, 1989.

160. K.W. Scotto. Transcriptional regulation of ABC drug transporters. Oncogene. 22: 7496–7511 (2003).

161. S. Teng and M. Piquette-Miller. Regulation of transporters by nuclear hormone receptors: implications during inflammation. Mol Pharm. 5:67-76 (2008).

162. B. L. Urquhart, R.G. Tirona, and R.B. Kim. Nuclear receptors and the regulation of drug-metabolizing enzymes and drug transporters: implications for interindividual variability in response to drugs. J Clin Pharmacol. 47:566-578 (2007).

163. S. Deferme, P. Annaert, and P. Augustijns. In Vitro Screening Models to Assess Intestinal Drug Absorption and Metabolism. In C. Ehrhardt and K.J. Kim (eds.), Drug Absorption Studies, Springer, US, 2008, pp 182-215.

164. C.H. Lee and J. Plutzky. Liver X Receptor Activation and High-density Lipoprotein Biology: a Reversal of Fortune? Circulation, 113:5-8 (2006).

165. A. Chawla, J.J. Repa, R.M. Evans, and D.J. Mangelsdorf. Nuclear Receptors and Lipid Physiology: Opening the X-Files. Science. 294:1866-1870 (2001).